

**Ecology and photosynthetic activity of a newly-discovered
Vaucheria sp. dominated Arctic microphytobenthos, Svalbard.**

Claude-Eric Souquieres



UNIVERSIDADE DO ALGARVE

Marine Biology Master (MBM) Programme

2016/2018

**Ecology and photosynthetic activity of a newly-discovered
Vaucheria sp. dominated Arctic microphytobenthos, Svalbard.**

Claude-Eric Souquieres



UNIVERSIDADE DO ALGARVE

Marine Biology Master (MBM) Programme

2016/2018

Student: Claude-Eric Souquieres (student n° a57343), claude.souquieres@gmail.com

Supervisor: Josef Elster (CPE), Josef.Elster@ibot.cas.cz

Co-Supervisors: Rui Santos (uAlg), rosantos@ualg.pt

Sending institution: Universidade do Algarve, Faro, Portugal – Faculty of Marine Biology
(uAlg)

Receiving organization/Enterprise: University of South Bohemia – Faculty of Science, Centre
for Polar ecology (CPE)

Declaração de autoria de trabalho

*Ecology and photosynthetic activity of a newly-discovered Vaucheria
sp. dominated Arctic microphytobenthos, Svalbard.*

Declaro ser o(a) autor(a) deste trabalho, que é original e inédito. Autores e trabalhos consultados estão devidamente citados no texto e constam da listagem de referências incluída.

A Universidade do Algarve reserva para si o direito, em conformidade com o disposto no Código do Direito de Autor e dos Direitos Conexos, de arquivar, reproduzir e publicar a obra, independentemente do meio utilizado, bem como de a divulgar através de repositórios científicos e de admitir a sua cópia e distribuição para fins meramente educacionais ou de investigação e não comerciais, conquanto seja dado o devido crédito ao autor e editor respetivos.

Acknowledgements

I would like to express my sincere gratitude to my supervisor and co-supervisor, Dr. Josef Elster & Dr. Jana Kviderova whose understanding, and knowledge of the Arctic have helped me through the achievement of this Master Thesis. Not only have I benefited from their skills and knowledge in several areas, but also from their attentive support, providing me with many opportunities to study and work in the exalting landscapes of the Norwegian archipelago of Svalbard.

I would also like to address a special thank you to all the people whom contributed to make this thesis possible, including all the staff of the Centre for Polar Ecology in Ceske Budejovice. Especially, Petra Luláková for her help regarding the granulometric analysis. Jakub Ondruch for his experienced help mapping the tidal flat by means of drone. Dr. Tomáš Hajek for the recommendations he provided us regarding the photosynthetic measurements. Tomáš Hubáček for the time he spent explaining me the Triple Quadrupole ICP-MS Technology and numerous other people whose names might have escaped my distracted mind.

I am grateful to this MBM Master Program for the opportunity I had to live and study in Portugal as well as in Czech Republic, with its ups and downs along the way but eventually coming together as an irrefutable uplifting experience.

Finally, I would like to thank with all my heart my parents and my family who have always showed an infinite support for every decision I took and regardless of their apparent madness at times. Far away in too many circumstances though always closely caring.

This work was supported by the University of South Bohemia (USB), Faculty of Science, Centre for Polar Ecology (projects LM2015075, EF16_013/0001782 – SoWa Ecosystems Research).

Resumo

Um estudo abrangente da ecologia e atividade fotossintética de uma espécie recém-descoberta no Ártico, *Vaucheria* sp., que domina o microfítobentos foi abordado neste estudo. O microfítobentos é uma comunidade muito diversificada de organismos microscópicos localizada nos sedimentos superficiais dos ecossistemas aquáticos. Ocorre geralmente nos vários milímetros superiores de sedimentos iluminados, formando um subtil biofilme acastanhado ou esverdeado no fundo do mar. O microfítobentos é constituído por vários grupos de diatomáceas fotossintéticas, cianobactérias, flagelados e algas. Esta comunidade fotossintética de microrganismos desempenha um papel ecológico central no ambiente estuarino. É responsável por uma fração significativa da produção primária total, podendo até exceder a produtividade pelágica em certas circunstâncias. Além disso, o microfítobentos desempenha um papel importante na mediação das trocas de nutrientes entre o sedimento e a água. Sabe-se também que melhora o acoplamento bento-pelágico e em algumas circunstâncias, afeta positivamente a bioestabilização do fundo do mar. Apesar da sua importância ecológica nas áreas costeiras, muito pouco se sabe sobre o microfítobentos ártico em relação à sua ecologia, desempenho fotossintético e produtividade. No litoral ártico, onde existem grandes variações inter-sazonais de luz, temperaturas e concentrações de nutrientes, juntamente com pressões crescentes, as comunidades microfítobênticas mostraram sinais de excelentes adaptações metabólicas. No estudo que foi realizado da planície de maré da costa ocidental de Svalbard em que habita a *Vaucheria* sp. foram encontrados bons desempenhos fotossintéticos. Demonstramos que neste ecossistema, existe um impacto forte das coocorrências marinhas e de água doce na qual a *Vaucheria* sp. habita. Sugere-se que a *Vaucheria* sp. pode tolerar uma grande variedade de conteúdo de salinidade até aproximadamente 40 PSU. A heterogeneidade ecológica desta planície de maré em que *Vaucheria* sp. ocorre foi descrita cuidadosamente. Através da amostragem da coluna de água, observou-se que o fósforo era um fator limitante. No entanto, no final de agosto de 2017, observou-se uma alteração temporal que afetou os níveis de nutrientes na coluna de água. Observou-se que ao alterar as condições, alterando o fósforo como fator limitante para sílica, observou-se a natureza altamente dinâmica desse ecossistema de maré e sugerindo uma transição na comunidade estuarina. Especula-se que o florescimento tardio de diatomáceas árticas no verão, deve-se a uma exaustão significativa de sílica na coluna de água, sendo responsável por esta mudança de nutrientes no final da amostragem. Outros compostos químicos foram relatados como variar significativamente ao longo da amostragem. Notavelmente, na coluna de água registou-se uma diminuição significativa no NO₂-N,

enquanto que no Azoto total, PO₄-P, Fósforo Total, Mg, SO₄, K, Na e Ca observou-se um aumento significativo. Da mesma forma, observou-se uma diminuição significativa nas concentrações de NO₃-N e PO₄-P no sedimento da planície de maré.

Em relação ao ecossistema, demonstrou-se que existe uma forte contribuição da *Vaucheria* sp. para a produtividade fotossintética local, afetando o ciclo de carbonatos na coluna de água. Portanto, esta comunidade de *Vaucheria* sp. afeta significativamente os fatores químicos da água, especialmente o ciclo de carbonato. O microfitobentos não afeta apenas os fatores hidroquímicos da planície de maré, afeta também as características físicas e químicas do sedimento. A comunidade de *Vaucheria* sp. está correlacionada com baixo teor de unidade sedimentar e baixa percentagem de carbono orgânico nos sedimentos da planície de maré. Essa observação pode indicar o forte impacto dessa comunidade microfitobêntica na biogeoquímica do leito marinho. Um efeito que foi estudado e que é bem conhecido dos microfitobentos no sedimento é a bio estabilização do fundo do mar. Os organismos microfitobentônicos desempenham um papel fundamental no aumento da estabilização de sedimentos, protegendo o leito marinho da erosão causada pelo constante movimento da maré, libertando substâncias poliméricas extracelulares resultantes da atividade fotossintética, auxiliando na-bio estabilização do leito marinho. Embora não se tenha investigado diretamente a estabilidade do sedimento, especula-se que as observações ecológicas podem ser uma consequência indireta da bio-estabilização local do sedimento induzido pela comunidade de *Vaucheria* sp.. Outras investigações seriam necessárias para confirmar o hipotético efeito bio-estabilizante desta comunidade no ecossistema.

Embora *Vaucheria* sp. pareça dominar este ecossistema de maré baixa, foram encontradas evidências da ocorrência de uma comunidade microfitobêntica muito mais dinâmica e complexa e na qual *Vaucheria* sp. parece desempenhar uma função essencial. A comunidade de *Vaucheria* sp. exibiu uma notável plasticidade fisiológica em relação a um amplo espectro de intensidades luminosas que variam de 10 a 650 $\mu\text{mol m}^{-2} \text{s}^{-1}$. A combinação de técnicas gasométricas e de várias técnicas de fluorescência de clorofila a foram utilizadas neste estudo, permitindo determinar os desempenhos fotossintéticos gerais da comunidade de *Vaucheria* sp. A comunidade de *Vaucheria* sp. foi capaz de utilizar um amplo espectro de intensidades PAR sem mostrar qualquer fotoinibição para intensidades PAR até um máximo de 650 $\mu\text{mol m}^{-2} \text{s}^{-1}$. Foram medidas características fotossintéticas gerais das *Vaucheria* sp. e, foi reportado nesta espécie uma eficiência fotossintética média (α) de 0,00641 (\pm 0,00061), a qual não se alterou com a intensidade PAR a que foi aclimatada. A fotossíntese máxima (Pmax)

variou de 0,756 a 1,188 nmol g⁻¹ s⁻¹, medida por via gasométrica. O Icomp médio foi de 38,53 μmol m⁻² s⁻¹, aproximadamente dez vezes menor do que o das algas bentônicas análogas extremamente sombreadas. Além disso, dados os valores de irradiância de saturação, Ek ou Isat, *Vaucheria* sp. parece estar adaptada à pouca luz. Por fim, *Vaucheria* sp. foi capaz de uma fotoaclimação rápida através da transição consecutiva entre a luz de baixa irradiância recebida e a de alta. Esta qualidade de fotoaclimação rápida de *Vaucheria* sp. está provavelmente ligada às transições de estado ou ao ciclo das xantofilas.

Palavras-chaves (4-6): Ecologia litoral ártica, microphytobenthos, ecofisiologia da *Vaucheria* sp.

English abstract

A comprehensive study of the ecology and photosynthetic activity of a newly-discovered *Vaucheria* sp. dominated arctic microphytobenthos was addressed here. The microphytobenthos is a very diversified community of microscopic organisms from the surficial sediment of aquatic ecosystems. It typically consists of various assemblages of substrate-dwelling photosynthetic diatoms, cyanobacteria, flagellates and algae. The microphytobenthos plays a central ecological role in estuarine environment, responsible for a significant fraction of the total primary production, mediating water-sediment nutrient exchanges, enhancing benthic-pelagic coupling and efficiently stabilizing the sediment. Despite their ecological value in coastal areas, very little is known about arctic microphytobenthos ecology and photosynthetic performances. Across the arctic coastline, where large inter-seasonal variations in light, temperatures and nutrient levels are experienced along with increasing pressures, microbenthic communities have shown signs of excellent metabolic adaptations. In case, across this arctic tidal flat, *Vaucheria* sp. was found to show a remarkable adaptation to the local ecological parameters. We demonstrated in this ecosystem the strong impacts of both marine and freshwater co-occurrences creating *Vaucheria* sp. environment. The heterogeneity of *Vaucheria* sp. habitat was described. Locally, the water column was phosphorus-limited and a temporal shift from phosphorous to silica-limited conditions occurred throughout the sampling period, witnessing of the highly dynamic nature of this tidal ecosystem. At the ecosystem level, the strong microphytobenthos' photosynthesis was supported by significant high water-pH values, correlated to *Vaucheria* sp. spatial occurrence. Even though *Vaucheria* sp. seemed to dominate, we found evidences of a more complex micro-phytobenthic community functioning. *Vaucheria* sp. community exhibited adaptability to large variations in abiotic factors. Gasometric and Chlorophyll fluorescence measurements did not show any limitation of the photosynthetic over the range of environmental PAR suggesting good photoacclimation of *Vaucheria* sp. to arctic conditions. Based on the compensation irradiance value of *Vaucheria* sp. we demonstrated this alga to be low-light adapted. Furthermore, *Vaucheria* sp. was capable of fast photo-acclimation through the consecutive transition from low to high incoming light irradiances. This quality of *Vaucheria* sp. fast photo-acclimation is thought to be linked to state transitions or effective xanthophyll cycle.

Keywords (4-6): Arctic coastal ecology, microphytobenthos, *Vaucheria* sp. ecophysiology.

Table of content

DECLARAÇÃO DE AUTORIA DE TRABALHO	II
ACKNOWLEDGEMENTS	III
RESUMO	IV
ENGLISH ABSTRACT	VII
LIST OF FIGURES	X
LIST OF TABLES	XII
CHAPTER 1 – INTRODUCTION	1
1. ARCTIC OCEAN HYDROGRAPHY	1
1.1. <i>Arctic ocean physical oceanography</i>	1
1.2. <i>Arctic Ocean bathymetry</i>	3
1.3. <i>Arctic Ocean hydrochemistry</i>	4
2. ARCTIC LIGHT REGIME AND POLAR DAY LENGTH	5
2.1. <i>Irradiance quantity (E)</i>	6
2.2. <i>Spectral composition</i>	6
3. THE CRYOSPHERE	7
3.1. <i>Sea-ice</i>	8
4. GEOSCIENCE OF SVALBARD	8
5. SVALBARD CLIMATIC CONDITIONS	10
6. ARCTIC MICROPHYTOBENTHOS	10
6.1. <i>Arctic microphytobenthos growth</i>	11
6.2. <i>Arctic microphytobenthic primary production</i>	11
6.3. <i>Arctic microphytobenthic biodiversity</i>	12
7. <i>VAUCHERIA</i> SP. – YELLOW-GREEN ALGA	13
7.1. <i>Morphology</i>	13
7.2. <i>Reproduction and reproductive features</i>	14
7.3. <i>Distribution and habitat</i>	14
8. OBJECTIVES	15
CHAPTER 2 – ECOLOGY AND PHOTOSYNTHETIC ACTIVITY OF A NEWLY- DISCOVERED <i>VAUCHERIA</i> SP. DOMINATED ARCTIC MICROPHYTOBENTHOS, SVALBARD	16
MATERIAL & METHODS	16
<i>Study area description</i>	16
<i>Sampling</i>	17
<i>Data collection and analysis</i>	17
<i>Statistical analysis</i>	22
RESULTS	23
<i>Physical environment & Topography</i>	23
<i>Spatial & temporal ecological heterogeneity</i>	24
<i>Data summary & ANOVA interpretation</i>	25
<i>Vaucheria sp. biogeographical & ecological dispersion</i>	27
<i>Spatial & temporal biochemistry</i>	28
<i>N:P:Si ratio and limiting nutrients</i>	34
<i>Hydrochemical spatial distribution patterns – Principal Component Analysis</i>	35
<i>Sediment biochemistry</i>	38
<i>Sediment chemistry spatial characterization – Principal Component Analysis</i>	40

<i>Vaucheria sp. photosynthetic activity</i>	42
DISCUSSION	45
<i>Tidal flat abiotic characterisation</i>	45
<i>General ecological parameters</i>	45
<i>Hydrochemical and biogeochemical parameters</i>	47
<i>Abiotic PCA summary</i>	47
<i>Hydrochemical and biogeochemical temporal evolution</i>	48
<i>Vaucheria sp. Ecological distribution</i>	50
<i>Vaucheria sp. community photosynthetic profile</i>	51
CONCLUSION.....	52
REFERENCES	53
ANNEX	- 60 -

List of figures

FIGURE I-1 MAP OF THE ARCTIC OCEAN SHOWING THE MAJOR OCEANIC CURRENTS CARRYING ARCTIC WATER MASSES IN AND OUT OF THE ARCTIC OCEANIC SYSTEM. CREDIT TO THE AUDUN IGGESUND, AND THE NORWEGIAN POLAR INSTITUTE.	1
FIGURE I-2 BATHYMETRIC MAP OF THE ARCTIC OCEAN (COORDINATES: LON1= -10, LON2= 66, LAT1= 60, LAT2= 82). MAP CREDIT TO NATIONAL OCEANOGRAPHIC AND ATMOSPHERIC ADMINISTRATION (NOAA). (RSTUDIO VERSION 3.4.4, PACKAGE: MARMAP)(RSTUDIO TEAM 2016).	3
FIGURE I-3 BATHYMETRIC PROFILE OF THE ARCTIC OCEAN. (COORDINATES: LON1= -10, LON2= 66, LAT1= 60, LAT2= 82). MAP CREDIT TO NATIONAL OCEANOGRAPHIC AND ATMOSPHERIC ADMINISTRATION (NOAA). (RSTUDIO VERSION 3.4.4, PACKAGE: MARMAP) (RSTUDIO TEAM 2016).....	4
FIGURE I-4 SUN DIAGRAM FOR LONGYEARBYEN, SVALBARD, 2018. PRODUCED BY SVALBARD SAMFUNNS DRIFT AS AND LONGYEARBYEN LOKALSTYRE.....	5
FIGURE I-5 DESCRIPTIVE SKETCH OF THE DIFFERENT ELEMENTS CONSTITUTING THE ARCTIC CRYOSPHERE SYSTEM. SOURCE: SWIPA (AMAP) 2011.	7
FIGURE I-6 GEOLOGICAL MAP OF SVALBARD. COLOR LEGENDS: SEE ANNEX. (QGIS 3.0) (QGIS DEVELOPMENT TEAM 2018)	9
FIGURE I-7 MICROSCOPIC PICTURE OF <i>VAUCHERIA SP.</i> FILAMENTS COLLECTED IN THE TIDAL FLAT ADJOINING LONGYEARBYEN, SVALBARD, 2017.	13
FIGURE I-8 PICTURE OF A DENSE BIOFILM OF <i>VAUCHERIA SP.</i> MICROBENTHIC ALGAE COVERING THE SEABED IN ADVENTDALEN-ADVENTFJORDEN TIDAL FLAT. SVALBARD, 2017. CREDIT PHOTO TO DR. ELSTER.....	14
FIGURE II-1 GEOGRAPHIC LOCATION OF THE STUDIED TIDAL FLAT, RED DOT = STUDIED LOCATION (UPPER MAP). DETAILED MAP OF THE SAMPLING AREA WITH TRANSECTS I, II AND III (LOWER MAP). SAMPLING SITES ALONG THE TRANSECT ARE NUMBERED FROM ONE TO FOUR FROM BOTTOM TO TOP STARTING FROM T1.1. THE RED ZONE DELIMITS THE HIGH TIDE FRONT AND IN BLUE THE LOW TIDE CHANNEL. SAMPLING SITES IN GREEN REFER TO THE PRESENCE OF <i>VAUCHERIA SP.</i> (QGIS 3.0 + GOOGLE EARTH PRO) (QGIS DEVELOPMENT TEAM 2018).	16
FIGURE II-2 EVOLUTION OF THE LIGHT ENVIRONMENT THROUGHOUT THE SAMPLING PERIOD STARTING FROM AUGUST 12, 2017, 14:00 UTC, TO AUGUST 31, 2017, 8:00 UTC.....	24
FIGURE II-3 SOIL TEXTURE TRIANGLE WITH RESULTS OF THE GRANULOMETRY ANALYSIS OVER THE STUDIED TIDAL FLAT.	24
FIGURE II-4 BOX PLOTS DATA ANALYSIS OF THE MAIN PHYSICAL ABIOTIC PARAMETERS INCLUDING WATER PH, SALINITY, DENSITY, SEDIMENT MOISTURE AND WATER TEMPERATURE.	26
FIGURE II-5 BIPLLOT DATA ANALYSIS OF <i>VAUCHERIA SP.</i> DISTRIBUTION BASED ON THE MAIN ABIOTIC PHYSICAL PARAMETERS (SCORES OF EACH SAMPLING STATIONS AND LOADINGS OF THE DIFFERENT PHYSICAL ABIOTIC PARAMETERS INCLUDING WATER PH, WATER	

<p>DENSITY AND SEDIMENT MOISTURE). EACH SMALL DOT REPRESENTS ONE SAMPLING SITE. BLUE = PRESENCE OF VAUCHERIA, RED = ABSENCE. THE LARGER DOT REPRESENTS THE OVERALL AVERAGE SCORE FOR THE RESPECTIVE GROUPS. (RSTUDIO TEAM 2016).</p>	28
<p>FIGURE II-6 BOX PLOTS DATA ANALYSIS OF THE HYDROCHEMICAL PARAMETERS INCLUDING: NH₄-N, NO₂-N, NO₃-N, TN, PO₄-P, TP, MG, SI, SO₄, K, FE, MN, NA, CA. (RSTUDIO TEAM 2016).</p>	33
<p>FIGURE II-7 SCATTER DIAGRAMS OF THE SI:N:P ATOMIC NUTRIENT RATIOS INTRINSIC TO THE TIDAL FLAT'S WATER COLUMN FOR THE MONTH OF AUGUST 2017. THE MOLAR QUOTIENTS ARE DELIMITED IN THIS LOGARITHMIC PLOT BY THE SI:N= 1:1 (VERTICAL LINE), N:P= 16:1 (HORIZONTAL LINE) AND SI:P= 16:1 (OBLIQUE LINE) LINES. THE LINES ENABLE TO DIVIDE THE PLOT INTO SIX DIFFERENT AREAS. EACH OF THESE AREAS INDICATES THE POTENTIALLY LIMITING NUTRIENT WATER PROFILE, WITH LIMITING NUTRIENTS LISTED BY ORDER OF IMPORTANCE. (RSTUDIO TEAM 2016).....</p>	35
<p>FIGURE II-8 BIPLLOT DATA ANALYSIS OF THE SPATIAL HYDROCHEMICAL DISTRIBUTION BY TRANSECTS (SCORES OF EACH SAMPLING SITES AND LOADINGS OF THE DIFFERENT CHEMICAL VARIABLES INCLUDING: NH₄-N, NO₂-N, NO₃-N, TN, PO₄-P, TP, MG, SI, SO₄, K, FE, MN, NA, CA) ON THE LEFT. THE LARGER DOT REPRESENTS THE OVERALL AVERAGE SCORE FOR THE RESPECTIVE GROUPS. (RSTUDIO TEAM 2016).</p>	37
<p>FIGURE II-9 BIPLLOT DATA ANALYSIS OF THE SPATIAL HYDROCHEMICAL DISTRIBUTION BY SITES (SCORES OF EACH SAMPLING SITES AND LOADINGS OF THE DIFFERENT CHEMICAL VARIABLES INCLUDING: NH₄-N, NO₂-N, NO₃-N, TN, PO₄-P, TP, MG, SI, SO₄, K, FE, MN, NA, CA). EACH SMALL DOT REPRESENTS ONE SAMPLING SITE. THE LARGER DOT REPRESENTS THE OVERALL AVERAGE SCORE FOR THE RESPECTIVE GROUPS. (RSTUDIO TEAM 2016).</p>	37
<p>FIGURE II-10. BOX PLOTS DATA ANALYSIS OF THE SEDIMENT CHEMICAL PARAMETERS INCLUDING: NH₄-N, NO₃-N, PO₄-P. (RSTUDIO TEAM 2016).</p>	39
<p>FIGURE II-11 BOX PLOT DATA ANALYSIS OF THE ORGANIC CARBON CONTENT PRESENT IN THE SURFACE LAYER OF THE SEAFLOOR ACROSS THE TIDAL FLAT. (RSTUDIO TEAM 2016).</p>	40
<p>FIGURE II-12 BIPLLOT DATA ANALYSIS OF THE SPATIAL SEDIMENT CHEMICAL DISTRIBUTION BY TRANSECTS (SCORES OF EACH SAMPLING SITES AND LOADINGS OF THE DIFFERENT CHEMICAL VARIABLES INCLUDING: NH₄-N, NO₃-N, PO₄-P). EACH SMALL DOT REPRESENTS ONE SAMPLING SITE. LEFT, RED = TRANSECT I, GREEN = TRANSECT II, BLUE = TRANSECT III. THE LARGER DOT REPRESENTS THE OVERALL AVERAGE SCORE FOR THE RESPECTIVE GROUPS. (RSTUDIO TEAM 2016).</p>	41
<p>FIGURE II-13 BIPLLOT DATA ANALYSIS OF THE SPATIAL SEDIMENT CHEMICAL DISTRIBUTION BY TRANSECTS (SCORES OF EACH SAMPLING SITES AND LOADINGS OF THE DIFFERENT CHEMICAL VARIABLES INCLUDING: NH₄-N, NO₃-N, PO₄-P). EACH SMALL DOT REPRESENTS ONE SAMPLING SITE. THE LARGER DOT REPRESENTS THE OVERALL AVERAGE SCORE FOR THE RESPECTIVE GROUPS. (RSTUDIO TEAM 2016).</p>	42
<p>FIGURE II-14 THE DEPENDENCE OF THE NET PHOTOSYNTHESIS (P_{NET}), GROSS PHOTOSYNTHESIS (P_{GROSS}) AND DARK RESPIRATION (RD) EXPRESSED AS CO₂ ASSIMILATION RATE (MEAN ± S.D., N = 3) AT DIFFERENT PAR INTENSITIES. THE LETTERS INDICATE HOMOLOGOUS GROUPS RECOGNIZED BY TUKEY HSD TEST AT P = 0.05. THE NUMBER IN LEGEND INDICATES PAR IN μMOL M⁻² S⁻¹.</p>	42
<p>FIGURE II-15 THE DEPENDENCE OF ETR MEASURED IN THE LIGHT (ETR-LIGHT) AND ETR MEASURED IN THE DARK (ETR-DARK) AT DIFFERENT PAR INTENSITIES (MEAN ± S.D., N = 3). THE LETTERS INDICATE HOMOLOGOUS GROUPS RECOGNIZED BY TUKEY HSD TEST AT P = 0.05. THE NUMBER IN LEGEND INDICATES PAR IN μMOL M⁻² S⁻¹.</p>	43
<p>FIGURE II-16 THE DEPENDENCE OF COMPENSATION (I_{COMP}; MEAN ± S.D., N = 3) AND SATURATION (I_{SAT}; MEAN ± S.D., N = 3) IRRADIANCES ESTIMATED FROM GASOMETRIC (CO₂ ASSIMILATION) AND FLUORESCENCE (ETR) MEASUREMENTS FOR DIFFERENT PAR INTENSITIES. THE LETTERS INDICATE HOMOLOGOUS GROUPS RECOGNIZED BY TUKEY HSD TEST AT P = 0.05.</p>	44
<p>FIGURE II-17 PHOTOSYNTHESIS-IRRADIANCE CURVES FOR CO₂ ASSIMILATION AND ETR (MEAN ± S.D., N = 3). LL – LOW LIGHT OF 10 μMOL M⁻² S⁻¹, ML – MEDIUM LIGHT OF 230 μMOL M⁻² S⁻¹, HL – HIGH LIGHT OF 650 μMOL M⁻² S⁻¹.</p>	44
<p>FIGURE II-18 QUALITATIVE TEMPORAL EVOLUTION OF A SPECIFIC SET OF BIOCHEMICAL PARAMETERS ACROSS ADVENTDALEN-ADVENTFJORDEN'S TIDAL FLAT INCLUDING: NO₂-N, TN, PO₄-P, TP, MG, SI, SO₄, K, NA, CA IN THE WATER SURFACE LAYER & NO₃-N, PO₄-P IN THE SEDIMENT SURFACE LAYER. THE MONITORING TOOK PLACE DURING THE MONTH OF AUGUST 2017 FROM THE 09/08 TO THE 25/08/17. RED = HIGH CONCENTRATED & BLUE = LOW CONCENTRATED.</p>	48

List of tables

TABLE II-1 SUMMARY OF THE MAIN ABIOTIC PARAMETERS	25
TABLE II-2 PCA SUMMARY OF THE MAIN PHYSICAL PARAMETERS & ASSOCIATED EIGEN VALUES SCORES.....	27
TABLE II-3 HYDROCHEMICAL PARAMETERS FROM THE WATER SURFACE OF ADVENTDALEN'S TIDAL FLAT.....	29
TABLE II-4 KRUSKAL-WALLIS STATISTICAL SCORES OF THE TIDAL FLAT HYDROCHEMICAL PARAMETERS (UPPER TABLE) & WILCOXON STATISTICAL SCORES OF THE HYDROCHEMICAL VARIABLES (LOWER TABLE). STATISTICALLY SIGNIFICANT FOR $P < 0.05$ (DISPLAYED IN RED).	34
TABLE II-5 PCA SCORES SUMMARY. IN GREEN VALUES <0.5 (NEGATIVELY CORRELATED) AND RED >0.5 (POSITIVELY CORRELATED)..	35
TABLE II-6 HYDROCHEMISTRY PCA EIGEN VALUES AND CUMULATIVE VARIANCE.....	36
TABLE II-7 SEDIMENT BIOCHEMICAL INVENTORY.	38
TABLE II-8 KRUSKAL-WALLIS STATISTICAL SCORES OF THE BIOCHEMICAL PARAMETERS (UPPER TABLE) & WILCOXON STATISTICAL SCORES OF THE SEDIMENT BIOCHEMICAL PARAMETERS (LOWER TABLE). STATISTICALLY SIGNIFICANT FOR $P < 0.05$ (DISPLAYED IN RED).....	40
TABLE II-9 PCA SUMMARY OF THE BIOCHEMICAL PARAMETERS & ASSOCIATED EIGEN VALUES. IN GREEN VALUES <0.5 (NEGATIVELY CORRELATED) AND RED >0.5 (POSITIVELY CORRELATED).	41

CHAPTER 1 – Introduction

1. Arctic ocean hydrography

The Arctic region is a fundamental and unique area among the Earth’s ecosystems, raising northwards from the 66° parallel north. This region is presently transforming at an unequivocal pace, exceeding any other regions globally (Serreze and Francis 2006). Furthermore, the rate of its change is predicted to accelerate in the coming future (Serreze and Francis 2006). Across its extent, the arctic ocean and its coastal zone are particularly vulnerable.

1.1. Arctic ocean physical oceanography

A substantial portion of the arctic region is occupied by a large Arctic Ocean, itself surrounded by several landmasses and rich industrialized countries. The Arctic Ocean forms a semi-enclosed system profoundly affected by diverse oceanic and atmospheric influences from neighbouring sub-arctic regions (Sakshaug, Johnsen, and Kovacs 2011; Hattermann et al. 2016). The Arctic ocean connects two of the world’s major oceans: connecting the Pacific Ocean through the Chukchi Sea and the Atlantic Ocean through the Greenland Sea and Labrador Sea (Cokelet, Tervalon, and Bellingham 2008; The Norwegian Polar Institute, n.d.). The Arctic Ocean is divided in the middle in two major basins, delimited by the Lomonosov ridge. The Canadian basin extends westwards from the Lomonosov ridge, while The Eurasian basin including Svalbard locates to the East (Jakobsson et al. 2012).

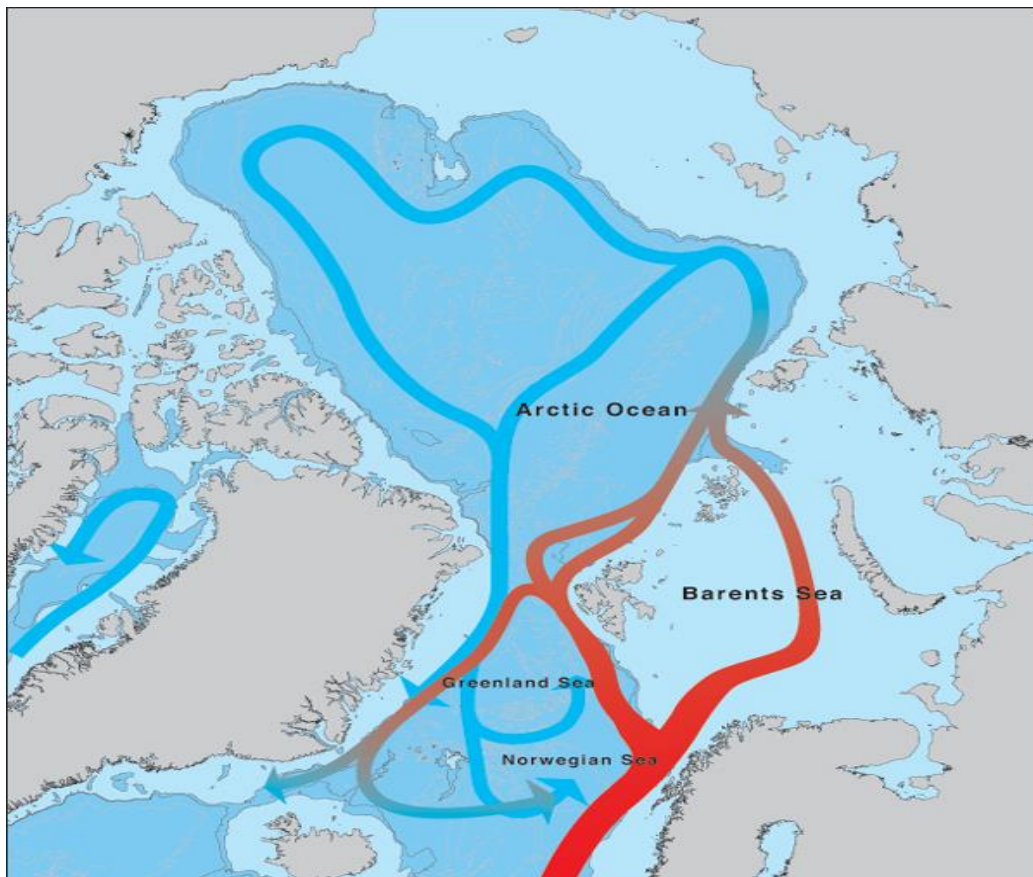


Figure I-1 Map of the Arctic ocean showing the major oceanic currents carrying Arctic water masses in and out of the Arctic oceanic system. Credit to the Audun Iggesund, and The Norwegian Polar Institute.

The Arctic Ocean's physical oceanography is tightly correlated to its hydrochemistry, hence affecting profoundly arctic marine productivity as a whole (Nikiforov, Colony, and Timokhov 2001; Rudels, Larsson, and Sehlstedt 2016). Water masses enter the Arctic Ocean system from two main passages. They enter through the Bering Strait driven along by the Bering Sea gyrotory current, but also and primarily via the Fram Strait as a powerful North Atlantic inflow (Figure I-1) (Cokelet, Tervalon, and Bellingham 2008; The Norwegian Polar Institute, n.d.). Subsequently, water masses exit the Arctic system either via deep currents from the Norwegian Sea toward the Atlantic, or via surface currents driven along by the Greenland and Labrador currents (Changsheng 2014) (Figure I-1). To the Pacific side, very little Arctic water flows out due to the narrow morphology of the seafloor (Changsheng 2014; Cokelet, Tervalon, and Bellingham 2008).

The Arctic Ocean's physical oceanography is strongly seasonally influenced (Rudels, Larsson, and Sehlstedt 2016). Likewise, spatially the Arctic Ocean's physical oceanographic differs remarkably throughout its extent (Rudels, Larsson, and Sehlstedt 2016). Across the Barents Sea, oceanographic variations are believed to be mainly of advective origin, depending primarily on the transfer of water masses (Sakshaug, Johnsen, and Kovacs 2011). Furthermore, in this shallow region, the water column is typically deep and strongly stratified (Rudels, Larsson, and Sehlstedt 2016). Along Svalbard's western littoral, the interplay of various oceanic currents produce together the set of environmental variables intrinsic to Svalbard coastal ecosystems (Cokelet, Tervalon, and Bellingham 2008; Howe, Moreton, & Morris, 2003). As warm North Atlantic currents gradually progress northwards, these dense Atlantic water masses are funnelled down underneath local Arctic water masses in the vicinity of Svalbard's western littoral (Cokelet, Tervalon, and Bellingham, 2008). Atlantic water masses are typically characterized by temperatures above 0°C and high salinity above 35 PSU (Cokelet, Tervalon, and Bellingham 2008). The warm and salty West Spitsbergen Current flows northwards along Svalbard's western continental ridge, mixing up with the inflow of Atlantic waters causing the relatively ice-free conditions inherent to western Svalbard (Vinje 2001). The mixing of Atlantic water masses and regional water masses results in the formation of a unique water mass referred as "Transformed Atlantic Water", with lower salinity and temperatures values compared to Atlantic water masses, around one degree Celsius and 34.7 PSU (Cokelet, Tervalon, and Bellingham 2008). This transformed water mass is principally confined to the intermediate layer of the water column. Beneath it the bottom water layer also called Local Water mass displays colder waters resulting from winter cooling, sea ice formation and seasonal convection processes (Cokelet, Tervalon, and Bellingham 2008; Rudels, Larsson, and Sehlstedt 2016). This bottom water layer originates from the local accumulation of brine-enriched water masses throughout the winter period. The accumulation of brine creates dense, very cold high-salinity waters which consecutively sink down in a process referred as convection (Rudels, Larsson, and Sehlstedt 2016). Eventually, the bottom water layer becomes too dense that these water masses are hardly resuspended to upper layers (Rudels, Larsson, and Sehlstedt 2016). This stratification has a strong influence on marine primary production and especially for the benthos, as it selectively keeps nutrients to the benthos (Gazeau et al. 2004).

With today’s strengthened and increasing north atlantic inflow, we currently observe what is referred as the “Atlantification” of the Arctic Ocean (Vesman, Ivanov, and Volkov 2017; Polyakov et al. 2017). More and more evidences report the profound impact of increasing atlantic inputs to the physical oceanography intrinsic to the arctic ocean (Berge et al. 2005; Pavlov et al. 2013). These observations in most cases were strongly linked to climate change effects, local atmospheric conditions and large-scale weather phenomenon such as the North Atlantic Oscillation (Sakshaug, Johnsen, and Kovacs 2011).

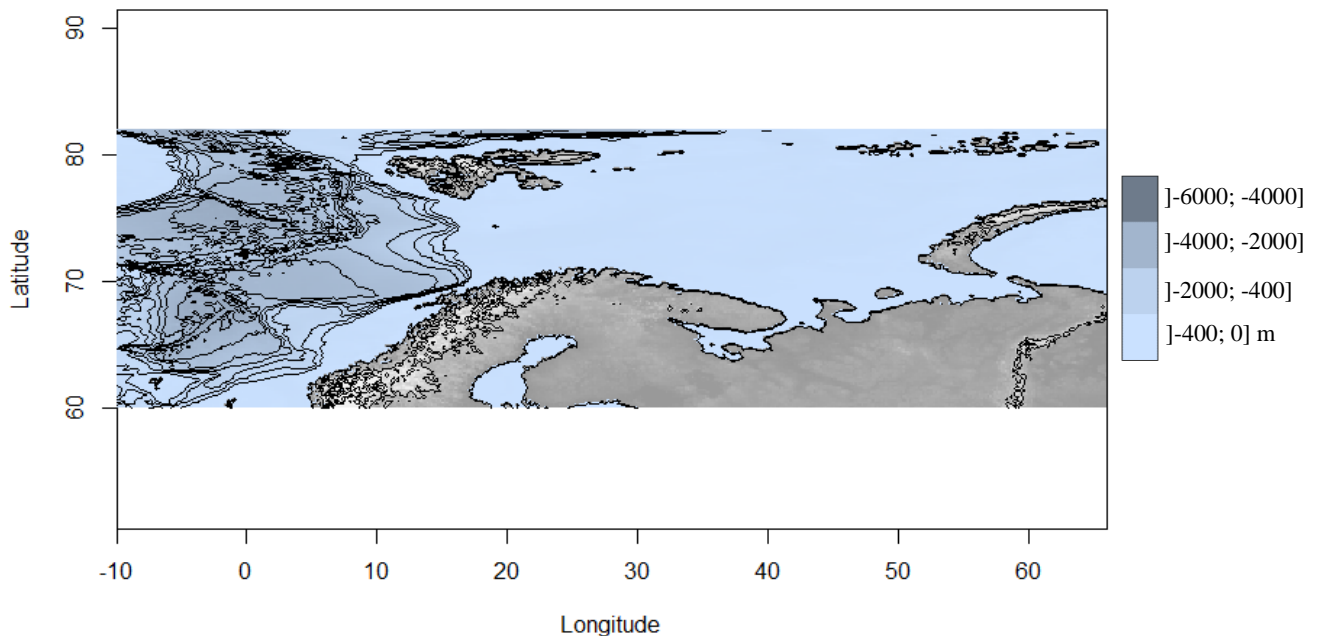


Figure I-2 Bathymetric map of the Arctic Ocean (coordinates: lon1= -10, lon2= 66, lat1= 60, lat2= 82). Map credit to National Oceanographic and Atmospheric Administration (NOAA). (Rstudio version 3.4.4, package: marmap)(RStudio Team 2016).

1.2. Arctic Ocean bathymetry

The Arctic Ocean expands over 15 558 000 km² of seafloor with a total average depth of 1 205 m, and a maximum depth reaching 5 549 m at the Litke Deep trench (Eakins and Sharman 2010). Arctic coastal regions occupy a total area of up to 5.8 to 6.1 million km² (Lantuit et al. 2012). Most of these Arctic coastal regions are characterized by shallow bathymetric profiles, especially along the Russian littoral (Figure I-2, I-3) (Jakobsson et al. 2012). More than 60% of the Arctic ocean consists of extensive stretches of shallow continental shelves laying on average at depths about 230 m (Stein et al. 2004; Gattuso et al. 2006; Sakshaug, Johnsen, and Kovacs 2011).

Along Svalbard’s littoral, or more generally in the Eurasian basin to the East side of Svalbard, most of the coastal seafloor lies at shallow depth reaching depths up to 400 meters maximum (Figure I-2, I-3) (Jakobsson

et al. 2012). Due to this shallowness A significant portion of this coastal seafloor is believed to accommodate large communities of benthic organisms (macrobenthic and microbenthic) (Gattuso et al. 2006).

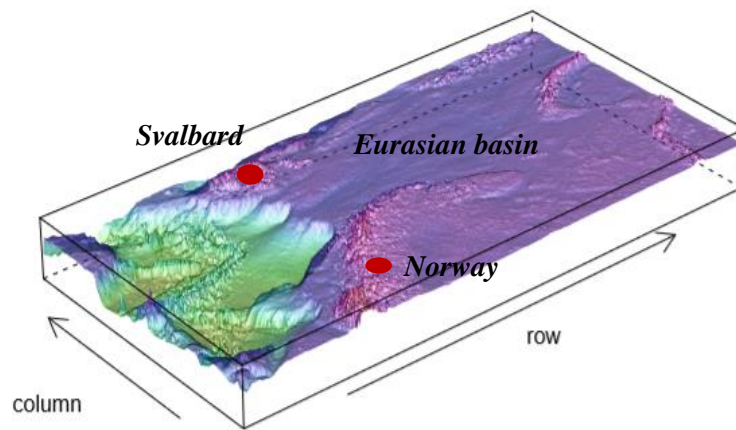


Figure I-3 Bathymetric profile of the Arctic ocean. (Coordinates: lon1= -10, lon2= 66, lat1= 60, lat2= 82). Map credit to National Oceanographic and Atmospheric Administration (NOAA). (Rstudio version 3.4.4, package: marmap) (RStudio Team 2016).

1.3. Arctic Ocean hydrochemistry

The Arctic Ocean is the world's smallest (14 056 000 km²), shallowest and coldest ocean on Earth (The world Factbook 2011). It is comprised of the following regional seas: the Barents Sea (1 405 000 km²), Kara Sea (880 000 km²), Laptev Sea (714 837 km²), Chukchi Sea (582 000 km²), Beaufort Sea (476 000 km²), Greenland Sea, Lincoln Sea and the East Siberian Sea (Briney 2018). Throughout the Arctic Ocean, nutrient concentrations are typically low and varies largely throughout the year (Sakshaug, Johnsen, and Kovacs 2011).

Arctic Ocean hydrochemistry is a key feature for arctic marine life as it produces the necessary ecological conditions for the development and inhabitancy of a specific flora and fauna (Nikiforov, Colony, and Timokhov 2001). A variety of ecological processes including oceanographic, cryogenic, atmospheric and biological processes, affects profoundly nutrients concentration and distribution throughout the Arctic Ocean and within the water column (Cokelet, Tervalon, and Bellingham 2008). Comparatively to light, nutrients concentration is the second most important limiting factor in marine ecosystems accountable for the growth of primary producers (Sakshaug, Johnsen, and Kovacs 2011). Marine nutrients comprise a highly diverse spectrum of chemical elements of which the dominant ones, include nitrogen, phosphorus, and silicate (Sakshaug, Johnsen, and Kovacs 2011). In the Barents Sea around Svalbard, the nutrient concentration is typically regarded as one of the poorest across the Arctic Ocean (Sakshaug, Johnsen, and Kovacs 2011). However, arctic spring nutrient admixtures (mainly nitrogen and silicic acid) from adjacent Arctic freshwater rivers seasonally supplies the Arctic Ocean from the onset of the springtime sea-ice melt (Stein et al. 2004). Yet the significance of these nutrient inputs to the Arctic Ocean must be contrasted, as it appears to be restricted only to very local coastal sites where nutrients are rapidly exhausted (Tremblay and Gagnon 2009). Arctic estuaries typically experience limiting phosphorous concentration because arctic rivers are relatively rich in nitrogen and silicic acid but poor in phosphate (Stein et al. 2004; Popova et al. 2010).

2. Arctic light regime and polar day length

The light regime corresponds to the properties of the light occurring over a certain interval of time in a given medium and by which photosynthetic activity is regulated (Mascarenhas et al. 2017). It comprises a set of different parameters including: irradiance quantity (E; amount of incoming energy), irradiance quality (spectral composition), and day length, which varies simultaneously as a function of astronomical parameters and cyclical movements (e.g; Milankovic cycle), latitude and local inherent optical properties (Sakshaug, Johnsen, and Kovacs 2011).

The light regime is an ecologically important factor, profoundly influencing a wide range of biological processes (Mascarenhas et al. 2017). In the poles, the light climate is unique displaying extreme temporal and spatial variations, ranging from polar night conditions in winter to midnight sun conditions in summer (Figure I-4) (Sakshaug, Johnsen, and Kovacs 2011). At latitudes beyond the 66° parallel north, while there are high variations in light regime throughout the year, there are significantly less fluctuations with respect to diurnal variations (Sakshaug, Johnsen, and Kovacs 2011). The polar night season is the period of the year when the night lasts for more than 24 hours while the midnight sun season is when the sun remains above the horizon for more than 24 hours. This period of long darkness differs with respect to the light regime produced, depending on the geographical position from the North pole (Ludvigsen et al. 2018). It is usually divided into 3 periods according to the position of the sun (Ludvigsen et al. 2018).

Civil polar night: The civil polar night occurs when the sun is between 0° and 6° below the horizon. It is perceived at latitudes above 72°.

Nautical polar night: The nautical polar night occurs when the sun is between 6° and 12° below the horizon. It is experienced at latitudes above 78°.



Figure I-4 Sun Diagram for Longyearbyen, Svalbard, 2018. Produced by Svalbard Samfunns drift AS and Longyearbyen Lokalstyre.

Astronomical polar night: The astronomical polar night occurs when the sun is between 12° and 18° below the horizon. It is limited to latitudes above 84° 33'.

2.1. Irradiance quantity (E)

The sun emits a uniform beam of electromagnetic radiations called the solar constant (Sakshaug, Johnsen, and Kovacs 2011). The Irradiance noted (E) refers to the sum of the incident spectral radiations that reached the Earth's surface (Stine and Geyer 2001). It is a measure of the sum of solar radiations striking a unit surface per unit time and given in μmol of photons per $\text{m}^{-2} \text{s}^{-1}$. At higher latitudes, the typical low sun angle reduces significantly the incoming irradiance from the sun (Stine and Geyer 2001). It is because at higher latitudes the incident solar radiations must travel through a thicker layer of air compared to zenith solar radiations (Sakshaug, Johnsen, and Kovacs 2011). This optical phenomenon is known as the cosine effect (Stine and Geyer 2001; Sakshaug, Johnsen, and Kovacs 2011). Despite the low solar elevation, the typical maximum solar irradiance experienced on a clear arctic summer day can reach up to 2000 μmol per $\text{m}^{-2} \text{s}^{-1}$ at a latitude of 60°N (Sakshaug, Johnsen, and Kovacs 2011).

The polar irradiance constitutes a significant actinic source for all organisms, not to mention the sun illumination period characteristic of the midnight sun season (Mascarenhas et al. 2017; Sakshaug, Johnsen, and Kovacs 2011). Hence, over a 24-h integrated irradiance period, the polar irradiance experienced at latitudes higher than 66° is considerable and potentially as large as the diurnal irradiance experienced at the equator (Sakshaug, Johnsen, and Kovacs 2011). Arctic primary productivity is strongly dependent upon light availability. In the Arctic region, the spatial and temporal variability of the light field plays a central ecological role profoundly affecting all organisms both directly and indirectly (Mascarenhas et al. 2017).

2.2. Spectral composition

The spectral irradiance is the respective intensity for every single wavelength of the incident light spectrum and measured in μmol of photons per $\text{m}^{-2} \text{s}^{-1} \text{nm}^{-1}$ (Sakshaug, Johnsen, and Kovacs 2011). Some of the constitutive wavelengths of this spectrum are attenuated along their paths, as they travel through the Earth's atmosphere or any other given medium (Sakshaug, Johnsen, and Kovacs 2011; Kirk 2011; Mascarenhas et al. 2017). Indeed atoms, particles, clouds, phototrophic organisms and gasses present in the distinct media along the light path (e.g: H₂O, O₂, CO₂, O₃, DOM, POM, CDOM) governs the fate of the light spectral composition (Kirk 2011). On average, about 50% of the total incident solar radiations is estimated to reach the Earth's surface producing the natural light spectrum available for terrestrial photosynthetic organisms (Sakshaug, Johnsen, and Kovacs 2011).

In aquatic medium, the solar light regime is even more attenuated, determined as a function of the medium inherent optical properties (Mascarenhas et al. 2017; Kirk 2011). The fate of the incident spectral irradiance is essentially shaped by absorption and scattering events taking place as the incident light penetrates deeper through the water column (Kirk 2011). Coloured dissolved organic matter (CDOM), total suspended matter (TSM) and phototrophic biomass within the water column constitute altogether the inherent optical

properties of one's aquatic medium (Kirk 2011). These properties are of particular importance for marine photosynthetic organisms as they regulate light availability for marine photochemistry (Kirk 2011; Mascarenhas et al. 2017). The actinic fraction of the solar light spectrum admitted to regulate photosynthesis is referred as the Photosynthetically Active Radiation (PAR) and spans between 400 and 700 nm (Kirk 2011). Yet, recently, several cyanobacteria have been reported to harvest radiations beyond this spectrum down to UV radiations at about 320 nm (Nürnberg et al., n.d.).

3. The Cryosphere

The cryosphere is comprised of the Earth's sea-ice and snow cover, glaciers and ice caps, ice sheets, lake ice and permafrost-dominated grounds altogether (Figure I-5) (SWIPA, 2011). Cryospheric processes have large-scale fundamental implications on global circulation patterns and global atmospheric events (Vesman, Ivanov, and Volkov 2017). Furthermore, they affect locally the ecology, the biodiversity and the physico-chemistry of Arctic coastal and marine ecosystems (Vesman, Ivanov, and Volkov 2017).

While in the sub-Arctic region a rather seasonal sea ice coverage is experienced, across the high-Arctic the sea ice is more or less permanent forming multiyear-old sea ice (Sakshaug, Johnsen, and Kovacs 2011). Arctic ice extent fluctuates on a yearly basis, typically reaching a maximum in February-March and a minimum in September (Sakshaug, Johnsen, and Kovacs 2011). Major large-scale atmospheric phenomenon such as the North Atlantic Oscillation may greatly affect cryospheric processes throughout the Arctic (Sakshaug, Johnsen, and Kovacs 2011). Due to the large contribution of marine ecosystems to the overall

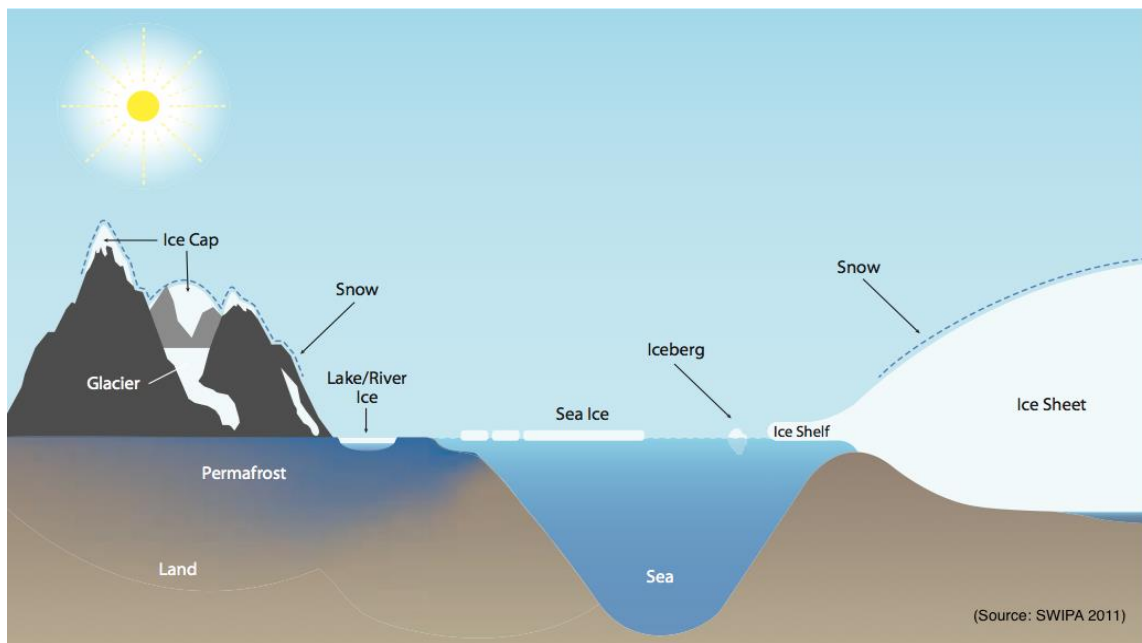


Figure I-5 Descriptive sketch of the different elements constituting the Arctic cryosphere system. Source: SWIPA (AMAP) 2011.

ecosystem production of Svalbard, sea-ice conditions in specific years may deeply affect coastal marine production throughout Svalbard's archipelago (Polyakov et al. 2017).

3.1. Sea-ice

Sea-ice is an exclusive feature of polar ecosystems and displays major structuring and insulating functions (Comiso et al. 2008; Muckenhuber et al. 2016). Sea ice comes in a variety of types. The structure of the sea ice depends mainly on its stage of development as well as the ambient meteorological and atmospheric conditions. Sea ice types include: new ice, young ice, first-year ice and old ice (second year and multiyear sea ice). Old ice is the most robust type of sea ice, established after at least one year surviving over the summer melting season. Other sea ice types are less than a year-old sea ice with respective thickness and morphological features. Fast ice is defined as sea-ice that is attached to the coastline while other sea ice forms are drifting, afloat at the surface of the water. The drifting patterns of afloat sea-ice forms are dependent on arctic oceanic currents (Sakshaug, Johnsen, and Kovacs 2011). Arctic sea ice drift patterns are presumably key biological processes for the distribution of several ice-related species across the Arctic ocean and have a huge impact on marine productivity (Sakshaug, Johnsen, and Kovacs 2011). Typically, bare sea-ice is characterized by a high albedo up to 0.7 (National Snow and Ice Data Center 2016). This key insulating physical property gives rise to the development of characteristic low-temperature across the Arctic and to its specific polar climate (Michon and Hansen 2016). Incidentally, a gradient of temperature spanning from the equator to the Arctic promote global atmospheric & oceanic circulations. Furthermore, Sea-ice has a great structuring role across the Arctic seafloor, shaping the morphology of the littoral (erosion, ice scouring etc...) and producing specific conditions for the development of sea-ice related communities.

As a result of climate change, over the last decade arctic sea ice has shown dramatic signs of retreat (Comiso et al. 2008). Due to the later freeze-up and earlier melting of the ice, the ice season has been markedly shortened over the past years (Meier et al. 2014). A study carried out in 2008 by Drobot et al. registered the extent annual fluctuation of the Arctic sea ice cover. The annual sea ice cover was reported to range from a minimum of approximately 5 million km² to a maximum extent of approximately 14 million km² (Drobot et al. 2008). In September 2012, sea ice extent was reported to set a new lowest minimum extent record (Beitler, J. 2012). The new record loss totalled to 3.41 million km² below the 1981 to 2010 Arctic sea ice minimum average according to the National Snow & Ice Data Centre (Beitler, J. 2012). This decline is magnifying the warming up in the Arctic through the Arctic amplification positive feedback phenomenon. The effect of climate change on the arctic cryosphere is predicted to increment progressively over the next 100 years, promising fundamental ecological, physical, social, and economic changes (Serreze and Francis 2006).

4. Geoscience of Svalbard

At mid-distance between Norway and the North Pole, between the latitudes 74° - 81° N, and longitudes 10° - 35° E, is located Svalbard. Svalbard is an archipelago system with a rich geological history comprising several islands and skerries, of which the main ones are: Spitsbergen, Nordaustlandet, Barentsøya, Edgeøya, Kong Karls Land, Prins Karls Forland, and Bjørnøya (Ingólfsson 2000). The present landscape of Svalbard

originates from a long and complex geological history, going as far back in time as the late Archean era, about 42.5 billion years ago (Dallman et al. 2015).

A disparate assemblage of bedrock types composes Svalbard's heterogenous geology including sedimentary, metamorphic and igneous rock types (Dallman et al. 2015) (Figure I-6). Long-term continental displacements have driven the gradual and heterogenous stratigraphic depositions responsible for Svalbard's present geology. Overtime, Svalbard's unique geological architecture was formed by the accumulation of large deposits deriving from various climate zones (Dallman et al. 2015). Extensive tectonic processes like uplift and subsidence, deposition and erosion, have progressively led to Svalbard's present geographical situation (Dallman et al. 2015; Elvevold, Dallmann, and Blomeier 2007)

Svalbard's chronostratigraphic succession is usually subdivided into three major components: The Basement (Precambrian and lower Palaeozoic), Sedimentary rocks (Devonian to Tertiary), and recent unconsolidated deposits (Quaternary) (Elvevold, Dallmann, and Blomeier 2007). The oldest metamorphic formation is described as "the Basement". This geological stratum spans large patchy areas across the north of the Archipelago encompassing parts of Wijdefjorden, Hinlopenstretet and further east in Nordaustlandet and across Spitsbergen forming a peripheral belt along the west littoral (Dallman et al. 2015). Amongst these three major geological components, recent unconsolidated deposits are mainly responsible for the majority of Svalbard's present geological formations (Dallman et al. 2015; Ingólfsson 2000).



Figure I-6 Geological Map of Svalbard. Color legends: see annex. (QGIS 3.0) (QGIS Development Team 2018)

It is only from the onset of the Cretaceous period that Svalbard locates within the polar circle (Dallman et al. 2015). In the course of the Quaternary, Svalbard's landscapes withstood several major episodes of glaciation (Elvevold, Dallmann, and Blomeier 2007; Dallman et al. 2015). Geological and cryogenic processes responsible for Svalbard's unique geology are profoundly linked to these major glaciation events (Dallman et al. 2015). Svalbard's unique geology was gradually shaped over a relatively long-timescale by the successive episodes of glaciation/deglaciation which produced the diversity of geological features, including: mountains, valleys, cirques, horns, arêtes, glaciated fjords, bays, beach terraces and beach ridges, we observe today (Ingólfsson 2000; Elvevold, Dallmann, and Blomeier 2007; Dallman et al. 2015).

Regarding Svalbard's coastline in particular, long periods of deglaciation have progressively induced the erosion of the littoral. The gradual erosion of coastal areas eventually produced the variety of raised beaches, postglacial marine terraces and fjord-systems (Elvevold, Dallmann, and Blomeier 2007).

5. Svalbard climatic conditions

The climate experienced in Svalbard is referred as polar climate. Polar climate zones occupy the utmost regions on Earth. These regions are typically characterized by very large inter-annual differences in mean precipitation and temperatures and huge seasonal solar intensity variations (Popova et al. 2010; Sakshaug, Johnsen, and Kovacs 2011). As we previously mentioned in the paragraph Arctic light regime and polar day length, a long season of darkness with cold temperatures and strong winds occurs in winter known as polar night, while in spring-summer a short light season with mild temperatures referred to as midnight sun is experienced. In the vicinity of Longyearbyen, in Svalbard, the average annual air temperature is about -6°C at sea level (Sakshaug, Johnsen, and Kovacs 2011). Lower temperatures are experienced at higher latitudes further north toward the high Arctic (Sakshaug, Johnsen, and Kovacs 2011). Throughout the Arctic, the total precipitations are amongst the lowest experienced worldwide with snow as the dominant form of precipitation, making up to half of the total precipitation (Stein et al. 2004).

6. Arctic microphytobenthos

The microphytobenthos represents this complex community of microscopic organisms inhabiting the surface layer of illuminated seafloor in aquatic ecosystems (MacIntyre and Cullen 1996; Miller, Geider, and MacIntyre 1996). Microphytobenthic organisms are major biotic components of aquatic ecosystems. They play a central ecological role in coastal environment, primarily as a major food supply for higher trophic levels, but also by mediating water-sediment nutrient exchanges and by enhancing benthic-pelagic coupling in the water column (Sigmon and Cahoon 1997; Brandini et al. 2001; Facca, Sfriso, and Socal 2002; Glud et al. 2009). Furthermore, the cohesive nature of microscopic benthic communities has the ability to reduce considerably resuspension and erosion of the benthic seafloor (Williams, Yarish, and Gill 1985; Jiménez Reyes 2013). This process is known as biostabilisation and relies on the release of extracellular polymeric substances (EPS or "slime") derived from the photosynthetic activity of benthic microphytes (Blanchard et al. 2000; De Brouwer and Stal 2001; Decho and Gutierrez 2017). In the arctic particularly, benthic microalgae

contribute significantly to the overall coastal productivity and typically exceed arctic pelagic productivity at shallow depths down to 30 m (Nelson et al. 1999).

6.1. Arctic microphytobenthos growth

Across the Arctic littoral, the biomass of coastal benthic communities exhibits huge spatial and annual variations (Sakshaug, Johnsen, and Kovacs 2011). One of the prevailing factors governing the occurrence and growth of the microphytobenthos is light availability. Other ecological factors add up for the regulation of the microphytobenthos across the Arctic seafloor. Arctic benthic microphytes are tightly dependent from regional oceanographic processes, atmospheric processes, seasonal nutrient admixtures, annual sea-ice distribution and sea-ice drift patterns (Rudels, Larsson, and Sehlstedt 2016; Slagstad, Wassmann, and Ellingsen, 2015). The texture, topography and organic content of the surface layer of the seafloor may also regulates the distribution of benthic microorganisms. This surface layer is extremely variable, affected periodically by strong physicochemical gradients due to the movement of tidal waters (Zacher et al. 2009). Arctic benthic microalgae typically display striking metabolic adaptations and resilient abilities allowing them to cope up with the extreme ecological variations occurring at the sediment-water interface of intertidal ecosystems (Zacher et al. 2009). Most benthic microalgae show indeed adaptive diurnal and tidal cycles adjusted with changing light conditions, tide cycles, desiccation, predation and resuspension (Paterson et al. 2011; Pushkareva et al. 2017). Arctic seasonal microphytobenthic variations in biomass typically exhibit a maximum during the spring and summer blooms and periods of low production (oligotrophy) in winter (Dalpadado et al. 2014). These maxima are believed to be triggered by enriched coastal nutrient concentration, increasing temperature and increasing day length coincident with coastal pelagic spring blooms. Consecutively, increased grazing pressure slows down microphytobenthic growth considerably. Toward the end of the summer season most microphytobenthic communities undergo changes in composition, coincident with variations in nutrient supplies potentially with the decrease in silicon concentration (Barranguet 1997).

6.2. Arctic microphytobenthic primary production

In the Arctic little is known on the productivity of coastal microphytobenthic communities mainly due to the logistic and technical limitations imposed by polar climatic constraints. Furthermore, in benthic tidal habitats productivity measurements may be erroneous and often are difficult to achieve due to large coastal disturbances (sea ice drifting, wind forcing, erosion, desiccation etc...). The major factors affecting the productivity of the microphytobenthos are light availability and local hydro-chemical parameters (salinity, temperature, nutrients, DIN/DIP ratio, etc...) (Longphuir, Sorcha Ni Leynaert et al. 2007; Longphuir et al. 2009; Vetrov and Romankevich 2004). The very first measurements of marine primary production in the Barents Sea date back to the end of the 1950s and focus mainly on the production of pelagic phytoplankton (Corlett 1953). More recent estimates were achieved by Dalpadado et al. in 2014, who estimated a mean annual net primary production for the Barents Sea of $59.0 \text{ Tg C year}^{-1}$ (Dalpadado et al. 2014). They monitored the evolution of the marine primary productivity over 13 years from 1998 until 2011 in distinct areas of the Arctic Ocean. Overall, they concluded that the marine net primary production intrinsic to the Barents Sea

region is significantly increasing in recent years, from 41.6 Tg C in 1999 to 80.9 Tg C in 2011 (Dalpadado et al. 2014). Moreover, the mean annual net primary production of the Barents Sea was determined to derive from the combinatorial contributions of the Atlantic (53%) coastal (37%) and arctic regions (10%) altogether (Dalpadado et al. 2014). However, over the whole studied period the specific mean annual net primary production of coastal regions comes out on top (Dalpadado et al. 2014). It suggests the significance of the coastal primary production around Svalbard's littoral as one of the highest across the Arctic Ocean and arctic coastal regions (Frey et al. 2017; Vetrov and Romankevich 2004). Arctic benthic microalgae contribute significantly to this coastal productivity (Nelson et al. 1999; Glud et al. 2009; Vetrov and Romankevich 2004). Even sometimes, when light availability is sufficient and nutrients are locally abundant, benthic primary production may even dominate the net coastal primary production at shallow depths (Gazeau et al. 2004).

6.3. Arctic microphytobenthic biodiversity

The arctic microphytobenthos represents a unique and complex community of microscopic organisms. These organisms selectively occupy the sediment surface of aquatic ecosystems where they are found on all types of substrates: rocks, logs, sand, soft sediments but also as epiphytes developing on macroalgae and aquatic plants (Ask, Rowe, and Brugel 2016). Various taxonomic groups develop across arctic microphytobenthic habitats and some of them distinctly predominate depending on the nature of the physical habitat and the local ecological parameters. Bacillariophyceae generally dominate microphytobenthic habitats but in certain conditions where microphytobenthic algal biofilms occur a few other groups can outcompete this previous class, notably: Cyanobacteria, Chlorophyceae, Haptophyceae and/or Dinophyceae (Nozaki, Misumi, and Kuroiwa 2003).

Microphytobenthic communities often develop as extensive microbial biofilms on top of the sediment. These benthic microbial biofilms generally exhibit a characteristically flat unstructured two-dimensional arrangement (D. C. Miller, Geider, and MacIntyre 1996). Given the large number and dynamic set of environmental variables operating at the arctic coastal interface, there are large inter-annual and spatial variations in the composition of coastal arctic communities, including microphytobenthic communities (Sakshaug, Johnsen, and Kovacs 2011). The composition of microbenthic communities is all the more dynamic as there is a very tight and complex relationship with the pelagic zone. Indeed, there is a very subtle line between pelagic and benthic communities since transfers are known to take place across the water column, notably due to resuspension and sedimentation processes (de Jonge 1995; Aberle-Malzahn 2004). The composition, distribution and abundance of coastal benthic biota is strongly dependant on the local environmental, physicochemical conditions (Water temperature, hydrochemistry, salinity, nutrients supply, hydrodynamic, substrate type etc...) and inter-species biological interactions (Stein et al. 2004). While some species show a strong affinity for hard substrata, others prefer soft sediment substrates such as in mudflat habitats. For instance, the brown alga *Chordaria* sp., the green alga *Ulotrix* sp. and the pennate diatoms *Navicula* sp. found across the littoral of Svalbard, have been reported to typically grow on sheltered beaches

with hard substrates (Sakshaug, Johnsen, and Kovacs 2011). *Vaucheria* sp. studied herein on the contrary, showed a strong affinity for soft sediments such as mud.

Despite large coastal disturbance (ice scouring, sea ice...) occurring along the Arctic littoral some algae have developed strategies to adapt. In the Arctic, coastal algae typically exhibit fast seasonal growing strategies, making them able to colonise coastal denuded substratum in less than 15 days (Sakshaug, Johnsen, and Kovacs 2011). Other species tend to grow heterotrophically in winter surviving on nutrient stocks accumulated over previous favourable growing seasons (e.g. *Acrosiphonia* sp. and *Spongomorpha* sp) (Sakshaug, Johnsen, and Kovacs 2011). To our knowledge, there has been to this date little study on the seasonal dynamics of arctic microphytobenthic communities. This scarce knowledge is greatly hindering our understanding of arctic coastal ecosystems and must be mended.

7. *Vaucheria* sp. – yellow-green alga

Vaucheria sp. is a xanthophycean algae, of the family Vaucheriaceae. The genus *Vaucheria* was first described in the book “Histoire des conferves d’eau douce”, by the botanist J-P Vaucher in 1803. This genus comprises to this date, about 70 species disseminated ubiquitously across all continents including Antarctica (Johnson et al. 2012; Guiry 2008). The most common species are the terrestrial species *V. sissilis* and the freshwater species *V. geminata* (Guiry 2008). Most species are terrestrial and/or limnic with only a few marine and estuarine representatives, so far reported and described (Wilcox 2012; Johnson et al. 2012).

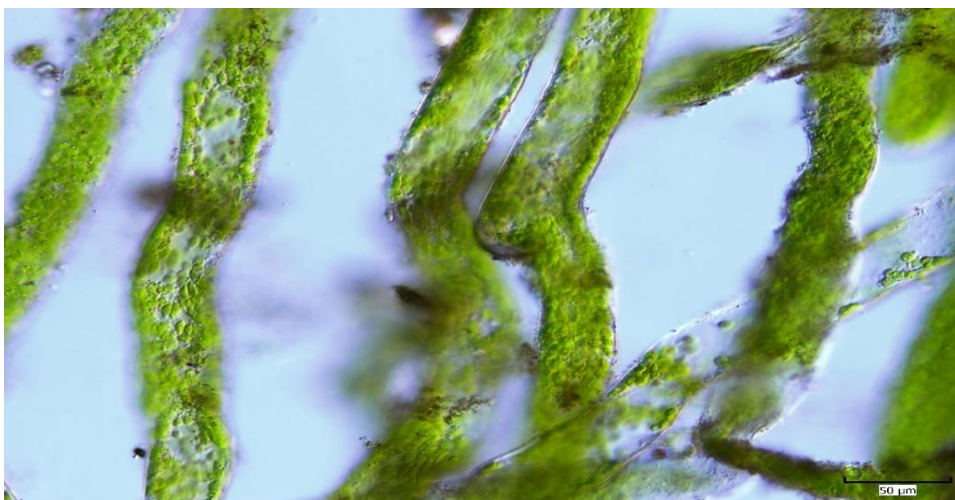


Figure I-7 Microscopic picture of *Vaucheria* sp. filaments collected in the tidal flat adjoining Longyearbyen, Svalbard, 2017.

7.1 Morphology

These algae may develop with different morphologies depending on the environmental parameters and the species' order such as motile unicells, coccoid, filamentous or motile colonial forms (Reddy 2001; Ott and Brown 1974). However, the most common form is filamentous, forming long cylindrical or siphonous yellow-green filaments (Elvebakk et al. 1996; Wilcox 2012; Johnson et al. 2012) (Figure I-7). The thallus of these algae is characterized by monopodial multinucleate tubular filaments and apical growth (Reddy 2001; Ott and Brown 1974). The algae are generally fixed to the substratum via a rhizoplast (rhizome) or holdfast (Reddy

2001). Each filament is covered by a rigid thin cell wall made up of 2 layers (Ott and Brown 1974; Lee 2008). The outer layer of the cell wall is made up of pectose while the inner layer is made up of a combination of cellulose and pectin (Lee 2008; Ott and Brown 1974). The cytoplasm contains multiple peripheral discoid chloroplasts without pyrenoids and a large central vacuole surrounded by numerous nuclei (Coenocyte) (Reddy 2001; Lee 2008; Ott and Brown 1974). The vacuole is continuous throughout the length of the filament with very little cross-walls or septa formation (Reddy 2001; Ott and Brown 1974). Food supplies are stored as oil droplets in the cytoplasm (Ott and Brown 1974).

7.2. Reproduction and reproductive features

Reproduction in *Vaucheria* sp. comes in many ways: by vegetative fragmentation of the filaments, by asexual multi-flagellate motile zoospores, or by oogamous sexual reproduction (Reddy 2001; Lee 2008). Typically, the respective female and male reproductive organs are produced on nearby branches. The female reproductive organ, called oogonium, is spherical while the male reproductive organ (antheridium) is hook-like in shape (The Editors of Encyclopaedia Britannica 2018; Reddy 2001). After fertilization of the egg, the zygote completes a resting phase before developing into a new alga. Out of these three, vegetative fragmentation is typically the most common mode of reproduction in *Vaucheria* sp. (Chapman, 1962). During this process, filaments break accidentally into small fragments each of which grows into a new functional plant (Reddy 2001; Lee 2008).

7.3. Distribution and habitat

The algae are widespread in almost any wetland habitat such as mudflats, salt marshes, estuaries, wet farmlands, mangroves, streams, channels, lakes and pond fringes (Baker et al. 2012; The Editors of Encyclopaedia Britannica 2018) (Figure I-8). *Vaucheria* sp. typically manifests a remarkable physiological



Figure I-8 Picture of a dense biofilm of *Vaucheria* sp. microbenthic algae covering the seabed in Adventdalen-Adventfjorden tidal flat. Svalbard, 2017. Credit photo to Dr. Elster.

resilience to desiccation (The Editors of Encyclopaedia Britannica 2018). The Algae may be submergent, amphibious, semi-emergent, or terrestrial and was reported to colonize habitats from the sublittoral to the intertidal zone and beyond in terrestrial habitats (Wilcox 2012; Baker and et al. 2012). Estuarine and Marine representatives of *Vaucheria* sp. have been discovered and described in various manuscripts across Europe (Christensen 1987; Kersen 2012) as well as across North America (Schneider et al. 2014). However the occurrence of Marine *Vaucheria* sp. does not seem to appear in the literature on Svalbard's coastal ecology (Elvebakk et al. 1996).

8. Objectives

The objective of this master thesis was primarily to characterise the abiotic environment intrinsic to this tidal flat and in which *Vaucheria* sp. occurs. We attempted to capture the environmental settings of *Vaucheria* sp. habitats at two different scales, by sites and to a larger extent by transects spanning across the tidal flat. This allowed us to accurately define the habitats of *Vaucheria* sp. with respect to local general abiotic parameters (salinity, temperature, sediment texture) as well as physico-chemical parameters from both the sediment and the water column. Incidentally, we could establish the abiotic profile of this arctic estuarine ecosystem, describing the temporal evolution of the local physico- and biogeochemical parameters characteristic of late summer arctic conditions (August 2017). Secondly, we attempted to measure the photosynthetic activity of this newly-discovered arctic marine *Vaucheria* sp. using a combination of gasometric and chlorophyll a fluorescence measurements.

The questions we attempted to answer were the following ones:

What are the characteristic abiotic parameters of this arctic tidal flat?

Which parameters defines *Vaucheria* sp. habitat? and how does *Vaucheria* sp. locally distribute?

Is *Vaucheria* sp. adapted to arctic late summer conditions?

What are the photosynthetic characteristics of *Vaucheria* sp.? Are these adapted to these specific arctic conditions?

We proposed to address this problem in this order:

- First, we characterised the physicochemical parameters inherent to this arctic estuarine ecosystem, in which *Vaucheria* sp. inhabits.

- Secondly, we described the photosynthetic performances of the benthic *Vaucheria* sp. community.

Chapter 2 – Ecology and photosynthetic activity of a newly-discovered *Vaucheria* sp. dominated arctic microphytobenthos, Svalbard.

Material & Methods

Study area description

The Field sampling was performed in one locality on the western coast of Svalbard during august 2017. The total surface of Svalbard is about 61 020 km² with a coastline extending across 8 782 km (Lantuit et al. 2012). Across the full stretch of its territory, up to 60% of Svalbard is markedly influenced by snow and ice cover, affecting mainly northern and easternmost territories for eight to nine months year-round (Sakshaug, Johnsen, and Kovacs 2011). These territories feature the most extreme climatic conditions, hosting untouched wilderness over large protected areas. However, milder climatic conditions are experienced on the west coast of Svalbard due to the impact of warm atlantic currents mixing with arctic water masses and subsequently flowing along the west littoral.

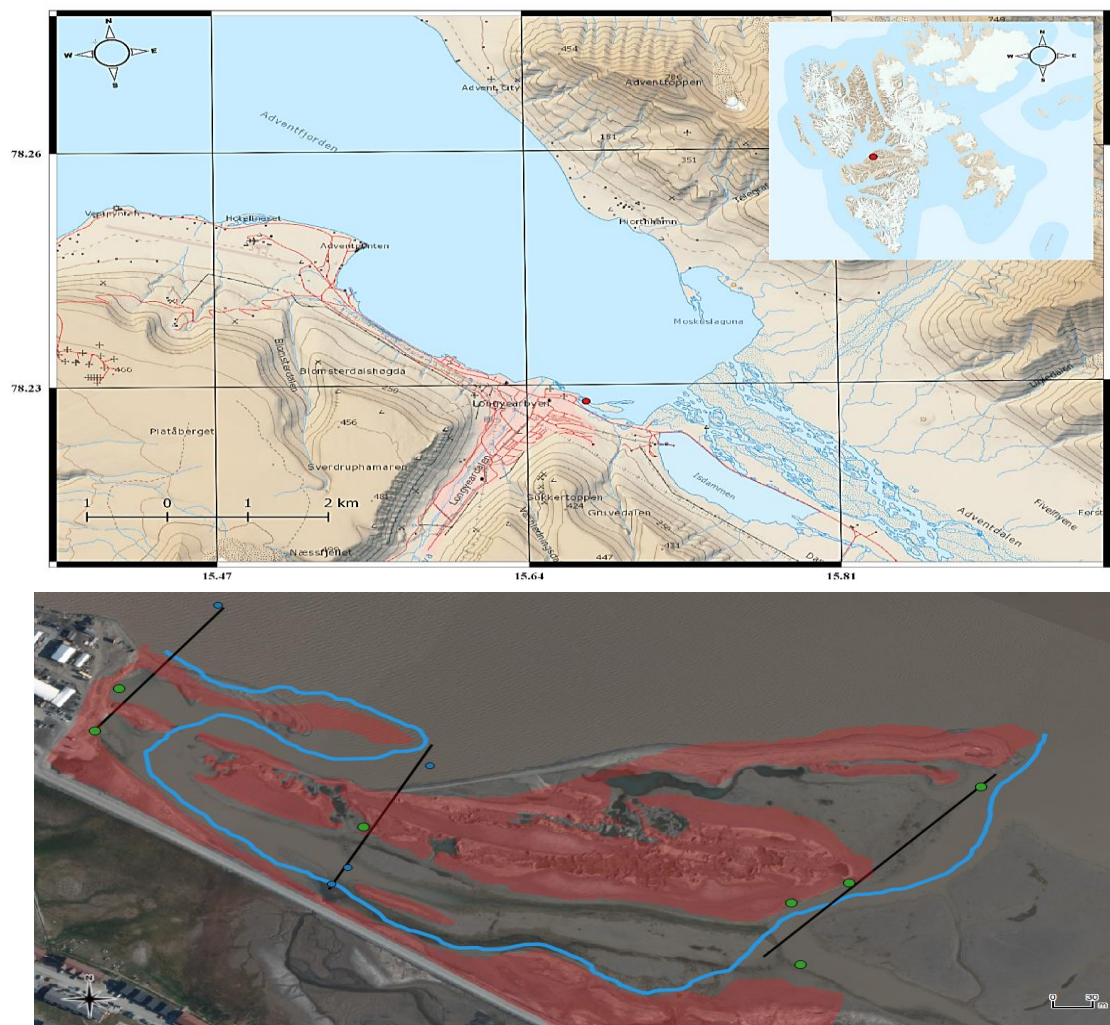


Figure II-1 Geographic location of the studied tidal flat, red dot = studied location (Upper map). Detailed map of the sampling area with transects I, II and III (Lower map). Sampling sites along the transect are numbered from one to four from bottom to top starting from TI.1. The red zone delimits the high tide front and in blue the low tide channel. Sampling sites in green refer to the presence of *Vaucheria* sp. (QGIS 3.0 + Google Earth pro) (QGIS

We observed across this tidal flat the presence of a newly-discovered *Vaucheria* sp. dominated microphytobenthos. The studied microphytobenthos occupied a tidal flat at the head of Adventfjorden within the larger fjord of Isfjorden, in central Spitsbergen. The field survey was performed over the month of August 2017, starting from the 9.8.17 and finishing on the 31.8.17. Around Svalbard, the annual sea-ice conditions are assumed to strongly influence marine coastal production, to a higher extent in particular years (Polyakov et al. 2017). The sea ice period in Isfjorden, generally starts between the end of November or mid-December and terminates between April - July (Muckenhuber et al. 2016). Over the past recent years ice-free conditions throughout winter in Isfjorden have become more and more frequent, with seasonal fast sea-ice occurring exceptionally (Muckenhuber et al. 2016). According to the Norwegian Meteorological Institute, Isfjorden has remained mostly ice-free since 2005. Throughout the duration of the field sampling, we did not report any influence of the sea ice on the studied microphytobenthos.

Sampling

The field sampling was achieved using several protocols expressed in HIMOM book of Protocols (Van Leeuwe, Morgan, and Brockmann 2005). The methods used for sampling were carefully carried out in respect with the requirements expressed in this manual. A total of three transects were defined across the tidal flat. A total of 11 sites were assayed along these transects and are illustrated on the map (Figure II-1) (QGIS Development Team 2018). The location of the transects and samples were specifically designed in the intention to embrace the scope of coastal influences acting on this tidal flat ecosystem. A comprehensive inventory of the physico-chemical parameters pertaining to this ecosystem was established. Nutrient supplies from the sediment and the overlying water were respectively and methodically quantified. Major cations, anions, nitrogen-based compounds, silica and phosphorus-based compounds were determined. The sediment was further analysed for organic carbon, and granulometry.

Data collection and analysis

Physical measurements

The temperature, pH and salinity profiles of the water column were determined using a low range pH/conductivity/TDS tester in combination with a refractometer for salinity measurements. Variations in the major four sea water ions mainly chloride, sulphate, sodium and magnesium accounted for the detected salinity by using the refractometer. Based on the TDS tester measurements, we calculated the consecutive sea water density (σ_t). The ambient climatic conditions for the month of August 2017 including: PAR [$\mu\text{mol}\cdot\text{m}^{-2}\text{s}^{-1}$] and air temperatures were recorded using QT_i datalogger (EMS Brno, Czech Republic). Furthermore, *in situ* air and seawater temperature were monitored in the close vicinity of *Vaucheria* sp. communities, respectively when unsubmerged during low tide or when submerged during high tide using Tie datalogger (EMS Brno, Czech Republic). The climatic data were taken from site TI.1 and were used to draw the overall climatic profile of the whole studied tidal flat ecosystem. Furthermore, the inter-tidal variations within the tidal flat were monitored and registered by time-lapse photography using two cameras (LTL-5310A, Acorn, China) and a graduated pole, throughout the duration of the field sampling.

Soil texture and granulometry

Laser diffraction methods were applied hereafter to determine the particle size distribution of the marine sediment occurring across Adventfjorden-Advendalen's tidal flat. An ANALYSETTE 22 MicroTec Plus laser device (FRITSCH company, Germany) was used for the following measurements. Laser diffraction methods rely on the specific scattering properties of a laser beam upon contact with a particle. Based on the physical characteristics of the suspension particle (size & optical properties), the resulting diffraction angles of the scattered laser beam differ characteristically from one particle to another. Hence, the specific properties of the scattered laser beam detected by the measuring unit provide reliable and solid information on the size distribution of the particles in suspension (Hrncirova, Pospil, and Spilacek 2013).

Prior to analysis, the samples were grinded and sieved through a 0.2 cm mesh size sieve to remove all particles bigger than 0.2 cm. The resulting fraction of the sample was then treated with a 30% hydrogen peroxide solution (H₂O₂). Each fraction was treated respectively with enough hydrogen peroxide to make sure that all organic material was oxidized. Hydrogen peroxide also aids to prevent particles' flocculation when in suspension. Subsequently, the resulting suspensions were sedimented and left aside until complete water evaporation. The processed samples were then introduced into ANALYSETTE 22 MicroTec Plus measuring unit and scanned by the laser beams for particle size analysis.

Each processed sample was measured 5 times at least. For the optimum evaluation of the particle size distribution, a Fraunhofer model approximation was used. The measurements were divided into 22 particle size categories and consequently counted as percentage proportion of clay (<2 µm), silt (2-50µm) and sand (50-2000µm) contained within the sediment of this studied Tidal flat.

Chemical measurements (Nutrients)

The concentrations of major cations, major anions, nitrogen-based compounds, silica and phosphorus-based compounds were determined, concurrently with general physical parameters from the respective surveyed sites along the three selected transects. Water samples were collected three times across the surveyed area for each site. Sediment samples were collected three times at low tides, the same days water samples were collected, respectively on the 08/09, 23/09 and 25/09/2017.

Chemical measurements, with respect to sampling collection and storage were carried out with extreme care, to the maximum extent of our technical and logistic capabilities. Acid washed plastic containers were not available instead new sterile plastic bottles were used to prevent samples' contamination. Blank samples were performed using distilled waters to ensure low residual contamination from the storing equipment. Differential storing methods were adopted depending on the chemical compounds analysed, in compliance with the recommendations expressed in HIMOM book of Protocols (Van Leeuwe, Morgan, and Brockmann 2005). When processing the respective data sets for multivariate analysis, we had to overcome one issue when at least one of the measurements was missing in the constituting data set. In such occurrence we chose to replace the missing value by the specific average of the data set to make the statistical visualization possible.

We acknowledge that it may have affected the distribution of the sites together with the average transect distribution in the visualization of the multivariate principal component analysis.

Water samples were taken by hand using pre-rinsed plastic bottles. Upon return to the station, within 24 hours maximum, water samples were filtered through a 0.45 µm filter membrane. All filter units and sample bottles were rinsed one to three times with filtrated water from the surveyed site. As for sediment samples, a mixture of 5 distinct surface sediment samples disseminated near each site was homogenized within Ziplock plastic bags. Upon return to the station, the samples were respectively processed: extracted, filtered or burnt and weighted for sediment moisture content, within the next 24 hours maximum. Consecutively, all samples were methodically stored with respect to their storage requirements.

- Silicate and other elements: 0-4 °C protected from light, no freezing as polymerization may occur.
- Total nitrogen/Total phosphorous - Freezing or 0–4 °C and protected from light.

The respective stored samples were then analysed within 4 months, in the laboratory in Ceske Budejovice, Czech Republic. The analytical methods adopted hereafter are described in the Methods Manual edited from Lachat Instrument (2004).

Hydrochemical and soil chemical sampling

The intrinsic hydrochemical parameters of this tidal flat were evaluated throughout the study period. A table was drawn from these results listing the following elements and compounds: Ammonium ($\text{NH}_4^+\text{-N}$), Sulfur (S), Calcium (Ca^{2+}), Chloride (Cl^-), Iron (Fe), Magnesium (Mg^{2+}), Manganese (Mn^{2+}), Nitrate ($\text{NO}_3\text{-N}$), Nitrite ($\text{NO}_2\text{-N}$), Orthophosphate ($\text{PO}_4\text{-P}$), Potassium (K^+), Silicic acid ($\text{Si}(\text{OH})_4$), Sodium (Na^{2+}), Total dissolved Phosphorus (TP), Total dissolved Nitrogen (TN) (Table II-4).

Orthophosphate ($\text{PO}_4\text{-P}$) and dissolved Total Phosphorus (TP). The filtered water samples were examined for dissolved Orthophosphate as phosphorus ($\text{PO}_4\text{-P}$) and total dissolved phosphorus also referred as organic phosphate (TP). Orthophosphate is a highly reactive compound, also known as “phosphate” or “reactive phosphorus” while total phosphorus (TP) are any phosphates forming part of a larger organic compound. Contrary to $\text{PO}_4\text{-P}$, organic phosphates (TP) are not directly measurable and require an additional procedure which consists in the digestion of their composite forms into the constitutive $\text{PO}_4\text{-P}$. The following chemical analysis used QuikChem 8000 Automated Ion Analyzer. Sub samples of 10 ml from the collected samples were run through the Analyzer methodically.

Water samples

- The concentration of dissolved $\text{PO}_4\text{-P}$ was calculated using ascorbic acid by flow injection analysis. The methodology adopted for this analysis was implemented according to QuikChem® method 10-115-01-1-A. The detection threshold for $\text{PO}_4\text{-P}$ was 0.01 mg P/L.

- The total dissolved Phosphorus (TP) was measured by flow injection colorimetric analysis combined with a persulfate digestion. The analytical procedure conformed to QuikChem® method 10-115-01-1-F as documented in the Methods Manual from Lachat Instrument (2004). The detection limit for TP was 0.9 µg P/L.

Sediment extract samples

- The relative bioavailability of inorganic ortho-phosphate (PO₄-P) in the sediment of the tidal flat was also measured. For this analysis, sediment subsamples of 10 g were weighted and extracted. The extraction of ortho-phosphate was performed based on an alkaline extraction method using 0.5 N sodium bicarbonate solution. The soil extracts were then filtered and examined for PO₄-P using QuikChem 8000 Automated Ion Analyzer. The analytical procedures for PO₄-P complied to the instructions formulated by QuikChem® Method 12-115-01-1-B. The method had a detection limit of 1.0 mg/kg.

Nitrogen-based compounds. Ammonium (NH₄⁺), Nitrate (NO₃⁻) and Nitrite (NO₂⁻) are nitrogen-based compounds which occur naturally in the water and sediment. Nitrogen naturally enters estuarine ecosystems carried along by freshwater runoff. Likewise decomposing organic matter and wildlife waste constitute significant nitrate sources for estuarine ecosystems. The quantitative analysis of ammonium (NH₄-N), nitrate (NO₃-N) and nitrite (NO₂-N) from filtered water samples and from soil extract samples were performed as followed. The following chemical analysis used QuikChem 8000 Automated Ion Analyzer. Sub samples of 10 ml and 10g were used for the respective hydrochemical analysis and soil chemical analysis.

Water samples

- Dissolved Nitrate (NO₃-N) and Nitrite (NO₂-N) were measured from the water surface by flow injection analysis, according to QuikChem® method 12-107-04-1-A. The detection limit in the water for nitrate and nitrite was 0.01 mg N/L.
- NH₄-N was determined from the water samples by flow injection analysis according to QuikChem® method 10-107-06-1-J. The detection threshold of this method was 0.01 mg N/L.
- Total dissolved Nitrogen (TN) from the water surface was measured by flow injection analysis combined with an alkaline persulfate/UV in-line digestion. The analytical procedure adopted here, followed the protocol formulated in QuikChem® method 10-107-04-3-C. All dissolved nitrogen compounds in the water samples were oxidized to nitrate before to be subsequently reduced to nitrite. Finally, both ambient and resulting nitrite were quantified accounting for the sample's TN. The method detection threshold for this test was 0.011 mg N/L.

Sediment extract samples

The relative bioavailability of soluble NO₃-N and NH₄-N across the studied seafloor was quantified. Sediment subsamples of 10 g were weighted and extracted for the following procedures. The extraction method used 50 ml of a solution of potassium chloride (2 M KCl). The soil extracts were filtered and analysed for soluble NO₃-N and NH₄-N using QuikChem 8000 Automated Ion Analyzer. The analytical protocol used

for these chemicals followed the instructions formulated by QuikChem® Method 12-107-04-1-B (Lachat Instruments, 1992) for NO₃-N and QuikChem® Method 12-107-06-2-A (Lachat Instruments, 1993) for NH₄-N.

Dissolved Silica. Dissolved Silica (Si) from the water surface were measured using Agilent 8800 triple-quadrupole spectrometer combined with an auto-sampler (Agilent Technologies, Japan). Prior to the chemical measurements a first step was implemented designed to analyse the concentration of macro cations (Cl⁻). Consecutively Si concentration was measured in diluted samples of the same salinity for the same nebulization and ionization effect. Sample nebulization was performed using a MicroMist device equipped with a tempered cell. Furthermore, to minimize the interference from analytes with multiatomic adduct, we used a collision cell (He collision gas) operating in a high-energy mode with double quadrupole filtration. The detection limit for this test was 25 ug/L.

Major cations

K⁺, Ca²⁺, and Mn²⁺. The analysis of certain cations from the water surface including: K⁺, Ca²⁺, and Mn²⁺, was performed following the same protocol and equipment we used for the analysis of dissolved Si. Sample nebulization was applied automatically using the MicroMist device mounted with a tempered cell. The test was performed in high-energy mode with double quadrupole filtration. The instrument detection limit for this analysis set respectively to 10 ug/l for K⁺ & Ca²⁺ and 0,1 ug/l for Mn²⁺.

Na⁺ and Mg²⁺. The cations Na⁺ and Mg²⁺ were measured using a similar protocol and equipment as we used above except that the test was performed in standard non-collision/reaction mode. The instrument limit of detection was around 20 ug/l for Na⁺ and 0,2 ug/l for Mg²⁺.

Fe²⁺. Fe²⁺ analysis from the water surface was performed in a high-energy mode with double quadrupole filtration following the same protocol and equipment we used for Dissolved Si. The instrument limit of detection for Fe was around 0,1 ug/l.

Major anion

S. For the trace element analysis of S in the surface water, the measurements involved a similar protocol as for dissolved Si. However, for these two elements we used a collision cell operating in a reaction oxygen mode with double filtration for interference masses' elimination. On first quadrupole was filtered 32+ - S. Subsequently the second quadrupole was set on mass shift +16. The instrument limit of detection for this element was 5 ug/L for S.

Photosynthetic measurements:

Small biological samples of the microphytobenthic biofilm dominated by *Vaucheria* sp. were collected and brought back to the laboratory in the attempt to best reproduce their natural conditions for consistent monitoring of their photosynthetic activity. The samples were washed using filtered water from the tidal flat

to remove sediment particles. The chambers containing the samples were partly submerged in filtered water collected from the tidal flat and were exposed to natural conditions. The water medium in the culture was changed on a regular basis throughout their preservation as well as during the measurements. Three replicates were used for the following measurements. To check the physiological state of the mat in exposition chambers during prolonged cultivation, effective quantum yield was recorded by two Monitoring Pen MP-100 fluorimeters with blue and red excitation lights (Photon Systems Instruments, Czech Republic) from August 20 to August 31, 2017. The ETR was calculated according to Eq. 3.

The rates of photosynthesis (P) and dark respiration (R_d) were measured using gasometric and variable chlorophyll a fluorescence methods. Gas Fluorescence System GFS-3000 (Walz, Germany) was used herein to monitor the physiological activity of the benthic samples collected from this Tidal flat. To mitigate the stress experienced by the samples from consecutive manipulations, the samples were pre-acclimatized for 15 min to the experimental conditions inside the measuring chamber. Before introduction of the samples inside the measuring chamber, the samples were dried using paper towels and weighted. The temperature within the chamber was kept constant throughout the measurements around 6°C. The P and R_d were measured in light adapted samples at 20, 60, 160, 265 and 650 $\mu\text{mol m}^{-2} \text{s}^{-1}$. The data for photosynthesis-irradiance (PE) curves were measured in the dark and at 10, 20, 50, 100, 300 and 500 $\mu\text{mol m}^{-2} \text{s}^{-1}$ in samples pre-acclimatized to low (LL, 10 $\mu\text{mol m}^{-2} \text{s}^{-1}$), medium (ML, 230 $\mu\text{mol m}^{-2} \text{s}^{-1}$) and high (HL, 650 $\mu\text{mol m}^{-2} \text{s}^{-1}$) light conditions. The data were normalized per gram of fresh weight.

The parameters of the PE curve, maximum photosynthesis rate (P_{max}), initial slope (α) and dark respiration (R_d) were estimated by fitting the data.

$$P = P_{max} \tanh \frac{\alpha I}{P_{max}} + R_d \quad (\text{Eq. 1, (Henley 1993)})$$

Where I is the irradiance. The compensation irradiance (I_{comp}) was calculated as follow

$$I_{comp} = \frac{-R_d}{\alpha} \quad (\text{Eq. 2})$$

Contrary to *in situ* measurements, electron transport rate (rETR) was calculated by the GSF-Win software (Walz, Germany).

$$ETR = 0.5 I ETR_{factor} \Phi_{PSII} \quad (\text{Eq. 3; (Genty, Briantais, and Baker 1989)})$$

Where I is the incident irradiance, ETR_{factor} is the ratio of absorbed photons (here 0.84) and Φ_{PSII} is the effective quantum yield.

Statistical analysis

The Statistical analyses were mainly performed in “Rstudio” (version 3.4.4) (RStudio Team 2016). The chemical data were converted into molar ratios for measurements ease and for comparative statistical testing outputs. Data were tested for normal distribution of residuals and homogeneity of variance. Upon

occurrence of very skewed data sets we consecutively apply a log-transformation on the data. Outliers or missing values were substituted by the overall mean data set value in some cases when required for the execution and visualization of the statistical analysis. In fact, when performing the PCA in R studio we had to overcome one issue regarding the absence of data within some datasets, due to the technical limit of detection of the instruments used. To overcome this difficulty, we decided to methodically input the average data set's value every time we were missing a data for the making of the PCA. We acknowledge that it might have affected our overall results especially when looking at the site-specific geochemical distribution over the tidal area and to a lesser extent in the consistent transect-specific evaluation. Statistical differences between transects (spatial heterogeneity) and overtime (temporal heterogeneity) were determined via ANOVA and Tukey-Kramer ($p < 0.05$) or Kruskal-Wallis and Wilcoxon rank sum tests when needed. To determine the potential relative contribution of different processes affecting nutrient concentrations, salinity, as well to give a broad abiotic background of this ecosystems, a comprehensive set of PCAs were produced in Rstudio using FactoMineR and factoextra packages. The descriptive statistics was done mostly in Rstudio except for the photosynthetic statistical results where Statistica 13.0 software was used (Dell 2012). Total of three testing and seven experimental measurements were performed. The photosynthesis and dark respiration expressed as CO₂ assimilation and ETR were measured at 5 different PAR levels ranging from 20 to 650 $\mu\text{mol m}^{-2} \text{s}^{-1}$, covering thus irradiance range encountered in the field. The differences were statistically significant for $p < 0.05$.

Results

Physical environment & Topography

Over the explored seabed, the sediment structure was reported to be predominantly composed of mud. This typical sediment composition suggested the weak impact of hydrodynamic forcing on the local ecosystem and the accumulation of huge supply of fine sediment. Clay particles (from 1 μm to 3.9 μm) were found to make up around 22% of the sediment structure of this local seabed, while silt particles (from 3.9 μm to 62.5 μm) made up around 71% and sand particles (from 62.5 μm to 2mm) around 6%. Based on the soil texture triangle and the USDA, the seafloor sediment of the studied tidal flat belongs to a silt loam type (Figure II-3). The detailed mapping of the topography of the tidal flat seabed can be visualized on the drone picture that was taken during the field sampling (see annex II). The picture shows a complex system of temporary tidal channels protected from the impact of waves by barrier beaches. The seabed was locally covered by extensive biofilms of microphytobenthic *Vaucheria* sp. algae. Tidal waters were reported to reside on average 4h per tidal cycles with a maximum amplitude registered at 70 cm locally at site TI.1. Major channels remained permanently wet even during low tide while minor channels serving as tributaries and distributaries dried out periodically.

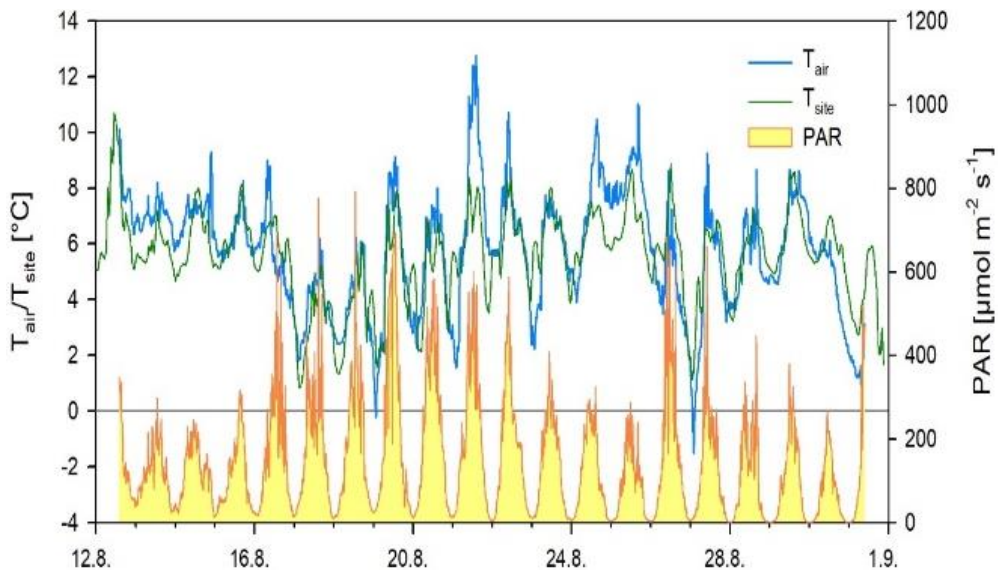


Figure II-2 Evolution of the light environment throughout the sampling period starting from August 12, 2017, 14:00 UTC, to August 31, 2017, 8:00 UTC.

The average air temperature throughout the duration of the field sampling set around 5.7°C (Figure II-2). While the air temperature dropped below freezing point on two occasions, the site temperature of the benthic community (TI.1) stayed above 0°C all through ($T_{DL1} - 0.7^{\circ}\text{C}$ $T_{DL2} - 0.8^{\circ}\text{C}$) (Table II-1). The minimum irradiance (PAR) registered during *in situ* measurements, reached 8 $\mu\text{mol m}^{-2} \text{s}^{-1}$ (25.08.2017) whereas the maximum irradiance set at 815 $\mu\text{mol m}^{-2} \text{s}^{-1}$ (19.08.2017) (Figure II-2). Across the seabed, extensive mats of *Vaucheria* sp. occurred in discrete localities (Figure II-1). They appeared to be more spread-out along transect III while they rather exhibited a patchy, less dense distribution across transects I & II.

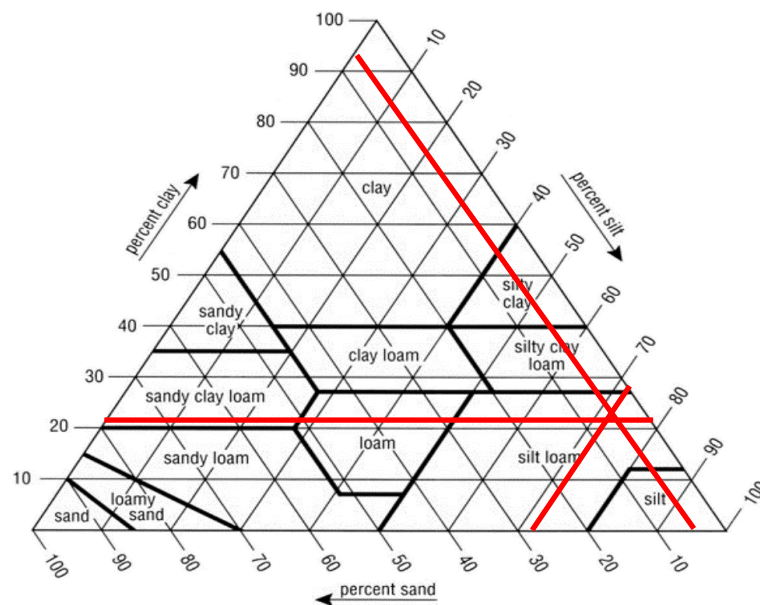


Figure II-3 Soil texture triangle with results of the granulometry analysis over the studied tidal flat.

Spatial & temporal ecological heterogeneity

We monitored the evolution of the physical environment including water salinity, sediment carbon content, sediment moisture, water pH, surface water density & water temperature, across the tidal flat

throughout the duration of the field sampling (25.8.17 - 31.8.17). Each set of data was summarized by means of boxplots mapping (RStudio – R package: ggplot2). Then a one-way ANOVA (RStudio – R package: stats) was performed to determine whether there were any statistically significant differences between the means of each response variables over the respective transects and between dates of sampling (Table II-2). At last, a post-hoc Tukey’s test was performed to compare all groups means for each variable and to identify which of them were statistically different (Table II-2).

Table II-1 Summary of the main abiotic parameters

Main abiotic parameters	<i>n</i>	Mean	(SE)	Range
Water Temperature (°C)	44	5.69	0.637	(1.4-7.4)
Salinity (PSU)	44	21.70	3.464	(14-40)
pH	44	7.18	0.118	(6.51-7.79)
sigma- <i>t</i>	44	17.06	1.127	(7.88-33.14)
PAR (μmol m ⁻² s ⁻¹)	1801	143	3.228	(0-793)
PAR* (μmol m ⁻² s ⁻¹)	11	267	71.156	(8-815)
UVR* (mW cm ⁻²)	11	0.257	0.053	(0.015-0.538)
T _{DL1} (°C)	451	5.4	0.254	(0.7-9.9)
T _{DL2} (°C)	451	5.5	0.259	(0.8-8.9)
T _{air} (°C)	1801	5.7	0.0494	(-1.5-12.8)

Data summary & ANOVA interpretation

The boxplots were clustered by transects (TI, TII, TIII) and differentiated based on their sampling date (25.8.17, 28.8.17, 29.8.17, 31.8.17).

Water salinity. The average salinity concentration was estimated at 21.70 PSU (Table II-1), suggesting the influence of strong local freshwater inputs. Salinity was reported to be statistically different between transects (ANOVA, p-value = 0.0278) and overtime (ANOVA, p-value = 0.000173). Among the transects, TIII and TI were reported to have significant differences in salinity (Tukey’s test, p-value = 0.0208363).

Water pH. The overall average water pH within the tidal flat was neutral about 7.18. pH was found to be statistically different spatially (ANOVA, p-value = 0.0336) although it was not statistically different overtime (ANOVA, p-value = 0.0667). The Tukey’s test scores supported this later observation, validating a significant difference in pH between TIII and TII. This may denote the major contribution of the microphytobenthos to the carbonate cycle through changes in pH, as we reported the presence of *Vaucheria* sp. in higher density across TIII compared to TI.

Surface water temperature. Throughout the field sampling, the average temperature set around 5.69°C (Table 3). We did not report any significant differences of temperature over the tidal flat between transects (ANOVA, p-value = 0.919). Yet, overtime the temperature has statistically decreased from the 25.8.17 to the 31.8.17 (ANOVA, p-value = <2E-16). We decided not to show the Tukey’s test scores for the previous as we did not intend to use this information.

Water density. The average density of the surface water was estimated at 17.06 across the studied area. The density was statistically different spatially-wise between transects (ANOVA, p-value = 0.0271) and overtime throughout the duration of the field sampling (ANOVA, p-value = 0.000164). Spatially we reported a significant difference in water density between T1 and TIII (Tukey’s test, p-value = 0.0202776), with the lowest density registered across TIII around 13.842.



Figure II-4 Box plots data analysis of the main physical abiotic parameters including Water pH, salinity, density, sediment moisture and water temperature.

Sediment moisture. The average sediment moisture for the explored surface seabed was estimated at 54.42%. Sediment moisture was reported to be statistically different across the seabed (ANOVA, p-value = 0.0174), though it did not show any significant difference throughout the sampling period (ANOVA, p-value = 0.795).

According to the Tukey's test, there is a significant difference with respect to the sediment moisture between TIII and TII (Tukey's test, p-value = 0.0202776). It seems that lower sediment moisture occurs in TIII compared to TII.

Table II-2 ANOVA's statistical scores (Upper table) & Tukey's Test statistical scores of the main in-situ physical parameters (Lower table). Statistically significant for $p < 0.05$ (displayed in red).

Explanatory variable	Response variable	F-statistic	P-value
Transects (Spatial)	Salinity	3.915	0.0278
	pH	3.689	0.0336
	Temperature	0.085	0.919
	Density	3.946	0.0271
	Moisture	4.653	0.0174
Dates (Temporal)	Salinity	8.502	0.000173
	pH	2.583	0.0667
	Temperature	87.18	<2E-16
	Density	8.56	0.000164
	Moisture	0.231	0.795
Tukey multiple comparisons of means 95% family-wise confidence level			
Response variable	P-value		
	TIII-TI	TIII-TI	TIII-TII
Salinity	0.2542582	0.0208363	0.41055
pH	0.1081096	0.964507	0.041216
Density	0.2534426	0.0202776	0.405229
Moisture	0.0956695	0.852539	0.017947

***Vaucheria* sp. biogeographical & ecological dispersion**

A PCA was performed using as independent variables water pH, water density and sediment moisture. The water temperature and salinity were not used in this PCA as we previously demonstrated no spatial heterogeneity of the temperature in the surface water across the tidal flat. Moreover, density is a function of water temperature and salinity. Hence to prevent graph overloading we decided to use only these 3 previous variables. The aim of this PCA was to show how *Vaucheria* sp. distributed based on the following environmental variables (water pH, water density, soil moisture). The set of data was normalized by log transformation. Likewise, the PCA was scaled and centred to allow the principal components to capture a maximum variance. Out of the 3 principal components we decided to consider only the two first components, together capturing a total of 80.86% of the variance in the data set (Table II-3).

Table II-2 PCA summary of the main physical parameters & associated eigen values scores.

	PC1	PC2
Standard deviation	1.2206	0.9676
Proportion of Variance	0.4966	0.312
Cumulative Proportion	0.4966	0.8086
	PC1	PC2
Water pH	0.8291	0.0941
Water density	0.7544	0.4436
Sediment moisture	-0.4829	0.8547

PCA interpretation

The eigenvalues produced for the two first components can be found in Table II-4. The first principal component was positively correlated with pH and density (Table II-4). While the 2nd principal component was negatively correlated with sediment moisture. *Vaucheria* sp. seemed to distribute slightly toward the lower right corner suggesting modest variances in pH & water density and low variances in sediment moisture. These observations confirm the photosynthetic contribution of *Vaucheria* sp. (pH variance) and indicate its adaptation to quasi-saline habitats (low moisture & modest density).

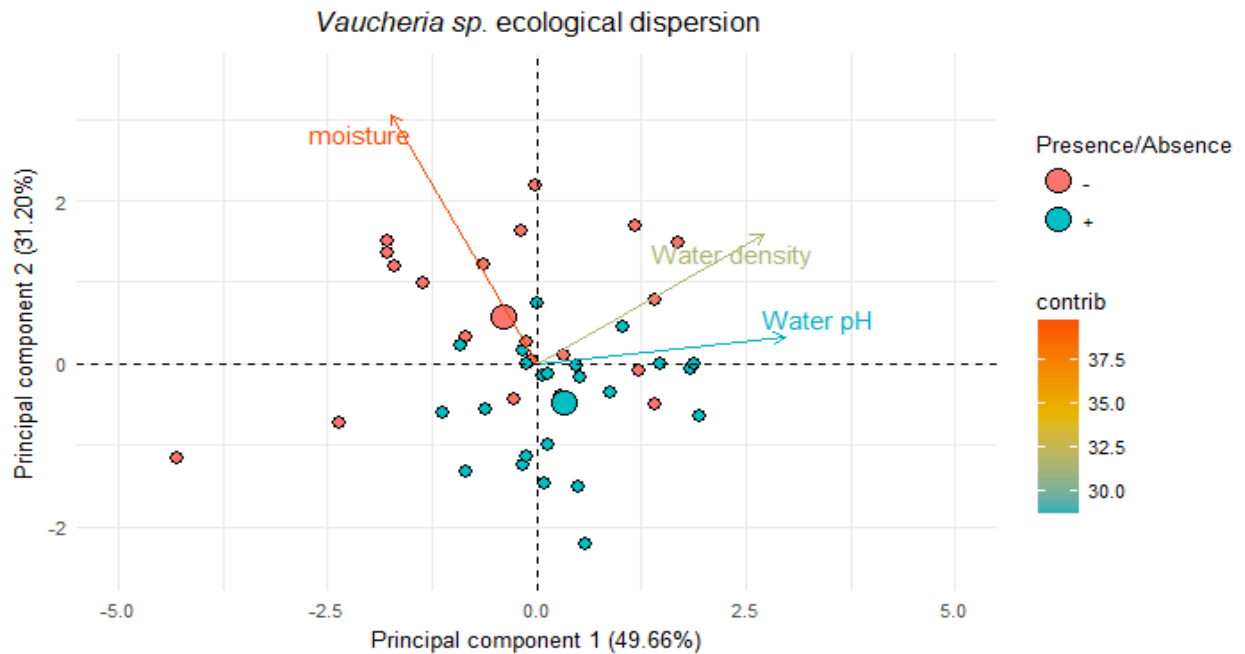


Figure II-5 Biplot data analysis of *Vaucheria* sp. distribution based on the main abiotic physical parameters (scores of each sampling stations and loadings of the different physical abiotic parameters including water pH, water density and sediment moisture). Each small dot represents one sampling site. Blue = Presence of *Vaucheria*, red = absence. The larger dot represents the overall average score for the respective groups. (RStudio Team 2016).

Spatial & temporal biochemistry

An extensive inventory of the biochemical supplies present in this tidal flat was established. A Table containing all compounds and elements assessed during the sampling period was laid down below (Table II-4).

Water biochemical inventory

A preliminary study of the distribution of our data sets was carried out to select the correct statistical procedure to apply. Most of the data sets were reported not to adopt a normal distribution (shapiro test and qqplot – $p < 0.05$), except for Nitrite (NO_2^-) with ($p > 0.05$). Hence, the Nitrite data set was individually studied via ANOVA and Tukey-Kramer ($p < 0.05$). Subsequently, statistical differences between the remaining water biochemical supplies, respectively across the tidal flat between transects and over the month of August 2017 at different sampling dates, were determined via Kruskal-Wallis rank sum test. At last, Wilcoxon signed rank pairwise tests adjusted using the Bonferroni correction were carried out for the respective pairs of groups both spatially and temporally ($p < 0.05$).

Table II-3 Hydrochemical parameters from the water surface of Adventdalen's tidal flat.

Nutrient concentration	n	Mean	(SD)	Range (min-max)
TP (mmoles/l)	22	2.432×10^{-4}	5.869×10^{-5}	$(1.810 \times 10^{-4} - 59.288 \times 10^{-4})$
TN (mmoles/l)	22	11.04×10^{-3}	8.182×10^{-3}	$(3.491 \times 10^{-3} - 35.758 \times 10^{-3})$
N-NO ₂ (mmoles/l)	22	9.385×10^{-5}	6.393×10^{-5}	(LoD - 23.536×10^{-5})
P-PO ₄ (mmoles/l)	22	3.015×10^{-4}	1.257×10^{-3}	(LoD - 59.288×10^{-4})
N-NH ₄ (mmoles/l)	22	4.467×10^{-3}	8.948×10^{-3}	(LoD - 42.78×10^{-3})
N-NO ₃ (mmoles/l)	22	2.310×10^{-3}	3.331×10^{-3}	$(0.135 \times 10^{-3} - 14.130 \times 10^{-3})$
K (mmoles/l)	22	3.090	2.959	(0.174 - 7.934)
Mg (mmoles/l)	22	16.030	15.759	(1.235 - 41.815)
Ca (mmoles/l)	22	4.425	3.583	(0.759 - 10.317)
Mn (mmoles/l)	22	6.99×10^{-3}	7.127×10^{-3}	$(0.353 \times 10^{-3} - 28.650 \times 10^{-3})$
Fe (mmoles/l)	22	6.157×10^{-5}	1.834×10^{-4}	(LoD - 80.089×10^{-5})
Na (mmoles/l)	22	139.425	138.381	(6.662 - 371.954)
Si(OH) ₄ (mmoles/l)	22	6.886×10^{-3}	5.929×10^{-3}	(LoD - 23.543×10^{-3})
SO ₄ (mmoles/l)	22	2.422	1.866	(0.321 - 5.443)
Average atomic ratios				
Si:N		1.016	1.134	(LoD - 4.471)
N:P		42.234	21.458	(18.772 - 98.426)

NH₄-N. The average ammonium concentration (NH₄-N) was reported at 4.467×10^{-3} mmol L⁻¹ ($\pm 8.948 \times 10^{-3}$) across the studied area and over the studied period from the 9.08.2017 to the 28.08.2017. The ammonium concentration ranged between a maximum of 42.78×10^{-3} mmol L⁻¹ and a minimum reported to exceed the instrument Limit of Detection (LoD). The lowest value detected was 1.776×10^{-4} mmol L⁻¹. No strong evidence of a spatial or temporal difference (p-value = 0.2074 & p-value = 0.5761) between the mean ranks of at least one pair of groups was found, suggesting no significant difference in [NH₄-N] in the surface water across the tidal flat and throughout the study period.

NO₂-N. The average nitrite concentration was registered at 9.385×10^{-5} mmol L⁻¹ ($\pm 6.393 \times 10^{-5}$) with a minimum exceeding the instrument Limit of Detection (LoD) and a maximum of 23.536×10^{-5} mmol L⁻¹. The lowest value detected was 8.346×10^{-6} mmol L⁻¹. A one-way ANOVA was specifically run for this data set because it met the normal assumption of the distribution of the data. While we reported no statistical differences spatially (p-value = 0.4303) a significant evidence of a difference (p-value = 0.006428) overtime was found. There was a significant decrease in [NO₂-N] in the surface water from the 9.08 to the 25.08. This observation may be correlated to a local shift in phytoplankton & microphytobenthic communities throughout the tidal flat, affecting nutrient removal overtime. Another hypothesis could be due to a local shift in the hydrodynamic of the tidal flat overtime.

NO₃-N. The average nitrate concentration (NO₃-N) across the tidal flat and over the sampling period was estimated at 2.310×10^{-3} mmol L⁻¹ ($\pm 3.331 \times 10^{-3}$). The nitrate concentration ranged from 0.135×10^{-3} to 14.130×10^{-3} mmol L⁻¹. We did not report any spatial or temporal significant difference (p-value =

0.08641 & p-value = 0.1783) between the mean ranks of at least one pair of groups. It indicated no significant difference in [NO₃-N] in the surface water over the tidal flat or throughout the study period.

TN. The average Total nitrogen concentration was estimated at 11.04×10^{-3} mmol L⁻¹ ($\pm 8.182 \times 10^{-3}$). It ranged across the tidal flat and over the sampling period between 3.491×10^{-3} and 35.758×10^{-3} mmol L⁻¹. Kruskal-Wallis scores indicated no significant spatial difference across the tidal flat (p-value = 0.09787). Yet, there was a strong evidence of a difference in [TN] overtime (p-value = 0.009493). [TN] in the surface water was reported to increase significantly from the 9.08 to the 25.08. Given that [TN] accounts for the sum of reduced nitrate [NO₃-N] plus original nitrite [NO₂-N] and total kjeldahl nitrogen (ammonia, organic and reduced nitrogen), and that [NO₂-N] was reported to decrease overtime. We speculate that higher decomposition toward the end of the summer season may occur hence building up TKN supplies and incidentally TN supplies overtime.

PO₄-P. The average Orthophosphate concentration (P-PO₄) across the studied area was estimated at 3.015×10^{-4} mmol L⁻¹ ($\pm 1.257 \times 10^{-3}$). [P-PO₄] ranged between a minimum that exceeded the instrument Limit of Detection (LoD) and a maximum of 59.2888×10^{-4} mmol L⁻¹. The lowest value detected was 1.357×10^{-6} mmol L⁻¹. We did not report any spatial significant difference (p-value = 0.0968). Yet, we reported a significant temporal difference between the mean ranks across the two respective sampling dates from the 9.08 to the 25.08 (p-value = 0.001631). [P-PO₄] was reported to increase overtime.

TP. The average Total phosphorus concentration was recorded at 2.432×10^{-4} mmol L⁻¹ ($\pm 5.869 \times 10^{-5}$) with a minimum of 1.810×10^{-4} mmol L⁻¹ and a maximum of 59.288×10^{-4} mmol L⁻¹. Although TP did not seem to differ spatially (p-value = 0.8441) there was a strong evidence of a temporal difference (p-value = 0.003477) over the month of August 2017. This temporal trend was in line with an increase in [P-PO₄] overtime as TP accounts for any phosphates forming part of a larger organic compounds including original dissolved orthophosphates compounds.

Na. The average sodium concentration (Na⁺) was registered at 139.425 mmol L⁻¹ (± 138.381). The sodium concentration varied from a minimum of 6.662 mmol L⁻¹ to a maximum of 371.954 mmol L⁻¹. The resulting Kruskal-Wallis scores indicated no significant spatial difference in [Na⁺] across the tidal flat (p-value = 0.3387). Yet, we reported a significant difference in [Na⁺] overtime (p-value = 0.001814). [Na⁺] was statistically higher on the 25.08 compared to the 09.08.

Mg. The average magnesium concentration (Mg²⁺) was reported at 16.030 mmol L⁻¹ (± 15.759). The [Mg²⁺] ranged from 1.235 to 41.815 mmol L⁻¹. Although we did not report any spatial significant difference (p-value = 0.3769) between the mean ranks of at least one pair of groups there was a strong evidence of a temporal difference (p-value = 0.001152) over the month of August 2017. [Mg²⁺] increased toward the end of the summer season.

Si(OH)₄. The average Silicic acid concentration (Si(OH)₄) measured across the tidal flat was recorded at 6.886×10^{-3} mmol L⁻¹ ($\pm 5.929 \times 10^{-3}$). [Si(OH)₄] ranged between and a maximum of 23.543×10^{-3} mmol L⁻¹ and a minimum reported to exceed the instrument's Limit of Detection (LoD). The lowest detected [Si(OH)₄] was 3.096×10^{-3} mmol L⁻¹. We did not report any spatial significant difference in [Si(OH)₄] across the tidal flat (p-value = 0.6186). Yet, we did report a significant temporal difference between the mean ranks across the two respective sampling dates from the 9.08 to the 25.08 (p-value = 0.009292). [Si(OH)₄] was reported to significantly decrease overtime. This might reveal a shift in the phytoplankton and/or microphytobenthic community structure of this tidal flat overtime. This observation could result in a decrease in the proportion of the diatom population correlated with the end of the summer season.

SO₄²⁻. The average Sulfate (SO₄²⁻) was registered at 2.422 mmol L⁻¹ (± 1.866) with a minimum of 0.321 mmol L⁻¹ and a maximum of 5.443 mmol L⁻¹. Kruskal-Wallis scores indicated no significant spatial difference in [SO₄²⁻] across the tidal flat (p-value = 0.228). However, there was a strong evidence of a statistical difference in [SO₄²⁻] overtime (p-value = 0.001152). [SO₄²⁻] over the course of the month of August 2017 was reported to increase from the 9.08 to the 25.08.

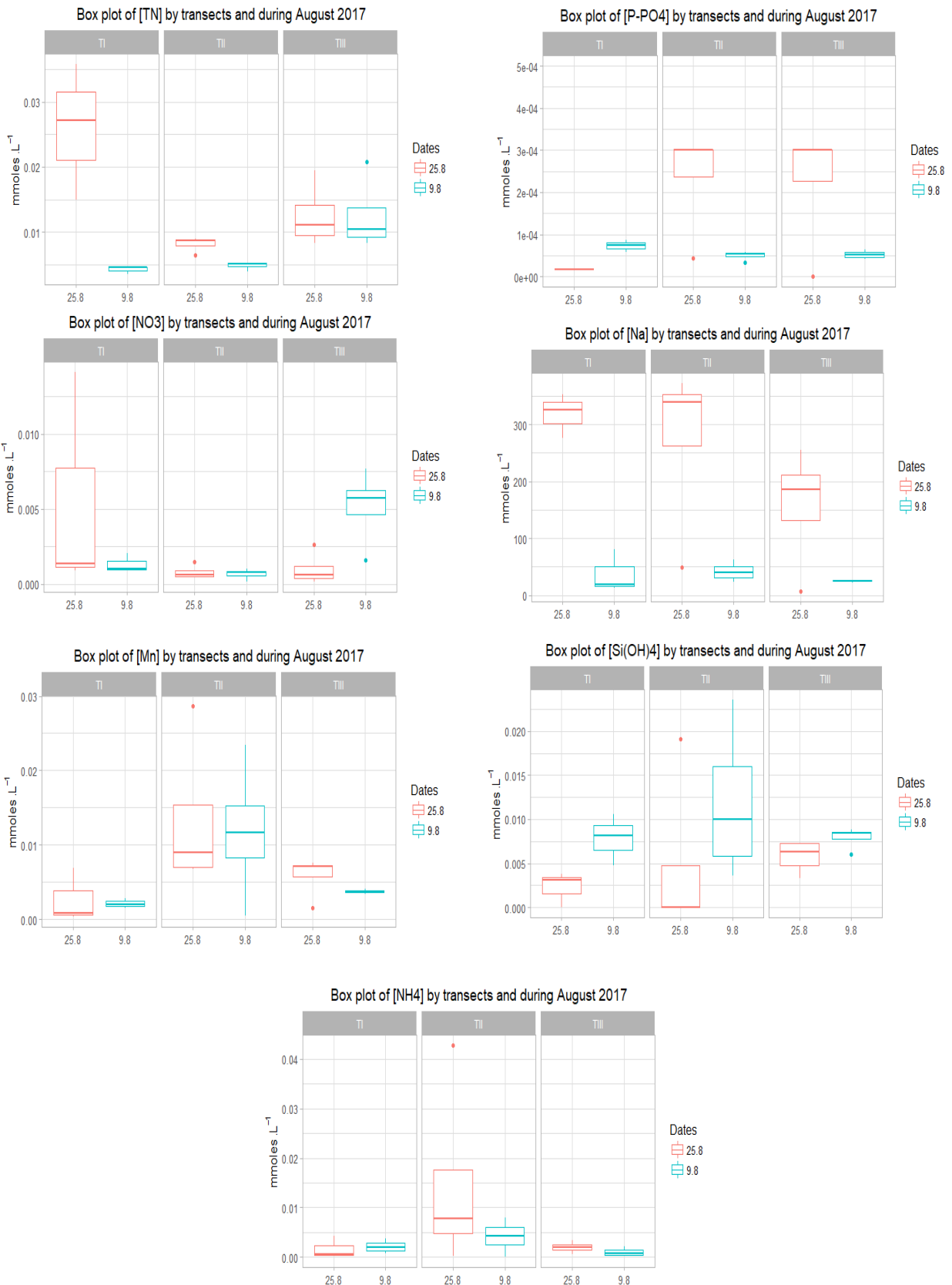
K. We reported an average Potassium concentration (K⁺) of 3.090 mmol L⁻¹ (± 2.959). [K⁺] ranged from 0.174 mmol L⁻¹ to 7.934 mmol L⁻¹. We found no significant spatial difference between the mean ranks of at least one pair of groups (p-value = 0.3174). Nevertheless, we reported a significant difference between the mean ranks for the two sampling dates (p-value = 0.001814). [K⁺] increased overtime from the first sampling date on the 9.08 to the 2nd sampling date on the 28.09.

Fe. The average iron concentration (Fe) across the tidal flat for the month of August 2017 was registered at 6.157×10^{-5} mmol L⁻¹ ($\pm 1.834 \times 10^{-4}$). The iron concentration ranged between and a maximum value of 80.089×10^{-5} mmol L⁻¹ and a minimum value reported to exceed the instrument's Limit of Detection (LoD). We did not report any spatial or temporal significant difference (p-value = 0.1082 & p-value = 0.6228) between the mean ranks of at least one pair of groups. It suggested no significant difference in the surficial iron water supplies over the tidal flat or throughout the study period.

Ca. The average calcium concentration (Ca²⁺) was registered at 4.425 mmol L⁻¹ (± 3.583). [Ca²⁺] varied from a minimum of 0.759 mmol L⁻¹ to a maximum of 10.317 mmol L⁻¹. Kruskal-Wallis scores indicated no significant spatial difference in [Ca²⁺] across the tidal flat (p-value = 0.2613). Yet, we reported a significant difference in [Ca²⁺] overtime (p-value = 0.001152). [Ca²⁺] was statistically higher on the 25.08 suggesting a significant increase overtime.

Mn. The average Manganese concentration (Mn) recorded across the tidal flat and for the month of August 2017 was 6.99×10^{-3} mmol L⁻¹ ($\pm 7.127 \times 10^{-3}$), with a minimum value of 0.353×10^{-3} mmol L⁻¹ and a maximum value of 28.650×10^{-3} mmol L⁻¹. We did report a spatial significant difference in Manganese (p-value = 0.01482) according to the resulting Kruskal-Wallis scores. Although when determining which of

the respective pair of transect groups held a significant difference using a Wilcoxon signed rank pairwise test adjusted with the Bonferroni correction, we did not manage to capture a significant spatial distribution. The manganese concentration at the surface of the water column has shown no evidence of changes over the period of the sampling in August 2017.



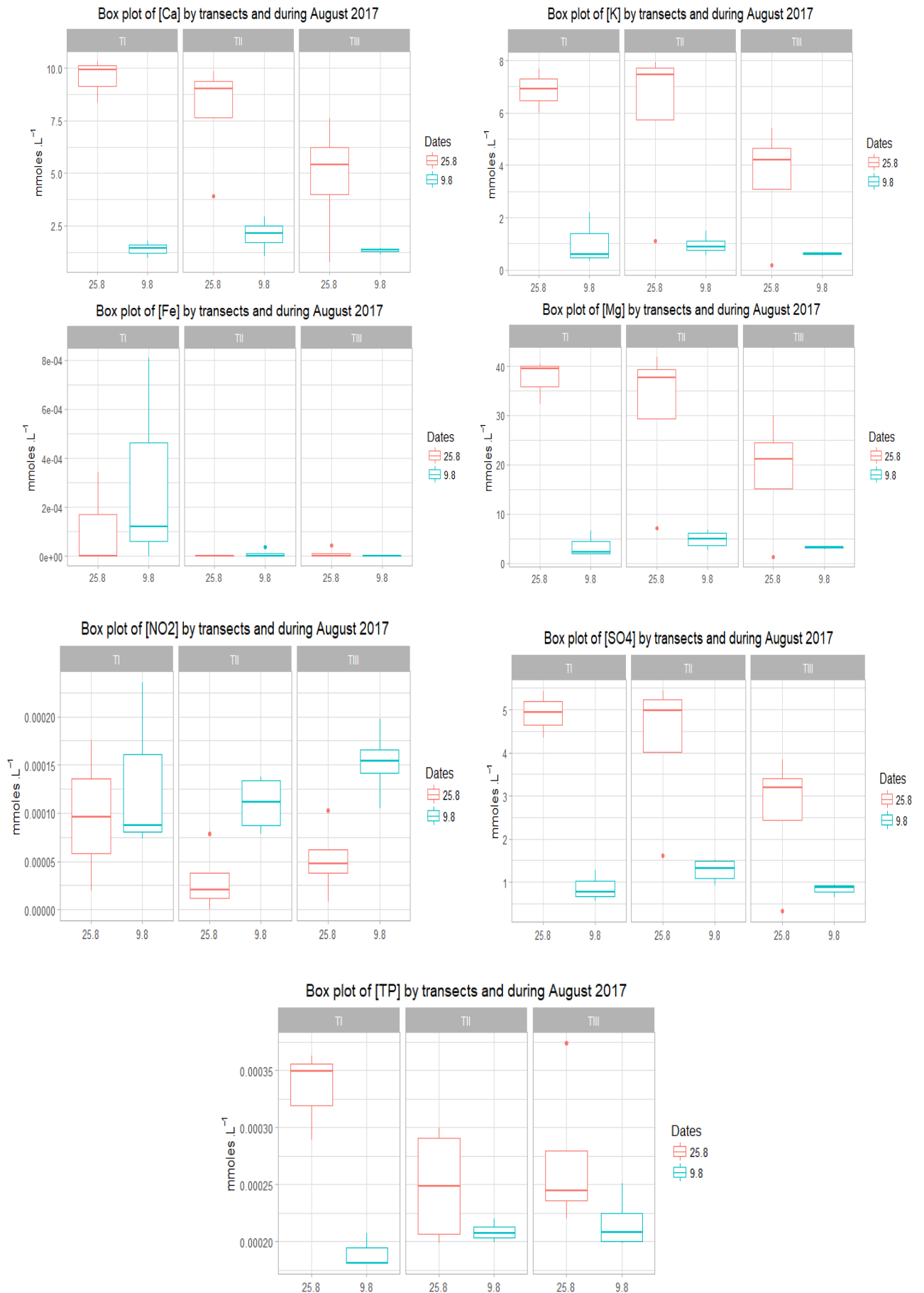


Figure II-6 Box plots data analysis of the hydrochemical parameters including: NH₄-N, N₂-N, N₃-N, TN, PO₄-P, TP, Mg, Si, SO₄, K, Fe, Mn, Na, Ca. (RStudio Team 2016).

Table II-4 Kruskal-Wallis statistical scores of the tidal flat hydrochemical parameters (Upper table) & Wilcoxon statistical scores of the hydrochemical variables (Lower table). Statistically significant for $p < 0.05$ (displayed in red).

Independent variables	Kruskal-Wallis rank sum test	
	dependent variable	P-value
Transects (Spatial) - T1/TII/TIII	NH ₄ -N	0.2074
	NO ₂ -N	0.4303
	NO ₃ -N	0.08641
	TN	0.09787
	P-PO ₄	0.09687
	TP	0.8441
	Na	0.3387
	Si	0.6186
	SO ₄	0.228
	K	0.3174
	Ca	0.2613
	Mn	0.01482
	Fe	0.1082
	Mg	0.3769
Dates (Temporal) - 09.08.2017/25.08.2017	NH ₄ -N	0.5761
	NO ₂ -N	0.006428
	NO ₃ -N	0.1783
	TN	0.009493
	P-PO ₄	0.001631
	TP	0.003477
	Na	0.001814
	Si	0.009292
	SO ₄	0.001152
	K	0.001814
	Ca	0.001152
	Mn	0.5327
	Fe	0.6228
	Mg	0.001152

N:P:Si ratio and limiting nutrients

The atomic N:P:Si ratio or Redfield ratio for phytoplankton growth is generally about 16:1:16 when nutrient levels are sufficient (Redfield 1963). Deviations from this ratio typically suggest potential for Nitrogen, Phosphorus and Silica limitation. We intended to provide herein an overall profile of the water biogeochemistry in which *Vaucheria* sp. occurs. The N:P ratio ranged from 18.77 to 98.43 across the tidal flat during august 2017. The average N:P atomic ratio was 42.23. The atomic Si:N ratio ranged from 0.132 to 4.471 with an average value of 1.11 across the tidal flat over the month of August. A scatterplot of the in-situ N:P and Si:N atomic ratios was built in RStudio and indicated an overall P limitation across the tidal flat (Figure II-7).

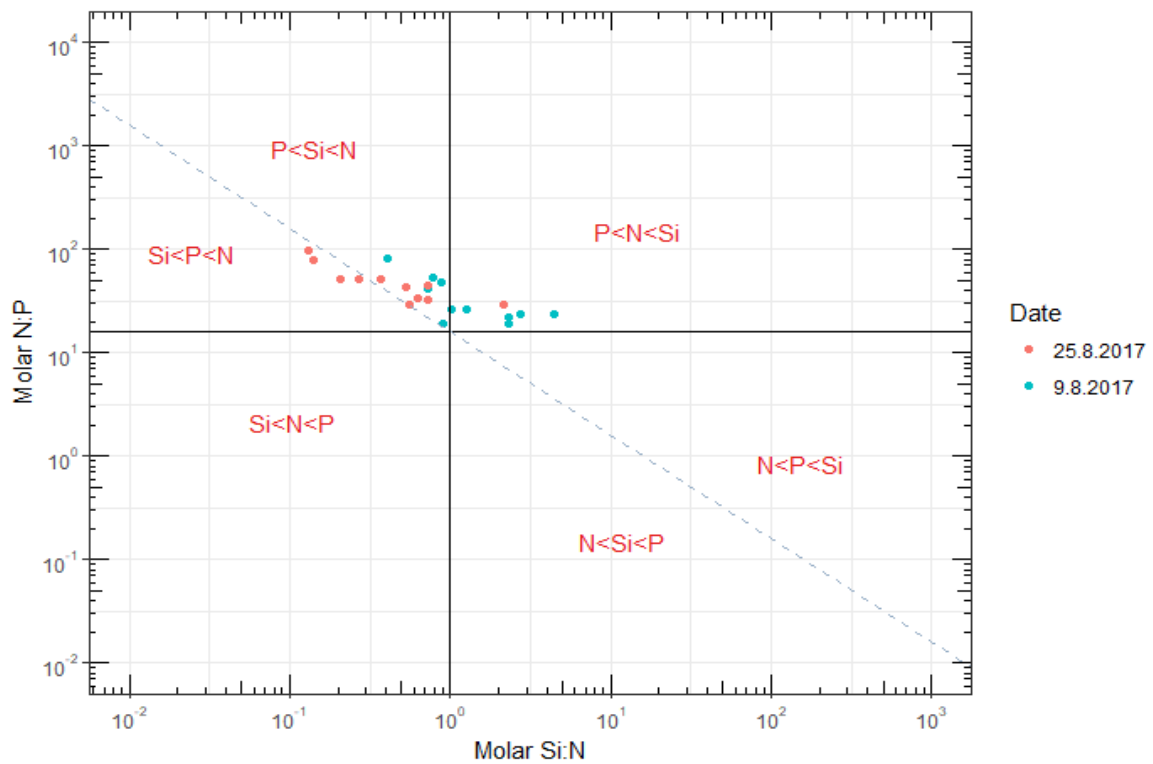


Figure II-7 Scatter diagrams of the Si:N:P atomic nutrient ratios intrinsic to the tidal flat's water column for the month of August 2017. The molar quotients are delimited in this logarithmic plot by the Si:N= 1:1 (vertical line), N:P= 16:1 (horizontal line) and Si:P= 16:1 (oblique line) lines. The lines enable to divide the plot into six different areas. Each of these areas indicates the potentially limiting nutrient water profile, with limiting nutrients listed by order of importance. (RStudio Team 2016).

Moreover, as a function of time we reported a shift from P limiting to Si limiting conditions when approaching the winter season. This may be due to a possible shift in pelagic phytoplankton community overtime.

Hydrochemical spatial distribution patterns – Principal Component Analysis

To get an overview of the spatial distribution of the above-measured chemicals and nutrients within the surface water layer across this tidal flat, we applied a set of statistical techniques. We used the entire biochemical inventory with each hydro-chemical respectively accounting for one single independent variable in the consistent making of our Principal Component Analysis. In a first place, we described the spatial distribution of the different biochemical compounds in the surface of the water over the tidal flat by transects (Figure II-8) and secondly by sites (Figure II-9). This first transect-specific PCA was intended to improve and support our previous statistical assay on inter-transect spatial hydro-chemical heterogeneity. Since many factors may have impacted and compromised our previous statistical test results, namely: tide variations, local tidal

	PC1	PC2
NH4-N	-0.009122467	-0.55188199
N02-N	-0.542114350	0.46576290
N03-N	-0.290961684	0.67849697
TN	0.525568385	0.66143572
PO4	0.582462699	-0.39568566
TP	0.659029886	0.30540342
Mg	0.979847132	0.01868244
Si	-0.408262590	-0.39920085
SO4	0.971893687	-0.02736688
K	0.967683589	0.02958995
Ca	0.961432152	-0.03158002
Mn	0.058852055	-0.52244944
Fe	-0.035059600	0.42502729
Na	0.972348042	0.01968548

Table II-5 PCA scores summary. In green values <0.5 (negatively correlated) and red >0.5 (positively correlated).

hydrodynamic, sampling time, weather conditions & related local river outflow. The second site-specific PCA served the purpose to more precisely characterize the tidal flat with the aim to identify specific spatial patterns, describing potential nutrient accretion site etc... The set of data was methodically normalized by log transformation to mend the skewness of some of the variables. Likewise, the PCA was scaled and centred to allow the principal components to capture a maximum variance. Out of the consistent set of resulting principal components we decided to consider only the two first components, together capturing a total of 58.76% of the variance in the data set (Table II-7). The first principal component was strongly positively correlated with P-PO₄, TP, Mg, SO₄, K, Na & Ca and negatively correlated with NO₂-N (Table II-6). While the 2nd principal component was negatively correlated with NH₄-N and positively correlated with NO₃-N and TN.

Table II-6 Hydrochemistry PCA eigen values and cumulative variance.

	PC1	PC2
Eigenvalue	6.3107	2.2855
Proportion of Variance	0.4507	0.1632
Cumulative Proportion	0.4507	0.6140

Transect-specific PCA interpretation

The principal component analysis suggested that the following variables: Mg, Na, K, Ca & SO₄ and to a lesser extent TP, P-PO₄, NO₃-N & TN were positively correlated. This may indicate that these biochemicals originate from a same source as they seem to increase concurrently. On the contrary, NO₂-N & NH₄-N seemed to decrease concurrently. Although we did not find any significant spatial differences between transects from the earlier statistical tests, except for Mn & P (Kruskal-Wallis rank sum test, p-value = ...), it might be due to changing conditions as a result of the local hydrodynamic, tidal variations and other environmental factors that might hinder the ability of our tests to identify inter-transect differences. The collective mean projection of all variables for each transect as illustrated on the PCA (Figure II-8) tends to occupy quite opposite positions from one another. TIII, where the highest biomass of *Vaucheria* sp. was assumed, seemed to locate toward the upper left corner correlated with low variance of NO₂-N and high variance of NO₃-N and TN. This may suggest a potential source of nitrogen locally across TIII in combination with high rates of nitrification. TI and TII seemed to locate toward the right-hand side accordingly, with high variance of Mg, Na, K, Ca, SO₄, TP & P-PO₄. Furthermore, while TI is situated in the upper corner together with high variance of NO₃-N and TN TII is situated in the lower corner together low NH₄-N. These observations indicate that TI and TIII, both colonized by *Vaucheria* sp., show collectively high variance of NO₃-N and TN that may be related to the local biogenic activity of the microphytobenthos. While we can cluster TI & TIII (y axis) based on TN, NH₄-N & NO₃-N we can similarly cluster TI & TII (x axis) based on Mg, Na, K, Ca, SO₄, TP, NO₂-N & P-PO₄. TI & TII are alike with respect to their variance in the concentration of mineral they present. This could suggest the hydro-chemical input of sea water to the tidal flat.

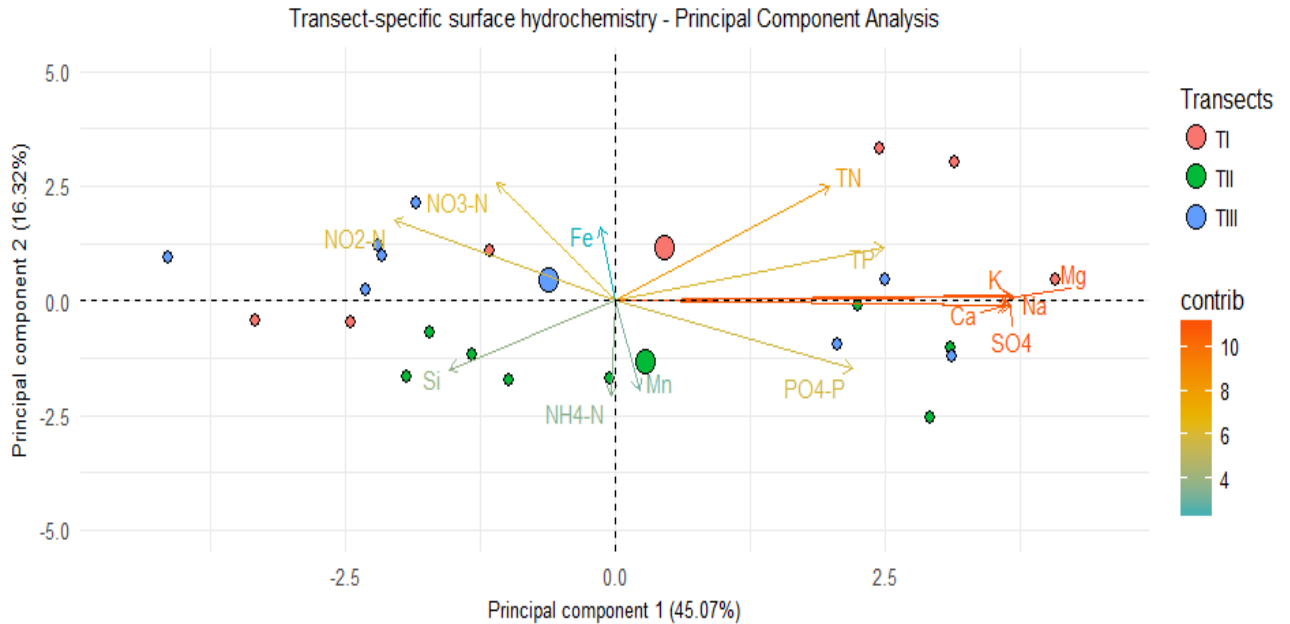


Figure II-8 Biplot data analysis of the spatial hydrochemical distribution by transects (scores of each sampling sites and loadings of the different chemical variables including: NH₄-N, NO₂-N, NO₃-N, TN, PO₄-P, TP, Mg, Si, SO₄, K, Fe, Mn, Na, Ca) on the left. The larger dot represents the overall average score for the respective groups. (RStudio Team 2016).

Site-specific PCA interpretation

The collective mean projection of all variables for each individual site revealed a rather homogeneous distribution. Yet two sites seemed to fall out, including TIII.4 and TII.1. TIII.4 displayed the lowest variance for NO₂-N together with the highest variance for NO₃-N for all sites included, suggesting potential nitrifying bioprocesses. TII.1 was found with the lowest variance for Si, NH₄ & Mn. The divergence of TII.1 was expected as TII.1 was situated directly where Longyearbyen's drinking water pond was flushing out within the tidal flat. This pond inputs to the tidal flat was found to be characterised by low levels of NH₄ & Silica.

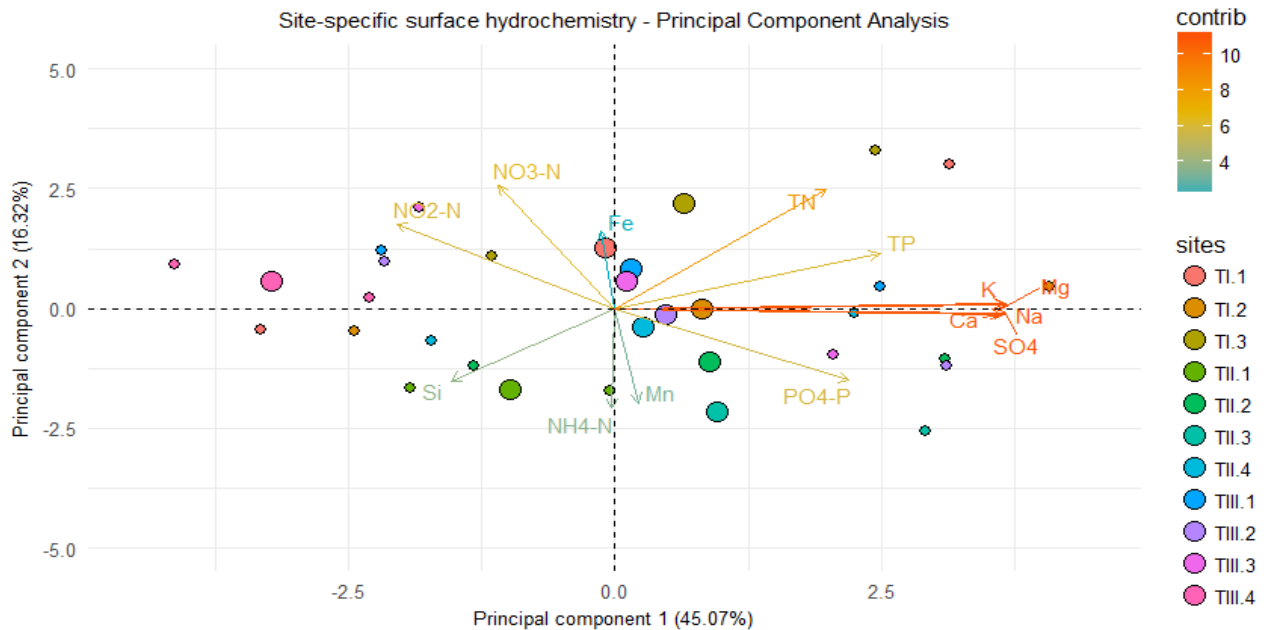


Figure II-9 Biplot data analysis of the spatial hydrochemical distribution by sites (scores of each sampling sites and loadings of the different chemical variables including: NH₄-N, NO₂-N, NO₃-N, TN, PO₄-P, TP, Mg, Si, SO₄, K, Fe, Mn, Na, Ca). Each small dot represents one sampling site. The larger dot represents the overall average score for the respective groups. (RStudio Team 2016).

Sediment biochemistry

Similarly to the tidal flat hydrochemistry assay, the surface of the substrate was extensively studied. It enabled us to produce a recording of the biochemical and physical structure, characteristic to this tidal flat. A Table containing all compounds and elements assessed during the sampling period over two dates on the 9.08 and the 25.08 was laid down.

Table II-7 Sediment biochemical inventory.

Sediment supply				
Nutrient concentration	<i>n</i>	Mean	(SD)	Range
N-NH₄ (mmoles/kg)	44	5.3570	1.6227	(1.6704 - 9.0838)
N-NO₃ (mmoles/kg)	44	0.2759	0.2498	(LoD - 1.4859)
P-PO₃ (mmoles/kg)	44	0.0346	0.0146	(0.01566-0.07864)
Org.C content (%)	33	9.5619	1.3989	(7.649-12.463)

NH₄-N. We reported across the total surface of the sediment of the tidal flat and over the sampling period an average ammonium concentration (NH₄-N) of 5.3570 mmol L⁻¹ (\pm 1.6227). The ammonium concentration overall ranged between 1.6704 to 9.0838 mmol L⁻¹. We did not report any statistical difference in [NH₄-N] geographically between the different transect of the tidal flat (ANOVA, p-value = 0.324). Likewise, no strong evidence of a temporal difference in [NH₄-N] was reported from the 9.08 to the 25.08.2017 (ANOVA, p-value = 0.913).

NO₃-N. The average nitrate concentration (NO₃-N) across the tidal flat and over the sampling period was estimated at 0.2759 mmol L⁻¹ (\pm 0.2498). The nitrate concentration ranged between a minimum value that exceeded the instrument Limit of Detection (LoD) and a maximum value of 1.4859 mmol L⁻¹. The lowest value detected was 0.009966 mmol L⁻¹. We found no significant spatial difference in [NO₃-N] between the mean ranks of at least one pair of groups (Kruskal-Wallis rank sum test, p-value = 0.3055). Nevertheless, we reported a significant difference in [NO₃-N] between the mean ranks for the two sampling dates (Kruskal-Wallis rank sum test, p-value = 0.006947). It seems that [NO₃-N] decreased significantly over the study period from the 9.08 to the 25.08.2017.

PO₄-P. The average Orthophosphate concentration (P-PO₄) across the studied area and during august 2017 was estimated at 3.46 x 10⁻² mmol L⁻¹ (\pm 1.46 x 10⁻²). [P-PO₄] was reported to range from 1.566 x 10⁻² mmol L⁻¹ to 7.864 x 10⁻² mmol L⁻¹. We did not report any spatial significant difference in [P-PO₄] (Kruskal-Wallis rank sum test, p-value = 0.9226). Yet, we reported a significant temporal difference between the mean ranks for the 2 respective sampling dates on the 9.08 and the 25.08.2017 (Kruskal-Wallis rank sum test, p-value = 0.001659).

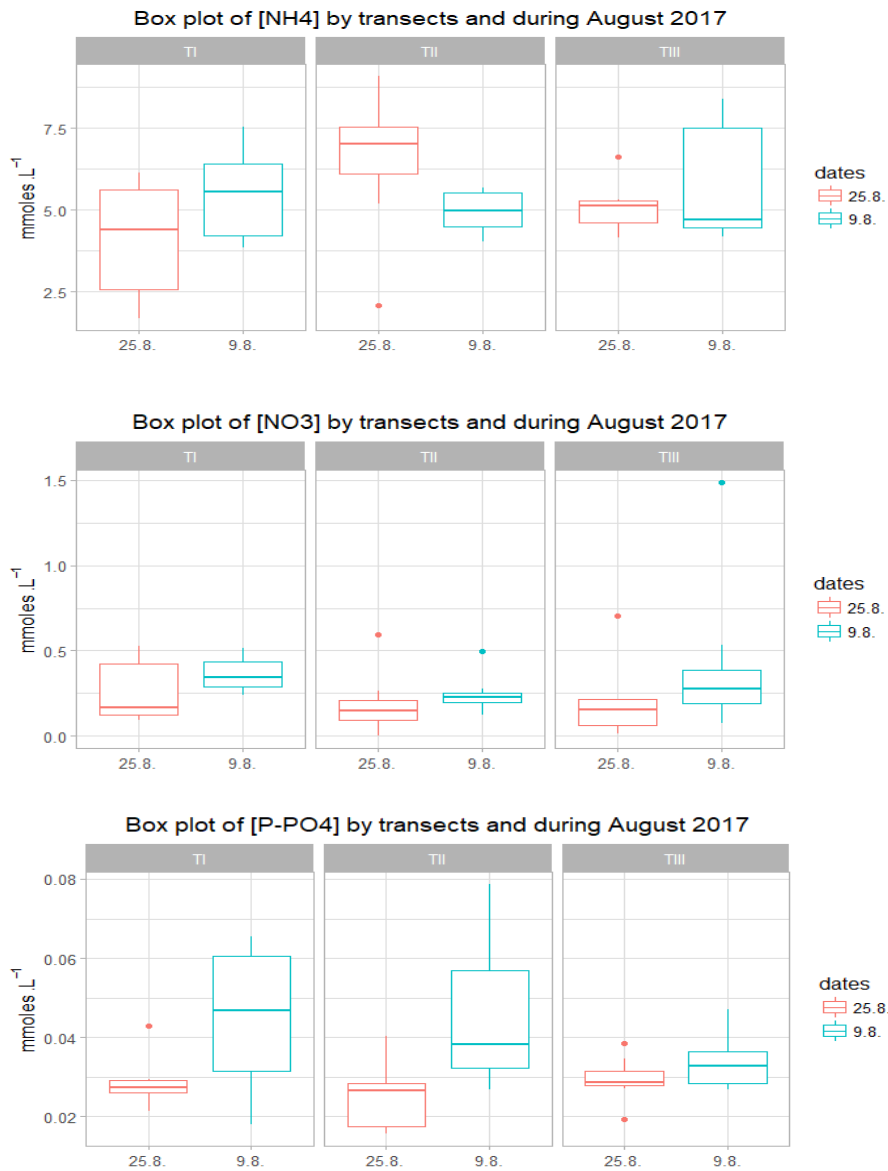


Figure II-10. Box plots data analysis of the sediment chemical parameters including: NH₄-N, NO₃-N, PO₄-P. (RStudio Team 2016).

Organic carbon content. The tidal flat sediment composition was inspected for organic carbon supply. The soil was found to be oligotrophic throughout the seabed with an average organic carbon content of 9.56% ($\pm 1.3989\%$). The proportion of organic carbon in the sediment surface ranged between 7.649% and 12.463%. The Kruskal-Wallis scores obtained suggested a significant spatial difference in the percentage of surface organic carbon between the transects of the tidal flat (Kruskal-Wallis rank sum test, p -value = 0.00675). To determine which of the respective pair of transect groups held a significant difference a Wilcoxon signed rank pairwise test adjusted using the Bonferroni correction was carried out. The results suggested a significant difference in surface organic carbon between the transects TIII and TII (Wilcoxon signed rank pairwise test, p -value = 0.0018). The transect TIII seemed to contain significantly lower surface organic content than transect TII. Organic carbon storage is a key component of the soil fitness affecting its physical, chemical, and biological properties. Our results are in line with the results pertaining to the surface moisture content, indicating that a higher soil organic carbon content improves water retention. Alike sediment

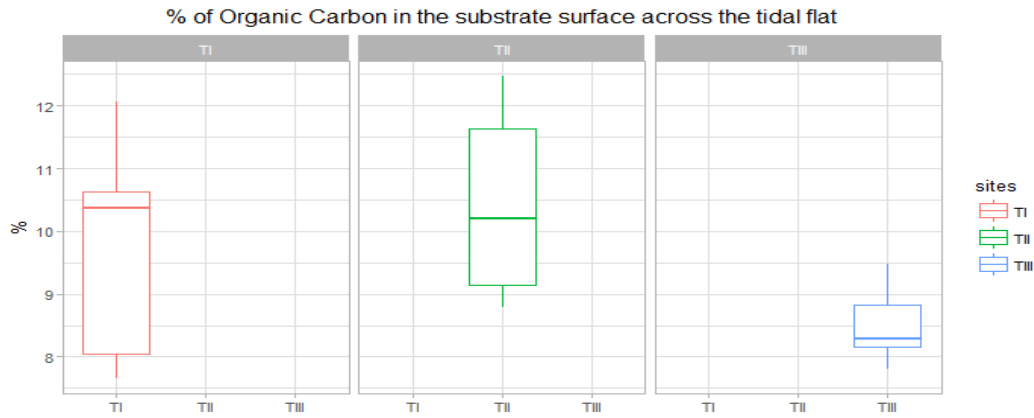


Figure II-11 Box plot data analysis of the Organic Carbon content present in the surface layer of the seafloor across the tidal flat. (RStudio Team 2016).

moisture, lower sediment organic carbon contents were specifically registered locally where *Vaucheria* sp. was the densest along TIII. We could speculate that *Vaucheria* sp. likely produces hot-spots of microbial activity where heterotrophic microbial decomposers benefit from algal biochemical inputs. Consecutively locally supporting optimised organic matter decomposition outcomes in the surficial layer of the sediment, according to a phenomenon known as priming effect (Guenet et al. 2010).

Table II-8 Kruskal-Wallis Statistical scores of the biochemical parameters (Upper table) & Wilcoxon statistical scores of the sediment biochemical parameters (Lower table). Statistically significant for $p < 0.05$ (displayed in red).

independent variables	Kruskal-Wallis rank sum test	
	dependent variables	P-value
Transects (Spatial) - TI/TII/TIII	NH ₄ -N	0.324
	NO ₃ -N	0.3055
	P-PO ₄	0.9226
	Organic carbon	0.00675
Dates (Temporal) - 09.08.2017/25.08.2017	NH ₄ -N	0.913
	NO ₃ -N	0.006947
	P-PO ₄	0.001659

Dependent variable	Pairwise comparisons using Wilcoxon rank sum test		
	P-value		
	TII-TI	TIII-TI	TIII-TII
Organic carbon	1.000	0.4974	0.0018

Sediment chemistry spatial characterization – Principal Component Analysis

Similarly to the hydrochemistry of the tidal flat, the surface layer of the sediment was spatially characterized based on the statistical collective mean projection of distinct variables, including NH₄-N, NO₃-N & P-PO₄. In a first place, we described the spatial distribution of the different biochemical compounds in the surface of the sediment over the tidal flat by transects (Figure II-12) and secondly by sites (figure II-15). The first PCA enabled us to distinguish biochemical similarities and dissimilarities locally across the sediment of the tidal flat between the distinct transects. The second PCA more precisely described the biochemical composition and spatial distribution of the sediment of the tidal flat per sites. The data were processed similarly to those in the previous hydrochemical PCA of the tidal flat. The data were methodically normalized by log

transformation to mend the skewness of the variables. The PCA was scaled and centred to allow the principal components to catch a maximum variance. We only consider the two first components to construct our PCA. Principal component 1 & Principal component 2 together captured a total of 84.34% of the variance (Table II-10). The first principal component was strongly positively correlated with $\text{NO}_3\text{-N}$ & $\text{NH}_4\text{-N}$ (Table II-10). The 2nd principal component was negatively correlated with $\text{NH}_4\text{-N}$ and positively correlated with P-PO_4 .

Table II-9 PCA summary of the biochemical parameters & associated eigen values. In green values <0.5 (negatively correlated) and red >0.5 (positively correlated).

	PC1	PC2
Eigenvalue	1.6415	0.8888
Proportion of Variance	0.5471	0.2962
Cumulative Proportion	0.5471	0.8434
	PC1	PC2
NH₄-N	0.7158	-0.5905
NO₃-N	0.8613	-0.0392
PO₄-P	0.6222	0.7338

Transect-specific PCA interpretation

The Principal Component Analysis suggested that P-PO_4 and $\text{NH}_4\text{-N}$ are inversely correlated. Furthermore $\text{NH}_4\text{-N}$ and $\text{NO}_3\text{-N}$ were positively correlated. Although we did not find any significant spatial differences between transects from the previous statistical tests, except for the organic carbon content (Kruskal-Wallis rank sum test, p-value = 0.00675), it might be due to the small sample size used. Yet, the collective mean projection of the variables for every transect as illustrated on the PCA (Figure II-12.) tends to show higher similarities between TI and TIII compared to TII. This may indicate the effect of microphytobenthic communities related with *Vaucheria* sp. occurrence on the sediment biochemistry. TI and TIII were found to be correlated with lower variance in $\text{NO}_3\text{-N}$ and higher variance in P-PO_4 while TII was correlated with lower variance in $\text{PO}_4\text{-P}$ and higher variance in $\text{NO}_3\text{-N}$.

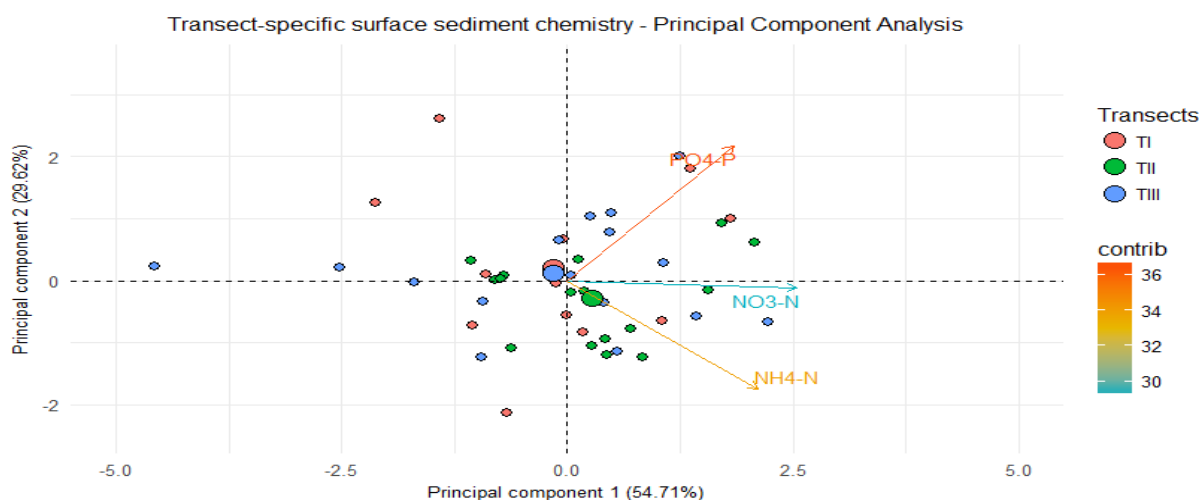


Figure II-12 Biplot data analysis of the spatial sediment chemical distribution by transects (scores of each sampling sites and loadings of the different chemical variables including: $\text{NH}_4\text{-N}$, $\text{NO}_3\text{-N}$, $\text{PO}_4\text{-P}$). Each small dot represents one sampling site. Left, red = Transect I, green = Transect II, Blue = Transect III. The larger dot represents the overall average score for the respective groups. (RStudio Team 2016).

Site-specific PCA interpretation

The collective mean projection of the variables for each individual site revealed a rather homogeneous distribution across the tidal flat. All sites tend to project toward the centre of the PCA with no big differences among sites. TII.1 was found to slightly diverge from the rest of the sites toward the right of the plot with higher variance in $\text{NO}_3\text{-N}$ probably due to the direct mechanical and biochemical impact of freshwater outflows from Longyearbyen's drinking water pond.

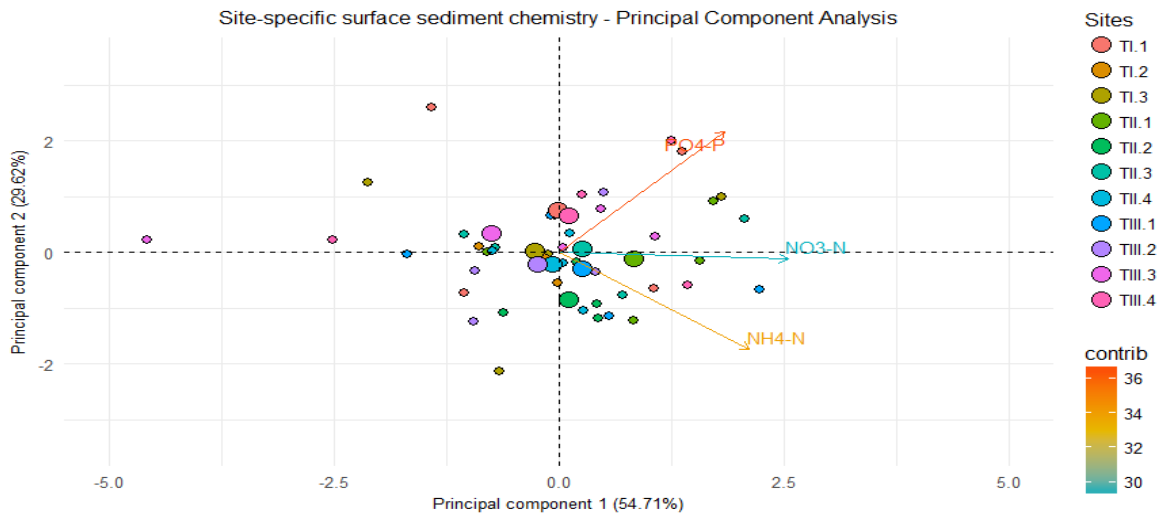


Figure II-13 Biplot data analysis of the spatial sediment chemical distribution by transects (scores of each sampling sites and loadings of the different chemical variables including: $\text{NH}_4\text{-N}$, $\text{NO}_3\text{-N}$, $\text{PO}_4\text{-P}$). Each small dot represents one sampling site. The larger dot represents the overall average score for the respective groups. (RStudio Team 2016).

Vaucheria sp. photosynthetic activity

Ex situ measurements combining gasometric and Chlo a fluorescence techniques were performed to assess the photosynthetic potential of *Vaucheria* sp. Prior to measurement *Vaucheria* sp. samples were carefully washed in the aim to clean the samples from associated benthic micro-organisms and sediment

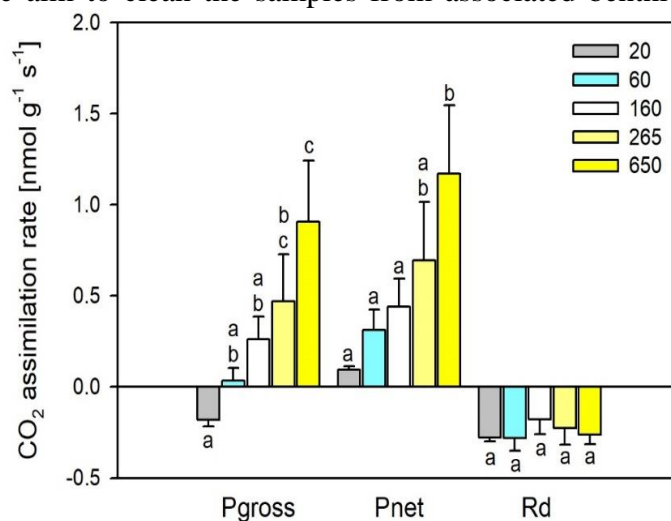


Figure II-14 The dependence of the net photosynthesis (P_{net}), gross photosynthesis (P_{gross}) and dark respiration (R_d) expressed as CO_2 assimilation rate (mean \pm s.d., $n = 3$) at different PAR intensities. The letters indicate homologous groups recognized by Tukey HSD test at $P = 0.05$. The number in legend indicates PAR in $\mu\text{mol m}^{-2} \text{s}^{-1}$.

particles. The thickness of *Vaucheria* sp. biofilm made this process difficult and several organisms may have remained enclosed inside. Hence, the resulting measurements most likely represent the biological response of *Vaucheria* sp. and a small fraction of the associated micro-organisms community. The photosynthesis and dark respiration measured, were respectively expressed as ETR and CO₂ assimilation. The measurements were reportedly performed over five distinct PAR intensities including 20, 60, 160, 265 and 650 $\mu\text{mol m}^{-2} \text{s}^{-1}$. The chosen PAR range was determined based on the natural in-situ irradiance detected during the study period (Table II-1). While the gross photosynthesis (P_{gross}; one-way ANOVA, F = 13.15, P < 0.001) and net photosynthesis (P_{net}; one-way ANOVA, F = 9.073, P = 0.002) significantly increased concurrently with elevated PAR intensities, the dark respiration (R_d; one-way ANOVA, F = 1.197, P = 0.370) remained stable with no significant differences at different PAR intensities (Figure II-14). The ETR measured in light (ETR-light; one-way ANOVA, F = 357.4, P < 0.001) significantly increased proportionally with elevated PAR (Figure III.28.). While, in the dark ETR (ETR-dark; one-way ANOVA, F = 6.289, P = 0.008) was reported to decrease slightly concurrently with high PAR intensities. The ratio of net photosynthesis to dark respiration increased continually with PAR (P_{net}:R_d ratio; one-way ANOVA, F = 1.197, P = 0.370) (see annex III). Overall, the results demonstrated a good photosynthetic activity under typical summer PAR intensities suggesting that *Vaucheria* sp. might relate to r-selected species mostly occurring over the summer season. Furthermore, *Vaucheria* sp. seems to be low-light adapted.

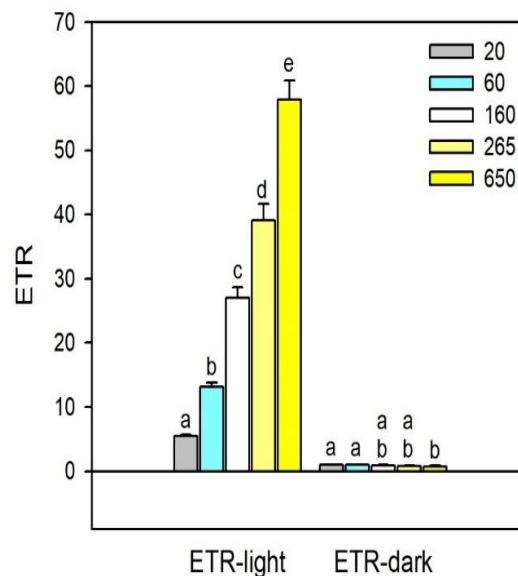


Figure II-15 The dependence of ETR measured in the light (ETR-light) and ETR measured in the dark (ETR-dark) at different PAR intensities (mean \pm s.d., n = 3). The letters indicate homologous groups recognized by Tukey HSD test at P = 0.05. The number in legend indicates PAR in $\mu\text{mol m}^{-2} \text{s}^{-1}$.

To further study the photoacclimation of *Vaucheria* sp. under different PAR intensities, the samples were respectively exposed to 3 different PAR intensities. The light intensities included: LL referring to low light with 10 $\mu\text{mol m}^{-2} \text{s}^{-1}$, ML for medium light with 230 $\mu\text{mol m}^{-2} \text{s}^{-1}$ and HL for high light with 650 $\mu\text{mol m}^{-2} \text{s}^{-1}$. The PI curves were then extrapolated and drawn from our measurements. The resulting curves were

expressed either as CO₂ assimilation rate or ETR (Figure II-17). We did not report significant photoinhibition at PAR of 500 $\mu\text{mol m}^{-2} \text{s}^{-1}$. No significant differences were observed between P_{max}, α and R_d values measured gasometrically (one-way ANOVA; F = 2.685, P = 0.215 for P_{max}; F = 3.855, P = 0.148 for α ; F = 6.593; P = 0.080 for R_d).

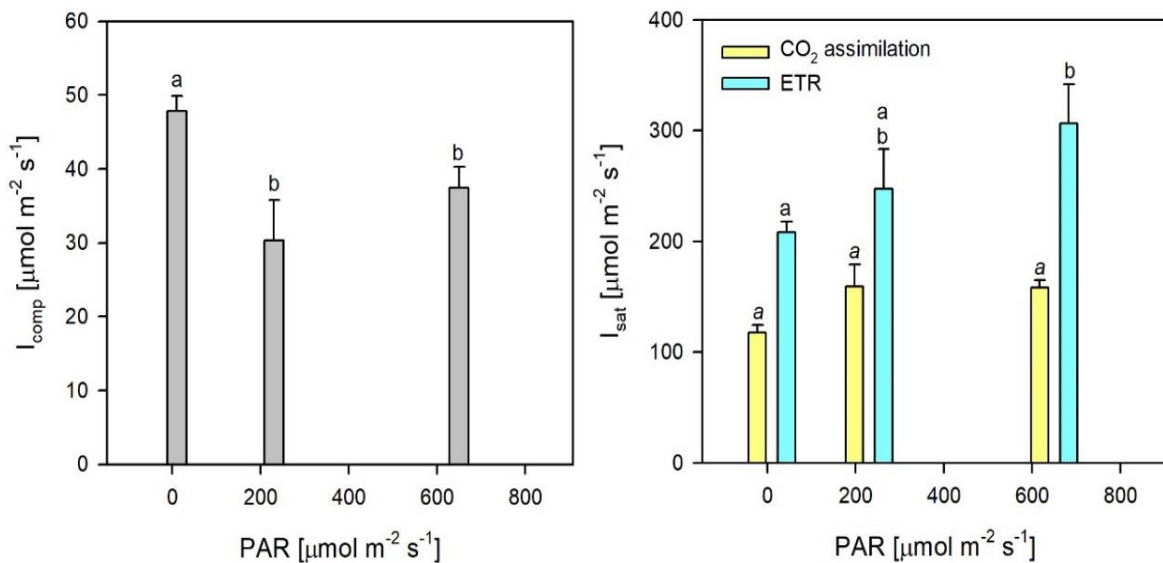


Figure II-16 The dependence of compensation (I_{comp} ; mean \pm s.d., $n = 3$) and saturation (I_{sat} ; mean \pm s.d., $n = 3$) irradiances estimated from gasometric (CO₂ assimilation) and fluorescence (ETR) measurements for different PAR intensities. The letters indicate homologous groups recognized by Tukey HSD test at $P = 0.05$.

However, the compensation irradiance (I_{comp}) was increased at low PAR (one-way ANOVA; F = 11.15, P = 0.041). The saturation irradiance (I_{sat}) based on CO₂ assimilation was not affected by PAR. When ETR was used to express the photosynthetic activity, the ETR_{max} (one-way ANOVA; F = 9.703, P = 0.019) and the saturation irradiance (I_{sat} ; F = 9.381, P = 0.020) increased significantly with the PAR, while the α remained the same (one-way ANOVA; F = 2.727, P = 0.158). The values of saturation irradiance (I_{sat}) based on CO₂ assimilation were lower than those estimated using fluorescence measurements (paired t-test; P = 0.002) (Figure III.31).

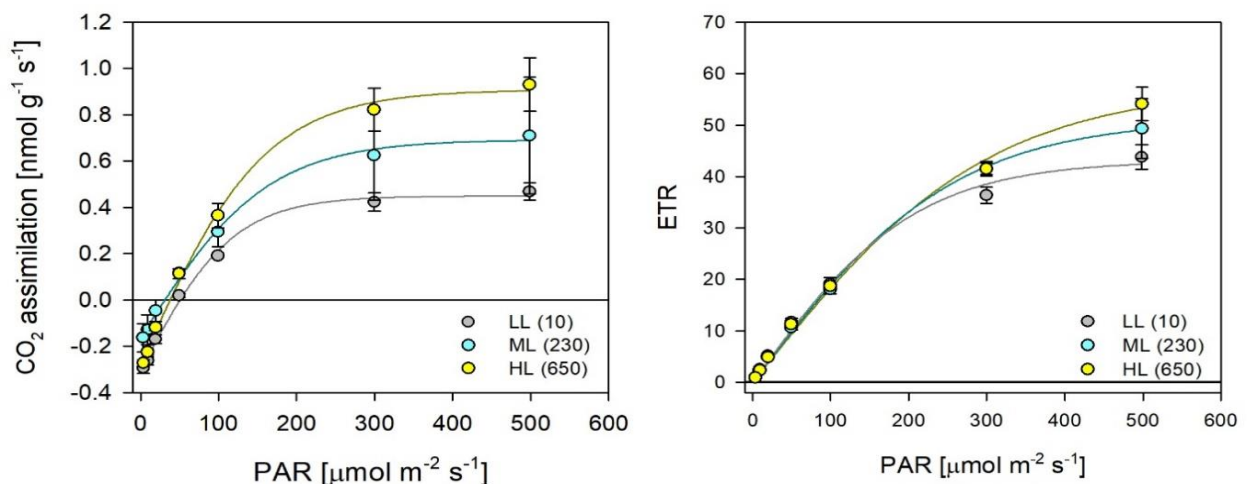


Figure II-17 Photosynthesis-Irradiance curves for CO₂ assimilation and ETR (mean \pm s.d., $n = 3$). LL – low light of 10 $\mu\text{mol m}^{-2} \text{s}^{-1}$, ML – medium light of 230 $\mu\text{mol m}^{-2} \text{s}^{-1}$, HL – high light of 650 $\mu\text{mol m}^{-2} \text{s}^{-1}$.

Discussion

A debut study and comprehensive assessment of the ecology and photosynthetic performances of a newly-reported *Vaucheria* sp. dominated arctic microphytobenthos from the coastlines of Svalbard was performed here. To our knowledge, no report of any brackish/marine *Vaucheria* sp. across Svalbard has been made to this date. However, there are evidences from the literature that Svalbard harbours *Vaucheria borealis* a terrestrial representative of the same family (Elvebakk et al. 1996).

Tidal flat abiotic characterisation

Microphytobenthic organisms inhabiting the eulittoral zones undergo large and rapid ecological variations on a daily-basis due to the periodic movement of tidal waters (Zacher et al. 2009). Additionally, numerous coastal pressures add up to this, inducing large disturbances across intertidal habitats (Anisimov et al. 2007; Meier et al. 2014). In Isfjorden, the inherent oceanographic, geologic and geographic characteristics have been reported to affect microbenthic communities (Berge et al. 2005; Pavlov et al. 2013; Vesman, Ivanov, and Volkov 2017). Local and seasonal river run-off are another important factor influencing microphytobenthic algae, typically from the onset of spring and throughout the summer period (Stein et al. 2004; Perrette et al. 2011). The abiotic parameters specific to this tidal flat exhibited a large spatial heterogeneity and temporally varying conditions.

General ecological parameters

The observed values of temperatures and light intensities measured throughout August were characteristic for late arctic summer conditions (Laska, Witoszova, and Prosek 2012). The *in situ* average irradiance reported throughout the study period was about $267 \mu\text{mol m}^{-2} \text{s}^{-1}$, suggesting predominant low-light conditions throughout August. While we reported sub-zero atmospheric temperatures occasionally during the study period, the water heat capacity allowed the water temperature to remain above zero preventing the microphytobenthos from freezing. Large daily temperature variations within the microphytobenthos were reported, ranging between 0.7°C to 9.9°C and were due to the periodic movement of tidal waters. Across the tidal flat, the transects III and I revealed significant differences in salinity concentrations and density properties. These observations support the clear differing impacts of both marine oceanic current (TI) and fresh water discharges (TIII) at play locally and highlight the importance of arctic riverine inputs during the summer period. We found consistency with this observation given the local topography and hydrography reporting two freshwater discharges; one across TIII (Adventelva river) and a second one across TII. TI was not reported to receive any direct freshwater inputs and hence was mostly dominated by transformed arctic water (~ 34.7 PSU) inputs gradually attenuated by local freshwater run-off. Although, we did obtain a significant statistical test score for salinity, we ought to contrast this result mentioning that all samples could not be taken strictly at the same time on the same day. Hence, the statistical scores may have been affected by the local hydrographic tidal evolution throughout the course of the sampling collection. An effort was made to carry out sampling procedures both during low tide and high tides in different days, as to obtain the most representative data set. However, because of the influence of the tidal cycle on the local salinity the time

between the first sampling and the last one may have influenced in-situ salinity readings. The sampling procedure was methodically collected by transect from T1.1 site to T11.4 site and lasted approximately between two to three hours. All salinity readings were retrieved from their respective sites across the tidal flat and at the specific in-situ temperature. Specific in-situ temperatures also may have slightly influenced salinity readings, as salinity decreases relatively to increasing temperature. This statement is in line with the observed concurrent temporal decrease of water temperature and water salinity overtime. As salinity is correlated to water density, similar findings and statistical results concerning water density give us additional weight to our conclusions.

Organic carbon was reported to be significantly different between T11 and T12 alike pH and sediment moisture spatial distribution patterns. We reported a significant decrease in sediment organic carbon content along T11 compared to T12 positively correlated with sediment moisture content and negatively correlated with water pH. It may suggest that *Vaucheria* sp. benthic community may actively affect the sediment structure across the seafloor, indirectly affecting sediment moisture and sediment organic carbon content. One referenced biological process developed by benthic microalgae and reported to affect the sediment is known as biostabilisation (Blanchard et al. 2000). This biological process depends on the release of extracellular polymeric substances (EPS or “slime”) as a secondary waste product of the photosynthetic microbial production. EPS acts as a cohesive agent, sticking sediment particles together, hence potentially improving the sediment stability locally and reducing resuspension (Decho and Gutierrez 2017). EPS is rapidly metabolized by various bacterial communities (Andersson, Dalhammar, and Kuttuva Rajarao 2011). Furthermore, although there have been only little recent studies focused on the priming effect occurring in aquatic ecosystems, we believe that this process may be herein linked to the spatial heterogeneity of organic carbon content across the seafloor. The priming effect is defined as the enhanced microbial decomposition response developed along with increased input of labile soil organic matter from neighbouring algal communities (Fontaine, Mariotti, and Abbadie 2003; Blagodatsky et al. 2010). The priming effect is not well studied in aquatic ecosystems, but it is a common response reported in terrestrial ecosystems (Guenet et al. 2010; Blagodatsky et al. 2010). The priming effect may be particularly important in peatland ecosystems where decomposition is often limited by the availability of labile organic matter (Bergman, Svensson, and Nilsson 1998). Herein, we speculate on the potential of algal-microbial ecological interactions by supposing that the presence of extensive algal mats produces hot-spots of microbial activity and where heterotrophic microbial decomposers receive subsidies boosting up the consecutive breakdown of organic matter. Overall it results locally in lower organic carbon content due to a higher systemic efficiency ratio at using and breaking down labile organic matter. Organic carbon storage is a key component of the soil fitness affecting its physical, chemical, and biological properties.

Hydrochemical and biogeochemical parameters

We did not detect any significant spatial differences between transects by means of statistical tests, with respect to the local hydrochemistry or sediment chemistry. This might have been due to the size of the sample size. A bigger sample size could have enabled us to better detect differences across the tidal flat and throughout the duration of the field sampling. Moreover, as mentioned before the duration of the sampling and the differential time of collection between the first site and the last site, may have affected the results. The tidal flat hydrodynamic although rather weak together with the periodic movement of tidal waters are other factors may have affected our results considerably, thus hindering the power of the statistical tests to detect any significant differences between transects. When estimating chemical concentrations, the need for a relevant methodology and efficiency in the processing of the sample must be adopted.

Abiotic PCA summary

Several principal component analyses were performed in this study, aiming at detecting specific abiotic patterns as well as to capture the full extent of the ecological scope found across this tidal flat. In the consistent set of PCAs assessing the distribution of the sites and transects over the tidal flat, we noticed some strong spatial heterogeneity. TIII was found correlated with low variance of NO₂-N and high variance of NO₃-N and TN. This may suggest a potential source of nitrogen locally across TIII in combination with high rates of nitrification further confirming the hypothesis of an adjacent associated benthic algae community. TI and TII seemed to locate toward the right-hand side of the PCA (Figure II-8) accordingly with high variance of Mg, Na, K, Ca, SO₄, TP & P-PO₄. While we can cluster TI & TIII (y axis) based on TN, NH₄-N & NO₃-N we can similarly cluster TI & TII (x axis) based on Mg, Na, K, Ca, SO₄, TP, NO₂-N & P-PO₄. TI & TII are alike with respect to their variance in the concentration of chemicals they present. This could suggest the hydro-chemical input of sea water to the tidal flat. Regarding the site-specific surface hydrochemistry, two sites seemed to fall out from a general clustered trend, including TIII.4 and TII.1. TIII.4 displayed the lowest variance for NO₂-N together with the highest variance for NO₃-N for all sites included, suggesting potential nitrifying bioprocesses. TII.1 was found with the lowest variance for Si, NH₄-N & Mn. The divergence of TII.1 was expected as TII.1 was situated directly where a freshwater input was flushing out inside the tidal flat.

Concerning the sediment chemistry spatial distribution over the tidal flat, we found a rather strong spatial uniformity at the site & transect scale. All sites were observed to project toward the centre of the PCA with no big differences among sites. In general, TII was found to be the most different of all transects with TII.1 observed to slightly diverge toward the right of the plot with higher variance in NO₃-N. This could indicate the direct mechanical and biochemical impact of freshwater outflows on the ecology of the tidal flat. As we did not find any differences specifically distinguishing TIII from the rest of the transects this goes against our initial hypothesis of the potential effect of the microphytobenthos on the sediment. We could speculate that either the differences are not fairly represented using this multivariate method especially knowing that we methodically inputted new values when we lacked some of the data as explained in the paragraph statistical analysis, or that there are no differences whatsoever.

Hydrochemical and biogeochemical temporal evolution

Overtime, several chemical compounds have revealed significant differences over the two sampling dates (9.08 and 25.08.2017) both in the water and in the sediment. We reported a significant temporal difference between the mean ranks for the two respective sampling dates on the 9.08 and 25.08.2017, for the following chemicals: NO₂-N, TN, P-PO₄, TP, Na, Si, SO₄, K, Ca, Mg and in the sediment NO₃-N and P-PO₄.

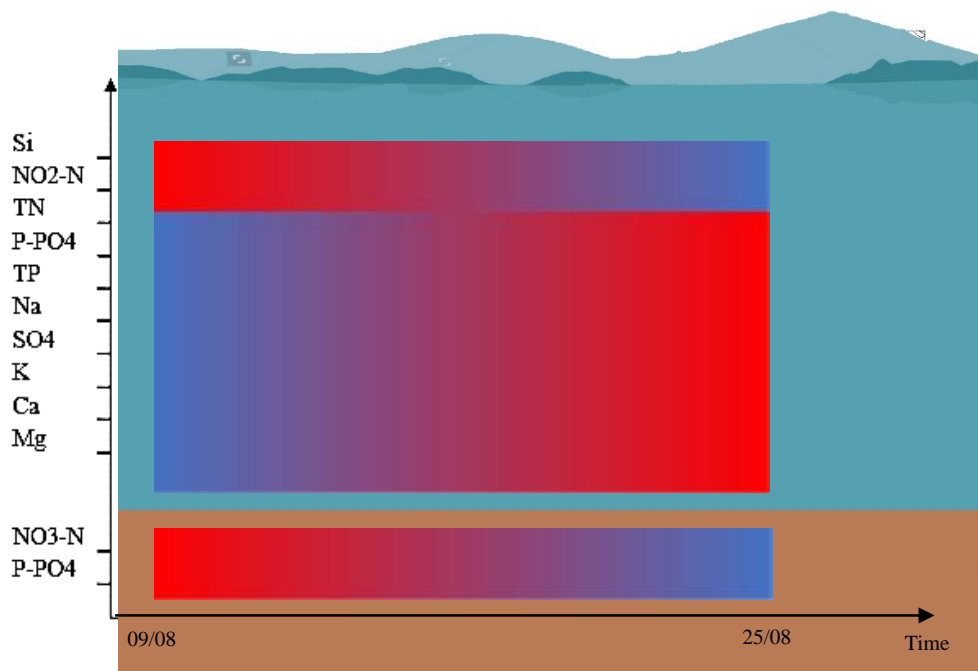


Figure II-18 Qualitative temporal evolution of a specific set of biochemical parameters across Adventdalen-adventfjorden's tidal flat including: NO₂-N, TN, PO₄-P, TP, Mg, Si, SO₄, K, Na, Ca in the water surface layer & NO₃-N, PO₄-P in the sediment surface layer. The monitoring took place during the month of August 2017 from the 09/08 to the 25/08/17. Red = high concentrated & Blue = low concentrated.

Across the water surface, Si & NO₂-N concentrations have revealed to significantly decrease while TN, PO₄-P, TP, Mg, SO₄, K, Na & Ca appeared to significantly increase overtime. Furthermore, across the sediment surface both NO₃-N & PO₄-P were found to significantly decrease overtime.

Nitrogen and phosphorus-based compounds are major nutrients for algal growth & productivity. Often in estuarine environments, algae represent a major sink of nitrogen and phosphorus-based compounds. Phosphorus is typically taken up by microalgae via two mechanisms. In the first mechanism, phosphorus is assimilated for the production of essential intracellular biomolecules such as phospholipids, ATP and nucleic acids. In the second mechanism referred as luxury uptake, microalgae can take up phosphorus when in excess and store it as inorganic polyphosphate granules (Schmidt, Gagnon, and Jamieson 2016). These polyphosphate reserves can sustain prolonged algal growth under limiting phosphorous conditions (Oliver and Ganf 2000). Microalgae actively assimilate phosphorus from the surrounding water column mainly as inorganic orthophosphate (Becker 1994). Similarly to phosphorus, Nitrogen can be assimilated directly for the production of key organic cellular compounds or can be internally stored under excess Nitrogen conditions in a mechanism alike the luxury phosphorous uptake (Larsdotter 2006). Nitrogen is mainly assimilated as ammonium (NH₄-N) and nitrate (NO₃-N) to a lesser extent nitrite (NO₂-N) can also be used as a nitrogen

source (Oliver and Ganf 2000). Typically, the preferred nitrogen source of microalgae is ammonium (NH₄-N) but alternative nitrogen sources may be used under specific ecological circumstances (Bhaya, Schwarz, and Grossman 2000). In addition to major nutrients (Carbon, Phosphorous, Nitrogen, Oxygen & Silica) microalgae also require oligo-elements (magnesium, potassium, calcium, iron, zinc & copper) for optimal algal growth and reproduction (Schmidt, Gagnon, and Jamieson 2016).

We observed locally a clear decrease in nitrite overtime, yet we did not find any significant temporal differences in ammonium or nitrate concentrations. The Total nitrogen concentration in the surface water did demonstrate a significant increase overtime though. We interpreted this overall temporal increase, with regard to our results, as a strong increase in total kjeldahl nitrogen (ammonia, organic and reduced nitrogen) overcasting the decrease in nitrite and suggesting post-bloom high decomposition rates toward the end of the summer season (post-growing season). We strongly doubt that ammonium concentrations remained stable overtime meaning that microphytobenthic algae solely based their nitrogen demands on nitrite as a nitrogen source. Especially when considering the potential toxicity of nitrite compounds uptake for microalgae, under high concentrations (Becker 1994). Our lack of success to identify any temporal differences with respect to ammonium concentrations may fall in an array of errors brought via the sampling procedure (hydrodynamic, tidal movement, sample size, time of sampling etc...) or errors in the methodology used. Nevertheless, based on these results, we could potentially report the ability of benthic *Vaucheria* sp. to tolerate alternative nitrogen sources. Orthophosphate was reported to be limiting across the tidal flat as suggested by N:P:Si ratio. As a result of the statistical tests we demonstrated an increase in P-PO₄ overtime within the tidal flat. This positive trend was further confirmed by the concurrent increase in Total phosphorus over the duration of the field sampling. These observations may be connected to the timing of the sampling. During the beginning of the sampling at the onset of August, observed P limiting conditions across the tidal flat may have suggested the significant impact of the local microbenthic algae removal. Then toward the end of August and the end of the growing season, microbenthic algae potentially filled up with polyphosphate reserves accumulated overtime, ceased from taking up available phosphate. In a context of arctic summer conditions, we could speculate that microalgae opt for early fast and short growth scenarios in which they build up phosphorous reserves to sustain post-growing season heterotrophic growth. The temporal increase in Total phosphorous also indicates the presence of a local input and accumulation of phosphorous within the tidal flat most likely brought by local marine currents as TP concentrations increased concurrently with Mg, Na, K, Ca & SO₄ concentrations overtime. This was further confirmed to be positively correlated from the hydro-chemical principal component analysis with TI closely distributed toward higher variances in TP, Mg, Na, K, Ca & SO₄.

In the consistent temporal evaluation of the chemical supplies in the surface of the sediment NO₃-N and P-PO₄ were reported to decrease significantly between the two sampling dates. Algae associated micro bacterial communities dwelling at the surface of the sediment may be one explanation for the significant decrease in NO₃-N and P-PO₄, directly in line with our previous hypothesis on the priming effect exerted by

benthic micro algae. In a second hypothesis, nutrients used by benthic microalgae may have originated not only from the water column but also from the sediment itself after bacterial decomposition. As we highlighted earlier the limiting phosphorus conditions observed in the water column along with no significant phosphorus supply difference overtime, we could speculate that *Vaucheria* sp. may be tightly associated with benthic surficial microbial communities potentially assimilating orthophosphate originating from the local decomposition of organic matter. Furthermore, benthic microorganisms and extensive algae surficial biofilms play a key role in capping the sediments and preventing nutrient resuspension to the overlying water column.

The study of the N:P:Si ratio inherent to this tidal flat concluded that the water column was overall P limited. It also showed that over the course of the field sampling, P limiting conditions were supplanted by Si limiting conditions when approaching the winter season. This significant depletion in silica concentration in the surface water overtime was further detected and confirmed, using a Kruskal-Wallis rank sum test (p-value = 0.009292). This decrease in silicon concentration in the overlying water toward the end of the summer season was recorded in other studies and typically associated with a shift in the estuarine community composition (Barranguet 1997; Facca, Sfriso, and Socal 2002). Either benthic diatoms may have undergone re-suspension (Koster and Pienitz 2006) or the local pelagic diatoms may have outcompeted the tidal flat ecosystem by forming a late summer abundance peak (June et al. 2007). Further investigations would be needed to more accurately determine the sink of this silica removal. At the beginning of August, the local P-limiting conditions suggest that mainly phosphate was removed from the water column supposedly by the prevailing microbenthic community. Towards the end of August, the increasing PO₄-P concentration in the water may suggest the end of the microphytobenthic growing period characterised by a gradual decline in phosphate removal rates.

***Vaucheria* sp. Ecological distribution**

We clearly demonstrated the strong contribution of *Vaucheria* sp. algae to the ecosystem photosynthetic productivity, affecting coastal carbonate cycle with higher pH associated to algal presence. Indeed, when bicarbonate is used by microalgae for photochemistry, the pH in the water medium incidentally increases as a function of the chemical reaction: $\text{HCO}_3^- \rightarrow \text{CO}_2 + \text{OH}^-$. This pH increase may significantly affect the overall water chemistry. With hardly no microphytobenthic algae over transect II the resulting pH was significantly lower than over transect III as the direct removal of CO₂ by phototrophic algae for photosynthetic production is increasing the pH. Similarly, to salinity samplings the same sampling procedure was adopted for all other measurements including pH. The samplings consecutively explored by transects from TI.1 site to TIII.4 site overall taking about two hours to be carried out. PH was registered both at low tide and high tide over the sampling period. Due to high turbidity at high tide no significant changes in pH was registered spatially across the tidal flat. Yet during low tide when turbidity did not affect the photosynthetic efficiency of microphytobenthic algae we reported significant differences between TIII and TII. The overall average pH combining low tide & high tide measurements provided a positive statistical score

validating the strong involvement of the microphytobenthos to the tidal flat ecosystem photosynthetic productivity. As moisture exhibited the same spatial heterogeneity over the tidal flat with lower percentage over algal inhabited areas. We concluded that there might be specific relationship between the presence of microphytobenthic algae and the sediment moisture content. Since moisture is function of the structure of the sediment. Microphytobenthic algae may have a strong effect on constitutive structure of the sediment indicating algal potential for bio stabilisation of the sediment (Blanchard et al. 2000).

Although we noticed a statistically significant difference between the salinity over TIII and TI, it did not seem to restrain *Vaucheria* sp. establishment over the seabed. Therefore, *Vaucheria* sp. was presumed to effectively withstand brackish salinity conditions as well as large sudden changes in salinity over daily tidal cycles.

***Vaucheria* sp. community photosynthetic profile**

With maximum irradiances potentially reaching up $1500 \mu\text{mol per m}^{-2} \text{ s}^{-1}$ in rare clear midsummer days, the arctic light climate constitutes a significant actinic source for photochemistry (Sakshaug, Johnsen, and Kovacs 2011). Yet, overall the annual mean incident arctic light climate is considered as low-light hindered by 11 weeks of 24-hour darkness polar night season. Typical arctic low-light conditions might be therefore selecting for low-light photoacclimated species, or fast high light photoacclimating species (Clark et al. 2013). The ex-situ photosynthetic monitoring of *Vaucheria* community did not show any signs of photoinhibition even when exposed to excess light for short periods of time. It suggested a remarkable physiological plasticity and good photoacclimation of *Vaucheria* sp. community, able to utilize a large range of incident light intensities with proportionally correlated photosynthetic outcomes. Indeed, under high PAR values (about $650 \mu\text{mol per m}^{-2} \text{ s}^{-1}$), CO_2 assimilation rates and ETR were not affected.

At the light intensity of $50 \mu\text{mol m}^{-2} \text{ s}^{-1}$ The $P_{\text{gross}}:R_d$ ratio was reported to be inferior to 1, suggesting that in this light conditions P_{gross} was inferior to R_d . It shows that under low-light conditions around $50 \mu\text{mol m}^{-2} \text{ s}^{-1}$ the primary production of the *Vaucheria* community becomes negative. Although, it has not been reported in this community of *Vaucheria* sp. so far, mixotrophy is common among polar microbenthic organisms. Algal mixotrophy was reported in several occasion across the polar regions and is regarded as an important ecological strategy developed by polar microorganisms (Laybourn-Parry and Marshall 2003; Moorthi et al. 2009).

The photosynthetic efficiency (α) was relatively stable around 0.00641 ± 0.00061 regardless of the light intensity to which *Vaucheria* sp. community was exposed. However, we observed significant positive changes in the maximum photosynthesis (P_{max} or ETR_{max}) when exposed to increasing irradiance. Since changes in the photosynthetic efficiency (α) are most likely related to changes in the photosystem stoichiometry or changes in the cell volume, respiration rates and chemical composition (Chow et al. 1990), such strategies may be inefficient for the fast acclimation to changing conditions typical for the eulittoral zone.

Yet, pigment-related changes such as changes in the amount and ratios of photosynthetic and photoprotective pigments may help *Vaucheria* sp. to fast acclimate to these hypervariable conditions, maybe explaining *Vaucheria* sp. remarkable physiological plasticity and concurrent increase in maximum photosynthesis (P_{max} or ETR_{max}) under higher light expositions. Further investigations regarding *Vaucheria* sp. pigment constitution in the course of diel and annual cycles would confirm the latter hypothesis.

The observed values of I_{comp} were approximately ten times higher than those recorded in extremely shaded benthic or sea ice algae (Clark et al. 2013; Glud, Rysgaard, and Kühl 2002; Kühl et al. 2001; Roberts et al. 2002; Roeselers et al. 2007), but they were comparable to water C3 plants (Van, Haller, and Bowes 1976). The higher values may either correspond to photoacclimation to higher irradiances on the surface, or it may reflect the high amount of non-photosynthetic rhizoid biomass in samples.

The observed I_{sat} values belonged to low-light adapted microbenthic species, as being about 10 times higher in comparison to high-light adapted polar benthic or sea ice algae (Clark et al. 2013; Glud, Rysgaard, and Kühl 2002; Kühl et al. 2001; Roberts et al. 2002; Roeselers et al. 2007). This observation was in line with the typical overall low-light conditions experienced across the Arctic (Clark et al. 2013). I_{sat} is an indicator of the efficiency of the photosynthetic electron transport rate. Hence, the higher I_{sat} the higher the ETR. As for CO_2 assimilation rate measurements they are dependent on the rate of enzymatic reactions of the Calvin-Benson cycle and therefore not light-dependent (Falkowski and Raven 2007). Indeed, while the CO_2 assimilation rate did not show any significant changes under increasing PAR irradiances, ETR was reported to be light-dependent. Since the P-E curve based on CO_2 assimilation showed increasing photosynthetic rates with no signs of enzymatic downturn under increasing PAR irradiances, the effective photoacclimation mechanism was further confirmed effectively supporting increasing photosynthetic productions.

Conclusion

As a conclusion, *Vaucheria* sp. microbenthic community showed signs of a remarkable physiological plasticity and good adaptation to these arctic hypervariable ecological conditions. *Vaucheria* sp. was found to be temperature-resilient as it was reported to tolerate large daily temperature variations due to the periodic movement of tidal waters. Alike polar terrestrial microorganisms, *Vaucheria* sp. was reported to tolerate rapid temperature changes of about 5 °C within one to two hours interval and low temperatures down to 1.4°C (Pushkareva et al. 2017). We reported strong evidences that this microbenthic community might hold a higher complexity than previously expected with signs of unidentified local nutrient sinks and temporally-varying hydro-chemical conditions as well as higher respiration outcomes to P_{gross} production under low-light PAR intensities. This latter observation may also suggest the hypothetic mixotrophic strategy adopted by *Vaucheria* sp. Further microscopic and genetic investigations would help us to adequately identify the complexity of this microphytobenthic community associated with *Vaucheria* sp. The significant spatial correlation between the presence of microphytobenthic algae and the local sediment moisture and organic carbon content across the studied area indicated the impact of the microphytobenthos on the sediment's

physicochemical characteristics. Although, we did not directly investigate the stability of the sediment herein, the microphytobenthos has been reported in several papers to improve the biostability of the seafloor via the secretion of “EPS or slime”. We speculate that the latter ecological observations may be an indirect consequence of the biostabilisation of the sediment by this microphytobenthic community. Further investigation would be necessary to confirm the hypothetical biostabilizing effect of this *Vaucheria* sp. community on its ecosystem.

At the ecosystem level, the significant microphytobenthos’ photosynthetic activity was supported by the detection of locally-high water pH values, correlated to *Vaucheria* sp. spatial occurrence. Ex situ measurements combining gasometric and Chlo a fluorescence methods provided a consistent and reliable profile of this *Vaucheria* sp. photosynthetic performances. *Vaucheria* sp. was able to utilize a wide spectrum of PAR intensities with no photoinhibition detected whatsoever from ten to 650 $\mu\text{mol per m}^{-2} \text{ s}^{-1}$. It demonstrated the good photoacclimation developed by *Vaucheria* sp.. In a brief summary, *Vaucheria* sp. photosynthetic activity was defined by an average photosynthetic efficiency (α) of 0.00641 ± 0.00061 relatively stable throughout the intensity range to which it was exposed. The maximum photosynthesis (Pmax) increased relatively with increasing light intensities ranging from 0,756 to 1,188 $\text{nmol g}^{-1} \text{ s}^{-1}$. The average Icomp was equal to 38,53 $\mu\text{mol m}^{-2} \text{ s}^{-1}$ approximately ten times lower than extremely shaded benthic or sea ice algae analogs (Clark et al. 2013; Glud, Rysgaard, and Kühl 2002; Kühl et al. 2001; Roberts et al. 2002; Roeselers et al. 2007). Based on the Icomp value *Vaucheria* sp. seemed to be low-light adapted. Furthermore, *Vaucheria* sp. was capable of fast photo-acclimation through the consecutive transition from low to high incoming light irradiances. This quality of *Vaucheria* sp. is probably linked to state transitions or effective xanthophyll cycle.

References

- Aberle-Malzahn, Nicole. 2004. “The Microphytobenthos and Its Role in Aquatic Food Webs.” *Mathematisch-Naturwissenschaftlichen Fakultät*, no. January 2004: 150.
- Andersson, Sofia, Gunnel Dalhammar, and Gunaratna Kuttuva Rajarao. 2011. “Influence of Microbial Interactions and EPS/Polysaccharide Composition on Nutrient Removal Activity in Biofilms Formed by Strains Found in Wastewater Treatment Systems.” *Microbiological Research* 166 (6): 449–57. <https://doi.org/10.1016/j.micres.2010.08.005>.
- Anisimov, Oleg A., Terry Callaghan, Christopher Furgal, Terry D. Prowse, and David G. Vaughan. 2007. “Polar Regions (Arctic and Antarctic),” 653–85.
- Baker, A.L., and et al. 2012. “Phycokey -- an Image Based Key to Algae (PS Protista), Cyanobacteria, and Other Aquatic Objects.” 2012. <http://cfb.unh.edu/phycokey/phycokey.htm>.
- Barranguet, C. 1997. “The Role of Microphytobenthic Primary Production in a Mediterranean Mussel Culture Area.” *Estuarine, Coastal and Shelf Science* 44 (6): 753–65. <https://doi.org/10.1006/ecss.1996.0153>.
- Becker, E.W. 1994. *Microalgae: Biotechnology and Microbiology*. Cambridge.
- Berge, Jørgen, Geir Johnsen, Frank Nilsen, Bjoørn Gulliksen, and Dag Slagstad. 2005. “Ocean Temperature Oscillations Enable Reappearance of Blue Mussels *Mytilus Edulis* in Svalbard after a 1000 Year Absence.” *Marine Ecology Progress Series* 303: 167–75. <https://doi.org/10.3354/meps303167>.

- Bergman, Inger, Bo H. Svensson, and Mats Nilsson. 1998. "Regulation of Methane Production in a Swedish Acid Mire by PH, Temperature and Substrate." *Soil Biology and Biochemistry* 30 (6): 729–41. [https://doi.org/10.1016/S0038-0717\(97\)00181-8](https://doi.org/10.1016/S0038-0717(97)00181-8).
- Bhaya, Devaki, Rakefet Schwarz, and Arthur R. Grossman. 2000. "Molecular Responses to Environmental Stress." *The Ecology of Cyanobacteria*, 397–442. https://doi.org/10.1007/0-306-46855-7_15.
- Blagodatsky, Sergey, Evgenia Blagodatskaya, Tatyana Yuyukina, and Yakov Kuzyakov. 2010. "Model of Apparent and Real Priming Effects: Linking Microbial Activity with Soil Organic Matter Decomposition." *Soil Biology and Biochemistry* 42 (8): 1275–83. <https://doi.org/10.1016/j.soilbio.2010.04.005>.
- Blanchard, G. F., D. M. Paterson, L. J. Stal, P. Richard, R. Galois, V. Huet, J. Kelly, et al. 2000. "The Effect of Geomorphological Structures on Potential Biostabilisation by Microphytobenthos on Intertidal Mudflats." *Continental Shelf Research* 20 (10–11): 1243–56. [https://doi.org/10.1016/S0278-4343\(00\)00021-2](https://doi.org/10.1016/S0278-4343(00)00021-2).
- Brandini, Frederico P., Eduardo T. da Silva, Franciane M. Pellizzari, Alessandra L.O. Fonseca, and Luciano F. Fernandes. 2001. "Production and Biomass Accumulation of Periphytic Diatoms Growing on Glass Slides during a 1-Year Cycle in a Subtropical Estuarine Environment (Bay of Paranaguá, Southern Brazil)." *Marine Biology* 138 (1): 163–71. <https://doi.org/10.1007/s002270000427>.
- Briney, Amanda. 2018. "Arctic Ocean or Arctic Seas?" ThoughtCo. 2018. [thoughtco.com/arctic-seas-overview-1435183](https://www.thoughtco.com/arctic-seas-overview-1435183).
- Brouwer, J.F.C. De, and L.J. Stal. 2001. "Short-Term Dynamics in Microphytobenthos Distribution and Associated Extracellular Carbohydrates in Surface Sediments of an Intertidal Mudflat." *Marine Ecology Progress Series* 218: 33–44.
- Changsheng, Chen. 2014. "The Circulation in the Arctic and Adjacent Oceans." 2014. <http://fvcom.smast.umassd.edu/2014/01/27/6-research-circulation-simulation/>.
- Christensen, T. 1987. "Seaweeds of the British Isles. Vol. 4. Tribophyceae (Xanthophyceae)." *London: British Museum (Natural History)*, 1–36.
- Clark, Graeme F., Jonathan S. Stark, Emma L. Johnston, John W. Runcie, Paul M. Goldsworthy, Ben Raymond, and Martin J. Riddle. 2013. "Light-Driven Tipping Points in Polar Ecosystems." *Global Change Biology* 19 (12): 3749–61. <https://doi.org/10.1111/gcb.12337>.
- Cokelet, Edward D, Nicole Tervalon, and James G Bellingham. 2008. "Hydrography of the West Spitsbergen Current , Svalbard Branch : Autumn 2001." *JOURNAL OF GEOPHYSICAL RESEARCH*. 113 (August 2007): 1–16. <https://doi.org/10.1029/2007JC004150>.
- Comiso, Josefino C, Claire L Parkinson, Robert Gersten, and Larry Stock. 2008. "Accelerated Decline in the Arctic Sea Ice Cover" 35 (October 2007): 1–6. <https://doi.org/10.1029/2007GL031972>.
- Corlett, C. 1953. "Measurement of Primary Production in the Western Barents Sea" 144: 76–78.
- Dallman, WK, D Blomeier, S Elvevold, A Mørk, S Olausen, S-A Grundvåg, D Bond, and A Hormes. 2015. *Geoscience Atlas of Svalbard*. Edited by WD Dallmann. Tromsø: Norwegian Polar Institute.
- Dalpadado, Padmini, Kevin R. Arrigo, Solfrid S. Hjøllø, Francisco Rey, Randi B. Ingvaldsen, Erik Sperfeld, Gert L. Van Dijken, Leif C. Stige, Are Olsen, and Geir Ottersen. 2014. "Productivity in the Barents Sea - Response to Recent Climate Variability." *PLoS ONE* 9 (5). <https://doi.org/10.1371/journal.pone.0095273>.
- Decho, Alan W., and Tony Gutierrez. 2017. "Microbial Extracellular Polymeric Substances (EPSs) in Ocean Systems." *Frontiers in Microbiology* 8 (MAY): 1–28. <https://doi.org/10.3389/fmicb.2017.00922>.
- Dell, I. 2012. "Dell Statistica (Data Analysis Software System), Version 13." [software.dell.com](https://www.dell.com).
- Drobot, Sheldon, Julianne Stroeve, James Maslanik, William Emery, Charles Fowler, and Jennifer Kay. 2008. "Evolution of the 2007 – 2008 Arctic Sea Ice Cover and Prospects for a New Record in 2008" 35: 1–5. <https://doi.org/10.1029/2008GL035316>.

- Eakins, B.W., and G.F. Sharman. 2010. "Volumes of the World's Oceans from ETOPO1."
- Elvebakk, Arve, Pal Prestrud, O.M Skulberg, G.R. Hasle, C Helium von Quillfeldl, V Aistrup, Li. Gjærum, et al. 1996. *A Catalogue of Svalbard Plants, Fungi, Algae and Cyanobacteria*. Norsk Polarinstitutt, Skrifter.
- Elvevold, Synnøve, Winfried Dallmann, and Dierk Blomeier. 2007. *Geology of Svalbard*. Edited by Synnøve Elvevold. Tromsø: Norwegian Polar Institute. www.npolar.no.
- Facca, C., A. Sfriso, and G. Socal. 2002. "Changes in Abundance and Composition of Phytoplankton and Microphytobenthos Due to Increased Sediment Fluxes in the Venice Lagoon, Italy." *Estuarine, Coastal and Shelf Science* 54 (5): 773–92. <https://doi.org/10.1006/ecss.2001.0848>.
- Falkowski, P., and J. Raven. 2007. *Aquatic Photosynthesis: (Second Edition)*. Princeton. <http://www.jstor.org/stable/j.ctt4cgbxs>.
- Fontaine, Sébastien, André Mariotti, and Luc Abbadie. 2003. "The Priming Effect of Organic Matter: A Question of Microbial Competition?" *Soil Biology and Biochemistry* 35 (6): 837–43. [https://doi.org/10.1016/S0038-0717\(03\)00123-8](https://doi.org/10.1016/S0038-0717(03)00123-8).
- Frey, K. E., J. C. Comiso, L. W. Cooper, L. B. Eisner, R. R. Gradinger, J. M. Grebmeier, and J. -É. Tremblay. 2017. "Arctic Ocean Primary Productivity." 2017. <https://arctic.noaa.gov/Report-Card/Report-Card-2017/ArtMID/7798/ArticleID/701/Arctic-Ocean-Primary-Productivity>.
- Gattuso, J.-P, B. Gentili, C.M. Duarte, J. A. Kleypas, J. J. Middelburg, and D. Antoine. 2006. "Light Availability in the Coastal Ocean : Impact on the Distribution of Benthic Photosynthetic Organisms and Their Contribution to Primary Production," 489–513.
- Gazeau, Frédéric, Stephen V. Smith, Bernard Gentili, Michel Frankignoulle, and Jean-pierre Gattuso. 2004. "The European Coastal Zone : Characterization and First Assessment of Ecosystem Metabolism" 60. <https://doi.org/10.1016/j.ecss.2004.03.007>.
- Genty, Bernard, Jean Marie Briantais, and Neil R. Baker. 1989. "The Relationship between the Quantum Yield of Photosynthetic Electron Transport and Quenching of Chlorophyll Fluorescence." *Biochimica et Biophysica Acta - General Subjects* 990 (1): 87–92. [https://doi.org/10.1016/S0304-4165\(89\)80016-9](https://doi.org/10.1016/S0304-4165(89)80016-9).
- Glud, Ronnie N., Søren Rysgaard, and Michael Kühl. 2002. "A Laboratory Study on O₂ Dynamics and Photosynthesis in Ice Algal Communities: Quantification by Microsensors, O₂ Exchange Rates, ¹⁴C Incubations and a PAM Fluorometer." *Aquatic Microbial Ecology* 27 (3): 301–11. <https://doi.org/10.3354/ame027301>.
- Glud, Ronnie N., Jana Woelfel, Ulf Karsten, Michael Kühl, and Søren Rysgaard. 2009. "Benthic Microalgal Production in the Arctic: Applied Methods and Status of the Current Database." *Botanica Marina* 52 (6): 559–71. <https://doi.org/10.1515/BOT.2009.074>.
- Guenet, Bertrand, Luc Abbadie, Michael Danger, and Gerard Lacroix. 2010. "Priming Effect: Bridging the Gap between Aquatic and Terrestrial Ecology," no. November 2017: 1–3. <https://doi.org/10.1890/09-1968>.
- Guiry, M.D. 2008. "AlgaeBase: Vaucheria." World-Wide Electronic Publication, National University of Ireland, Galway. 2008. <http://www.algaebase.org>.
- Hattermann, Tore, Pål Erik Isachsen, Wilken Jon Von Appen, Jon Albretsen, and Arild Sundfjord. 2016. "Eddy-Driven Recirculation of Atlantic Water in Fram Strait." *Geophysical Research Letters* 43 (7): 3406–14. <https://doi.org/10.1002/2016GL068323>.
- Henley, W.J. 1993. "Measurement and Interpretation of Photosynthetic Light-Response Curves in Algae in the Context of Photoinhibition and Diel Changes." *Journal of Applied Phycology* 29: 729–39. <https://academic.oup.com/jxb/article-lookup/doi/10.1093/jxb/51.345.659>.
- Hrncirova, Michaela, Jiri Pospsil, and Michal Spilacek. 2013. "SIZE ANALYSIS OF SOLID PARTICLES USING LASER" 20 (3): 309–18.
- Ingólfsson, Ólafur. 2000. "Outline of the Geography and Geology of Svalbard."

- Jakobsson, Martin, Larry Mayer, Bernard Coakley, Julian A Dowdeswell, Steve Forbes, Boris Fridman, Hanne Hodnesdal, et al. 2012. "The International Bathymetric Chart of the Arctic Ocean (IBCAO) Version 3 . 0" 39: 1–6. <https://doi.org/10.1029/2012GL052219>.
- Jiménez Reyes, Ariam. 2013. "The ' Secret Garden ' : Microphytobenthic Biofilms and the Foraging Ecology of Calidridine Sandpipers."
- Johnson, L.R., R. Merritt, David M. John, Brian A. Whitton, and Alan J. Brook. 2012. "The Freshwater Algal Flora of the British Isles, 2nd Edition." In , John, D.M., 627:896.
- Jonge, V. N. de. 1995. "Dynamics and Distribution of Microphytobenthic Chlorophyll-a in the Western Scheldt Estuary (SW Netherlands)." *Hydrobiologia* 311 (1–3): 21–30. <https://doi.org/10.1007/BF00008568>.
- June, Published, Abigail Mcquatters-gollop, Dionysios E Raitsos, Martin Edwards, and Martin J Attrill. 2007. "Spatial Patterns of Diatom and Dinoflagellate Seasonal Cycles in the NE Atlantic Ocean" 339 (Micheli 1999): 301–6.
- Kersen, Priit. 2012. "First Findings of the Benthic Macroalgae *Vaucheria* Cf . *Dichotoma* (Xanthophyceae) and *Punctaria tenuissima* (Phaeophyceae) in Estonian Coastal Waters" 1995: 135–47. <https://doi.org/10.3176/eco.2012.2.05>.
- Kirk, John T. O. 2011. *Light and Photosynthesis in Aquatic Ecosystems, Third Edition*. Cambridge.
- Koster, Dorte, and Reinhard Pienitz. 2006. "Seasonal Diatom Variability and Paleolimnological Inferences – a Case Study," 395–416. <https://doi.org/10.1007/s10933-005-1334-7>.
- Kühl, Michael, Ronnie N. Glud, Jens Borum, Rodney Roberts, and Søren Rysgaard. 2001. "Photosynthetic Performance of Surface-Associated Algae below Sea Ice as Measured with a Pulse-Amplitude-Modulated (PAM) Fluorometer and O₂microsensors." *Marine Ecology Progress Series* 223 (November): 1–14. <https://doi.org/10.3354/meps223001>.
- Lantuit, Hugues, Pier Paul Overduin, Nicole Couture, Sebastian Wetterich, Felix Aré, David Atkinson, Jerry Brown, et al. 2012. "The Arctic Coastal Dynamics Database : A New Classification Scheme and Statistics on Arctic Permafrost Coastlines." *Estuaries and Coasts*, no. 35: 383–400. <https://doi.org/10.1007/s12237-010-9362-6>.
- Larsdotter, Karin. 2006. *Microalgae for Phosphorus Removal from Wastewater in a Nordic Climate*. <https://doi.org/ISBN: 91-7178-288-5>.
- Laska, Kamil, Denisa Witoszova, and Pavel Prosek. 2012. "Weather Patterns of the Coastal Zone of Petuniabukta, Central Spitsbergen in the Period 2008–2010." *Polish Polar Research* 32 (4): 1–6. <https://doi.org/10.2478/v10183>.
- Laybourn-Parry, Johanna, and William A. Marshall. 2003. "Photosynthesis, Mixotrophy and Microbial Plankton Dynamics in Two High Arctic Lakes during Summer." *Polar Biology* 26 (8): 517–24. <https://doi.org/10.1007/s00300-003-0514-z>.
- Lee, Robert Edward. 2008. *Phycology - Fourth Edition*. Cambridge University Press. <https://doi.org/10.1017/CBO9780511812897.002>.
- Leeuwe, M. A. Van, G. Morgan, and C. Brockmann. 2005. "Book of Protocols. A System of Hierarchical Monitoring Methods for Assessing Changes in the Biological and Physical State of Intertidal Areas" 3: 199.
- Longphuir, Sorcha Ni Leynaert, Aude, Jacques Grall, Jacques Clavier, François Le Loc'H, Iwan Le Berre, Laurent Chauvaud, Sainte-Marie Flye, and J. Joëlle Richard. 2007. "Primary Production and Spatial Distribution of Subtidal Microphytobenthos in a Temperate Coastal System, the Bay of Brest, France." *Estuarine, Coastal and Shelf Science, Elsevier*. 74 (3): 367–80.
- Longphuir, Sorcha Ní, Jae Hyun Lim, Aude Leynaert, Pascal Claquin, Eun Jung Choy, Chang Keun Kang, and Soonmo An. 2009. "Dissolved Inorganic Nitrogen Uptake by Intertidal Microphytobenthos: Nutrient Concentrations, Light Availability and Migration." *Marine Ecology Progress Series* 379: 33–44. <https://doi.org/10.3354/meps07852>.
- Ludvigsen, Martin, Jørgen Berge, Maxime Geoffroy, Jonathan H Cohen, Pedro R De La Torre, Stein M Nornes,

- Hanumant Singh, and Asgeir J Sørensen. 2018. "Use of an Autonomous Surface Vehicle Reveals Small-Scale Diel Vertical Migrations of Zooplankton and Susceptibility to Light Pollution under Low Solar Irradiance," no. January.
- Macintyre, H L, and J J Cullen. 1996. "Primary Production by Suspended and Benthic Microalgae in Aturbid Estuary: Time-Scales of Variability in San Antonio Bay,Texas." *Marine Ecology-Progress Series* 145 (1–3): 245–68. <https://doi.org/10.2307/24857330>.
- Mascarenhas, V. J., D. Voß, J. Wollschlaeger, and O. Zielinski. 2017. "Fjord Light Regime: Bio-Optical Variability, Absorption Budget, and Hyperspectral Light Availability in Sognefjord and Trondheimsfjord, Norway." *JOURNAL OF GEOPHYSICAL RESEARCH.*, 3828–47. <https://doi.org/10.1002/2016JC012610>.Received.
- Meier, Walter N., Greta K. Hovelsrud, Bob E.H. Van Oort, Jeffrey R. Key, Kit M. Kovacs, Michel Christine, Christian Haas, et al. 2014. "Arctic Sea Ice in Transformation: A Review of Recent Observed Changes and Impacts on Biology and Human Activity." *Rev. Geophys.*, no. 51: 185–217. <https://doi.org/10.1002/2013RG000431>.Received.
- Michon, Scott, and Kathryn Hansen. 2016. "Sea Ice." 2016. <https://earthobservatory.nasa.gov/Features/SeaIce>.
- Miller, Douglas C., Richard J. Geider, and Hugh L. MacIntyre. 1996. "Microphytobenthos: The Ecological Role of the 'Secret Garden' of Unvegetated, Shallow-Water Marine Habitats. II. Role in Sediment Stability and Shallow-Water Food Webs." *Estuaries* 19 (2): 202. <https://doi.org/10.2307/1352225>.
- Moorthi, Stefanie, David A. Caron, Rebecca J. Gast, and Robert W. Sanders. 2009. "Mixotrophy: A Widespread and Important Ecological Strategy for Planktonic and Sea-Ice Nanoflagellates in the Ross Sea, Antarctica." *Aquatic Microbial Ecology* 54 (3): 269–77. <https://doi.org/10.3354/ame01276>.
- Muckenhuber, S, F Nilsen, A Korosov, and S Sandven. 2016. "Sea Ice Cover in Isfjorden and Hornsund , Svalbard (2000 – 2014)," 149–58. <https://doi.org/10.5194/tc-10-149-2016>.
- National Snow and Ice Data Center. 2016. "All About Sea Ice." 2016. [/cryosphere/seaice/index.html](http://cryosphere/seaice/index.html).
- Nelson, James R., James E. Eckman, Charles Y. Robertson, Roberta L. Marinelli, and Richard A. Jahnke. 1999. "Benthic Microalgal Biomass and Irradiance at the Sea Floor on the Continental Shelf of the South Atlantic Bight: Spatial and Temporal Variability and Storm Effects." *Continental Shelf Research* 19 (4): 477–505. [https://doi.org/10.1016/S0278-4343\(98\)00092-2](https://doi.org/10.1016/S0278-4343(98)00092-2).
- Nikiforov, Sergey L, Roger Colony, and Leonid Timokhov. 2001. "Hydrochemical Atlas of the Arctic Ocean." *Arctic and Antarctic Research Institute of the Russian Federal Service for Hydrometeorology and Environmental Monitoring, International Arctic Research Center, University of Alaska, Fairbanks, St. Petersburg, CD-ROM Version 1.0*.
- Nürnberg, Dennis J, Jennifer Morton, Stefano Santabarbara, Alison Telfer, Pierre Joliot, Laura A Antonaru, Alexander V Ruban, et al. n.d. "Photochemistry beyond the Red Limit in Chlorophyll F–containing Photosystems." <https://doi.org/10.1126/science.aar8313>.
- Oliver, R.L., and G.G Ganf. 2000. *Freshwater Blooms*. In: Whitto. Springer, Dordrecht. https://doi.org/https://doi.org/10.1007/0-306-46855-7_6.
- Ott, Donald W., and R. Malcolm Brown. 1974. "Developmental Cytology of the Genus Vaucheria e Organisation of the Vegetative Filament." *British Phycological Journal* 9 (2): 111–26. <https://doi.org/10.1080/00071617400650151>.
- Paterson, Author D M, K H Wiltshire, A Miles, J Blackburn, I Davidson, M G Yates, J A Eastwood, D M Paterson, and S Mcgrorty. 2011. "Cohesive Sediments from Intertidal Reflectance of Spectral Mediation Microbiological" 43 (6): 1207–21.
- Pavlov, Alexey K, Vigdis Tverberg, Boris V Ivanov, Frank Nilsen, Stig Falk-, Alexey K Pavlov, Vigdis Tverberg, et al. 2013. "Warming of Atlantic Water in Two West Spitsbergen Fjords over the Last Century (1912–2009)" 8369 (May). <https://doi.org/10.3402/polar.v32i0.11206>.

- Perrette, Mahé, Graham D. Quartly, Andrew Yool, and Ekaterina E. Popova. 2011. "Near-Ubiquity of Ice-Edge Blooms in the Arctic," no. February. <https://doi.org/10.5194/bgd-7-8123-2010>.
- Polyakov, I V, Igor V Polyakov, Andrey V Pnyushkov, Matthew B Alkire, Igor M Ashik, Till M Baumann, C Eddy, et al. 2017. "Greater Role for Atlantic Inflows on Sea-Ice Loss in the Eurasian Basin of the Arctic Ocean" 8204 (April): 1–14.
- Popova, E E, A Yool, A C Coward, Y K Aksenov, S G Alderson, B A De Cuevas, and T R Anderson. 2010. "Control of Primary Production in the Arctic by Nutrients and Light : Insights from a High Resolution Ocean General Circulation Model," 3569–91. <https://doi.org/10.5194/bg-7-3569-2010>.
- Pushkareva, Ekaterina, Jana Kviderová, Miloslav Šimek, and Josef Elster. 2017. "Nitrogen Fixation and Diurnal Changes of Photosynthetic Activity in Arctic Soil Crusts at Different Development Stage." *European Journal of Soil Biology* 79: 21–30. <https://doi.org/10.1016/j.ejsobi.2017.02.002>.
- QGIS Development Team. 2018. "QGIS Geographic Information System. Open Source Geospatial Foundation Project." <http://qgis.osgeo.org>.
- Reddy, S.M. 2001. *University Botany – 1. Algae, Fungi, Bryophyta and Pteridophyta*. New Age. New Delhi: New Age International Publishers.
- Roberts, Rodney D., Michael Kühn, Ronnie Nøhr Glud, and Søren Rysgaard. 2002. "Primary Production of Crustose Coralline Red Algae in a High Arctic Fjord." *Journal of Phycology* 38 (2): 273–83. <https://doi.org/10.1046/j.1529-8817.2002.01104.x>.
- Roeselers, Guus, Tracy B. Norris, Richard W. Castenholz, Søren Rysgaard, Ronnie N. Glud, Michael Kühn, and Gerard Muyzer. 2007. "Diversity of Phototrophic Bacteria in Microbial Mats from Arctic Hot Springs (Greenland)." *Environmental Microbiology* 9 (1): 26–38. <https://doi.org/10.1111/j.1462-2920.2006.01103.x>.
- RStudio Team. 2016. "RStudio: Integrated Development for R." RStudio, Inc., Boston, MA. <http://www.rstudio.com/>.
- Rudels, Burt, Anne-marie Larsson, and Per-ingvar Sehlstedt. 2016. "Stratification and Water Mass Formation in the Arctic Ocean : Some Implications for the Nutrient Distribution" 8369. <https://doi.org/10.3402/polar.v10i1.6724>.
- Sakshaug, E., G. Johnsen, and K. Kovacs. 2011. *Ecosystem Barents Sea*.
- Schmidt, Jordan J., Graham A. Gagnon, and Rob C. Jamieson. 2016. "Microalgae Growth and Phosphorus Uptake in Wastewater under Simulated Cold Region Conditions." *Ecological Engineering* 95: 588–93. <https://doi.org/10.1016/j.ecoleng.2016.06.114>.
- Schneider, Craig W, Christopher E Lane, Source Northeastern Naturalist, Craig W Schneider, and Christopher E Lane. 2014. "Eagle Hill Institute TWO SPECIES OF VAUCHERIA NEW FOR NEW ENGLAND , V . LII AND V . RACEMOSA" 7 (1): 25–32.
- Serreze, Mark C, and Jennifer A Francis. 2006. "The Arctic on the Fast Track of Change" 65 - 69.
- Sigmon, D. E., and L. B. Cahoon. 1997. "Comparative Effects of Benthic Microalgae and Phytoplankton on Dissolved Silica Fluxes." *Aquatic Microbial Ecology* 13 (3): 275–84. <https://doi.org/10.3354/ame013275>.
- Stein, R., R.W. Macdonald, R.M.W. Amon, E. Bauerfeind, A. Boetius, G.I. Batova, J. Christensen, et al. 2004. *The Organic Carbon Cycle in the Arctic Ocean*. Edited by R. Stein and R.W. Macdonald. Springer.
- Stine, William, and Michael Geyer. 2001. *Power From The Sun*.
- The Editors of Encyclopaedia Britannica. 2018. "Vaucheria." Encyclopædia Britannica, Inc. 2018. <https://www.britannica.com/science/Vaucheria>.
- The Norwegian Polar Institute. n.d. "The Arctic System." <http://www.arcticsystem.no/en/outsideworld/oceancurrents/>.
- The world Factbook. 2011. "Oceans: Arctic Ocean." Central Intelligence Agency. 2011. https://www.cia.gov/library/publications/the-world-factbook/geos/print_xq.html.






























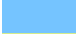
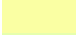

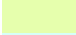

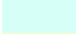

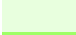















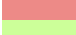







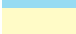
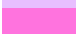
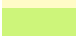
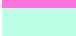

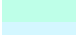

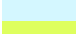

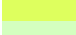





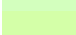

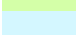


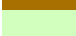

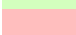

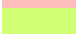

- Tremblay, J.E., and Jonathan Gagnon. 2009. "The Effects of Irradiance and Nutrient Supply on the Productivity of Arctic Waters : A Perspective on Climate Change Provided for Non-Commercial Research and Education Use . Not for Reproduction , Distribution or Commercial Use .," no. January. <https://doi.org/10.1007/978-1-4020-9460-6>.
- Van, T. K., W. T. Haller, and G. Bowes. 1976. "Comparison of the Photosynthetic Characteristics of Three Submersed Aquatic Plants." *Plant Physiology* 58 (6): 761–68. <https://doi.org/10.1104/pp.58.6.761>.
- Vesman, Anna V, Boris V Ivanov, and Vladimir A Volkov. 2017. "Changes in Thermohaline System on the West Spitsbergen Shelf since 1950 to Present Time Changes in Thermohaline System on the West Spitsbergen Shelf since 1950 to Present Time," no. June. <https://doi.org/10.5817/CPR2017-1-7>.
- Vetrov, Alexander, and Evgeny Romankevich. 2004. *Carbon Cycle in the Russian Arctic Seas*. <https://doi.org/10.1007/978-3-662-06208-1>.
- Vinje, Torgny. 2001. "Anomalies and Trends of Sea-Ice Extent and Atmospheric Circulation in the Nordic Seas during the Period 1864 – 1998," 255–67.
- Wilcox, M. D. 2012. "Occurrence of the Marine Yellow-Green Algae *Vaucheria Velutina* C. Agardh and *Vaucheria Longicaulis* Hopppaugh (Xanthophyceae: Vaucheriaceae) in Auckland, New Zealand." *New Zealand Journal of Marine and Freshwater Research* 46 (2): 285–90. <https://doi.org/10.1080/00288330.2011.622444>.
- Williams, SI, Sm Yarish, and Ip Gill. 1985. "Ammonium Distributions, Production, and Efflux from Backreef Sediments, St. Croix, US Virgin Islands ." *Marine Ecology Progress Series* 24 (2): 57–64. <https://doi.org/10.3354/meps024057>.
- Zacher, Katharina, Ralf Rautenberger, Dieter Hanelt, Angela Wulff, and Christian Wiencke. 2009. "The Abiotic Environment of Polar Marine Benthic Algae." *Botanica Marina* 52 (6): 483–90. <https://doi.org/10.1515/BOT.2009.082>.

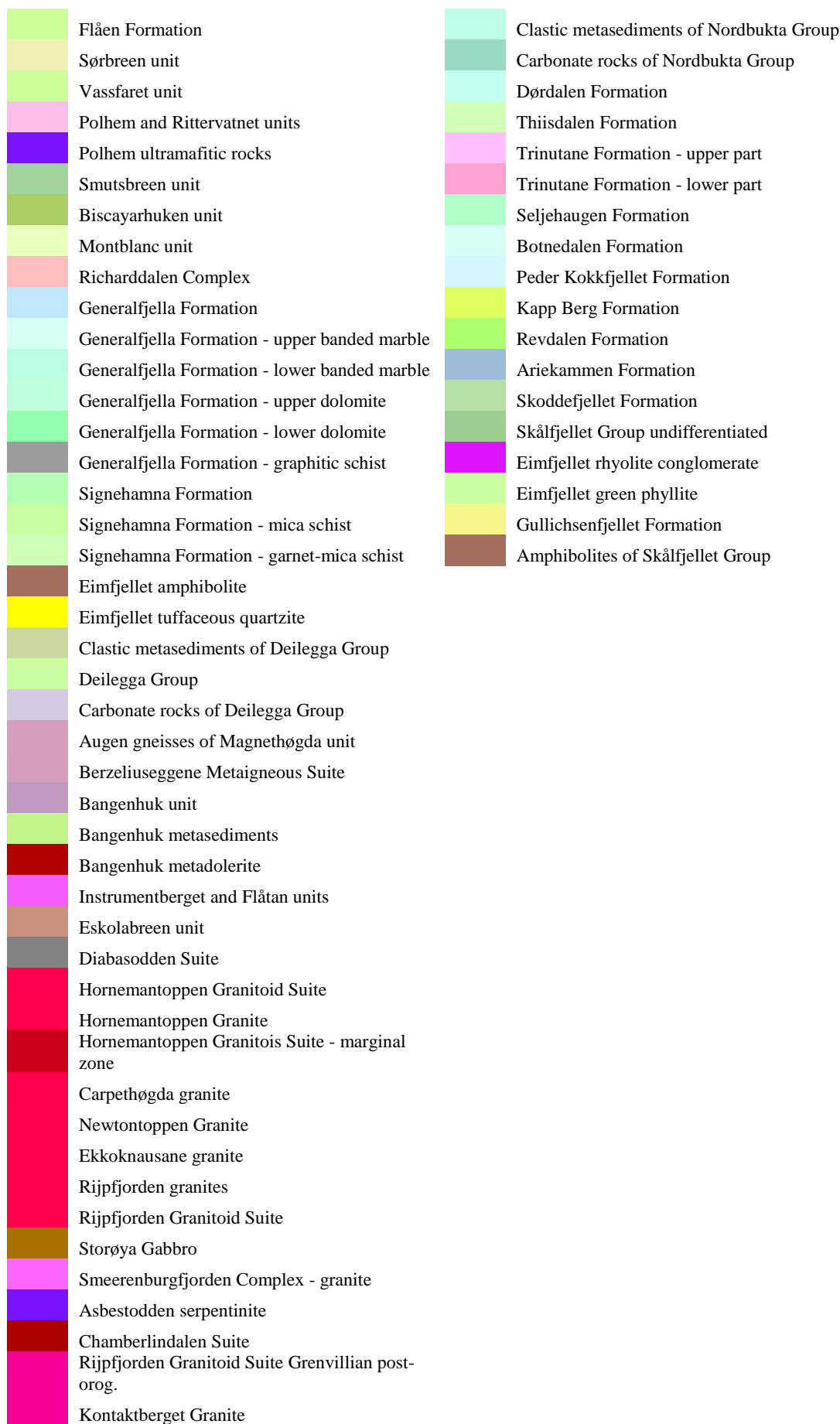
Annex

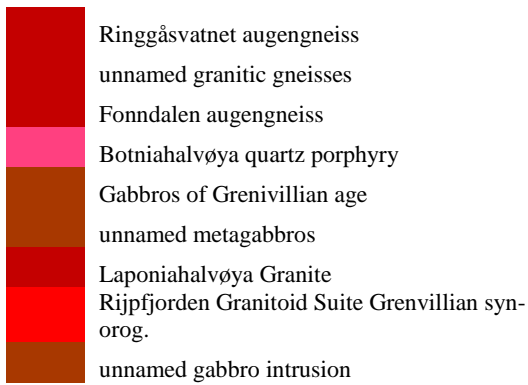
I. Legend Figure II.1. Geological Map of Svalbard

RGB	Value	RGB	Value
	marble in Comfortlessbreen Group		De Geerdalen Formation
	amphibolite in Nissenfjella Formation		Tschemakfjellet Formation
	moraine - unconsolidated		Skuld Formation
	Glacial deposits		Sassendalen Group
	marine deposit - unconsolidated		Botneheia Formation
	glaci-fluvial deposit - unconsolidated		Bravaisberget Formation
	other unconsolidated deposit		Vikingshøgda Formation
	Seidfjellet Formation		Vardebukta and Tvillingodden formations
	Marine and fluvial deposits		Tvillingodden Formation
	Bockfjorden Volcanic Complex		Vardebukta Formation
	Sverrefjellet Volcano		Urd Formation
	Halvdanpiggen Eruptive Centre		Tempelfjorden Group
	Sigurdfjellet Eruptive Centre		Kapp Starostin Formation
	Seidfjellet Formation		Miseryfjellet Formation
	Calypsostranda Group		Hambergfjellet Formation
	Buchananisen Group		Gipsdalen Group
	Sarstangen Formation		Dickson Land Subgroup
	Sarsbukta Formation		Gipshuken Formation
	Aberdeenflya Formation		Wordiekammen Formation
	Marchaislaguna Formation		Malte Brunfjellet Formation
	Krokodillen Formation		Malte Brunfjellet and Hårbardbreen formations
	Reinhardpynten Formation		Kapp Dunér Formation
	Sesshøgda Formation		Kapp Hanna Formation
	Selvågen Formation		Kapp Kåre Formation
	Van Mijenfjorden Group upper part		Landnørdingsvika Formation
	Van Mijenfjorden Group lower part		Treskelen Subgroup
	Brøggerbreen Formation		Treskelodden Formation
	Kongsfjorden Formation		Hyrnefjellet Formation
	Aspelintoppen Formation		Charlesbreen Subgroup
	Battfjellet Formation		Tårnkanten Formation
	Frysjaodden Formation		Petrellskaret Formation
	Grumantbyen Formation		Scheteligfjellet Formation
	Grumantbyen and Hollendardalen formations		Brøggertinden Formation
	Basilika Formation		Campbellryggen Subgroup
	Firkanten Formation		Minkinfjellet Formation
	Helvetiafjellet and Carolinefjellet formations		Ebbadalen Formation
	Carolinefjellet Formation		Hultberget Formation
	Helvetiafjellet Formation		Billefjorden Group
	Kong Karls Land Flows		Vegardfjellet Formation
	Janusfjellet Subgroup		Orustdalen Formation
	Rurikfjellet Formation		Sergejevffjellet Formation

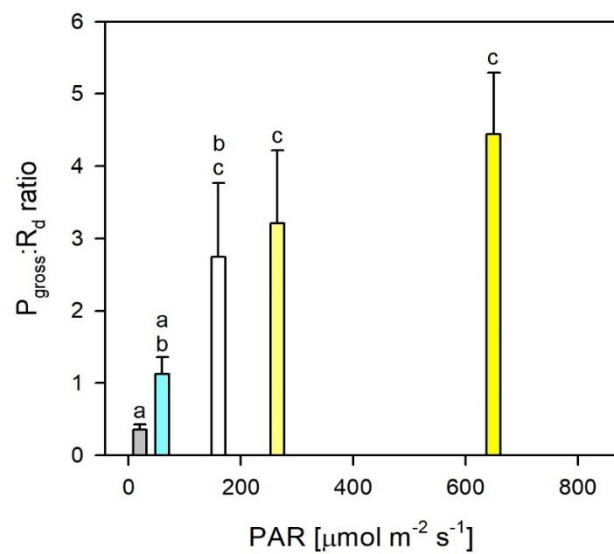
	Agardhfjellet Formation		Hornsundneset Formation
	Kapp Toscana Group		Nordkapp Formation
	De Geerdalen Form. & Wilhelmøya Subgroup		Røedvika Formation
	Wilhelmøya Subgroup		Carboniferous and Permian formations undiff.
	Svenskøya Formation		Adriabukta Formation
	Flatsalen Formation		Sutorfjella conglomerate
	Storfjorden Subgroup		Mimerbukta sandstone
	Småbreen sandstone		Vestgötabreen Complex
	Brotfjellet conglomerate		Vestgötabreen Complex - undifferentiated
	Germaniabekken conglomerate		blueshist and eclogite units
	Fotkollen sandstone - upper		schistose limestone unit
	Fotkollen sandstone - lower		phyllite unit
	Mimerdalen Subgroup		greenstone unit
	Plantekløfta Formation		magnesite rock unit
	Planteryggen Formation		Sørflya carbonate unit
	Fiskekløfta Member		Sørflya phyllite and mica schist unit
	Estheriahaugen Member		Malmberget unit - undifferentiated
	Wijde Bay Formation		Malmberget metapelite unit
	Grey Hoek Formation		Malmberget quartzite unit
	Forkdalen Member		Malmberget carbonate unit
	Tavlefjellet Member		Mefonna marble unit
	Skamdalen Member		Mefonna quartzite and mica schist unit
	Wood Bay Formation		Grampianfjella Group
	Verdalen Member		Grampianfjella Group - undifferentiated
	Dicksonfjorden Member		Craigtoppane unit
	Austfjorden Member		Antoniabreen carbonate rocks
	Marietoppen Formation		Gotiahelvøya Group
	Red Bay Group		Polarisbreen Group
	Widerøefjella Subgroup		West Coast Diamictite unit
	Ben Nevis Formation		Sofiebogen Group possible equivalents
	Schivefjellet Member		Scotiafjellet Group
	Drakehaugen member		Scotiafjellet Group
	Fränkelryggen Formation		West Coast Diamictite Unit possible equivalents
	Andréebreen Formation		Comfortlessbreen quartzite unit
	Svalisstranda Subgroup		Comfortlessbreen diamictite 1 unit
	Prinsesse Alicefjellet Formation		Comfortlessbreen carbonate unit
	Rabotdalen Formation		Comfortlessbreen greenschist unit
	Wulffberget Formation		Comfortlessbreen diamictite 2 unit
	Siktefjellet Group		Bellsund Group - undifferentiated
	Albertbreen Formation		Lågneset unit
	Lilljeborgfjellet Formation		Bellsund phyllite unit
	Bullbreen Group		Ferrierpiggen Group
	Holmesletta Formation		Kapp Platen shale unit
	Bulltinden conglomerate		Kapp Platen sandstone unit
	Motalafjella Formation		Roaldtoppen Group
	Aavatsmarkbreen Formation		Celsiusberget Group

	Sarsøyra Formation		Raudstupet-Sälodden Formation
	Arkfjellet unit		Nordvika Formation
	Ymerdalen Formation		Floraberget Formation
	Oslobreen Group		Franklinsundet Group
	Sørkapp Land Group		Kapp Lord Formation
	Sørkapp Land Group - without Wiederfjellet F		Westmannbukta Formation
	Wiederfjellet Formation		Persberget Formation
	Sofiekammen Group		Galtdalen Group
	Sofiekammen Group - without Vardepiggen F.		Meyerbukta Formation
	Vardepiggen Formation		Akademikarbreen Group
	Macnairrabbane unit		Veteranen Group
	Veteranen Group - undifferentiated		Signehamna Formation - mica schist w. aplites
	Oxfordbreen Formation		Signehamna Formation - quartzite
	Glasgowbreen Formation		Signehamna Formation - metasediments
	Kingbreen Formation		Signehamna Formation - marble
	Kortbreen Formation		Signehamna Formation - sericite-chlorite schist
	Geikie and Peachflya groups - undifferentiated		Nissenfjella Formation
	Konowfjellet marble		Nissenfjella Formation - garnet-biotite gneiss
	Konowfjellet slates and phyllites		Nissenfjella Formation - banded gneiss
	Sparrefjellet metapsammite		Smeerenburgfjorden Complex - felsic gneiss
	Sparrefjellet quartzite		Smeerenburgfjorden Cplx porphyroblast. Gneiss
	Gåshamna calcareous green phyllite		Smeerenburgfjorden Complex granitic orthogneiss
	Greenstone within Gåshamna Formation		Smeerenburgfjorden Complex - banded gneiss
	Jens Erikfjellet Formation		Smeerenburgfjorden Complex - migmatite
	Thiisfjellet Formation		Smeerenburgfjorden Complex migmatite w. aplites
	Kosibapasset-Vimsodden Zone deformed rocks		Smeerenburgfjorden Complex - quartzite
	Kosibapasset-Vimsodden Zone deformed rocks		Smeerenburgfjorden Complex - marble with skarn
	Kosibapasset-Vimsodden Zone deformed rocks		Gneisses of Smeerenburgfjorden Complex
	Russhamna Formation		Migmatite/gneiss altern. Smeerenburgfj. Complex
	Sørhamna Formation		Pinkie unit
	Gåshamna Formations and suggested equivalents		Alkhornet Formation
	Gåshamna Formation		Alkhornet Formation - carbonate part
	Höferpynten Formation		Alkhornet Formation - phyllitic part
	Höferpynten Formation and suggested equivalents		Løvliebreen Formation
	Jens Erikfjellet Formation and sugg. equivalents		Løvliebreen Formation
	Slyngfjellet Formation		Løvliebreen Formation - phyllitic part
	Slyngfjellet Formation and sugg. equivalents		carbonate layers in St. Jonsfjorden Group
	Kapp Hansteen Group		Trollheimen Volcanic Suite
	Brennevinsfjorden Group		Moefjellet Formation
	Duvefjorden Migmatite Complex		Trondheimfjella Formation
	Mosselhalvøya Group		Nielsenfjellet Formation
	Vildadalen Formation - upper member		Steenfjellet Formation
	Vildadalen Formation - lower member		Bogegga Formation





IV. Time-lapse pictures taken from Transect I site 1. The picture on the left was taken on the 10th of August 2017 at low tide. The picture on the right was taken on the 21/08/2017 at high tide.



III. Dependence of the ratio of net photosynthesis to dark respiration ($P_{\text{net}}:R_d$ ratio) on PAR (mean \pm s.d., $n = 3$). The letters indicate homologous groups recognized by Tukey HSD test at $P = 0.05$. The number in legend indicates irradiance in $\mu\text{mol m}^{-2} \text{s}^{-1}$

List of chemical abbreviations

Abbreviation	Description	Molecular/Formula Weight (g/mol)	Valence
Ca	Calcium	40.078	2+
Cl	Chlorine (chloride)	35.454	1-
Fe	Fer	55.845	2+
K	Potassium	39.0978	1+
Mg	Magnesium	24.3039	2+
Mn	Manganese	54.936948	2+
Na	Sodium	22.9892207	1+
NH ₄ -N	Ammonium (nitrogen)	18.0379	1+
NO ₂ -N	Nitrite (nitrogen)	46.0055	1-
NO ₃ -N	Nitrate (nitrogen)	62.0049	1-
Ntot	Total nitrogen	42.0161	
pH	Hydrogen ion activity		
PO ₄ -P	Phosphate (phosphorus)	97.9952	3-
Ptot	Total phosphorus		
Si	Silicon	28.085	1+
sigma-t	Water density		
SO ₄	Sulphate (Sulphur)	96.063	2-

Glossary

Terms and parameters	Description and physiological meanings
ETR	Electron transport rate.
F ₀	Minimum fluorescence in dark-adapted state. The primary quinone (Q _A) is oxidized (qP=1), non-photochemical quenching is relaxed (NPQ=0).
F ₀ '	Min. fluorescence calculated immediately after light exposure. Calculated estimate: qP=1, NPQ>0.
F _M	Maximum fluorescence in dark-adapted state. QA reduced (qP=0), NPQ relaxed (NPQ=0).
F _M '	Maximum fluorescence in light. qP=0, NPQ at maximum (NPQ _{max}).
F _P	Peak fluorescence during the initial phase of the Kautsky effect. Local maximum fluorescence resulting from rapid reduction of plastoquinone pool (PQ) and slower activation of re-oxidation mechanisms and of NPQ.
F _{PSII} (ΦPSII)	Effective quantum yield. The fraction of photons from incoming light that can be used for photochemistry (PSII).
F _V	Variable fluorescence increment that is due the transition from dark-adapted state with all-open RC to the all-closed state during saturating flash of light.
F _V /F _M	Maximum quantum yield. Maximum fraction of photons from incoming light that can be used for photochemistry. Basic parameter describing the physiological status of a photosynthetic (micro)organism.
HL	High light. (Herein above ca 500 μmol m ⁻² s ⁻¹).

I	Irradiance.
I_{comp}	Compensation irradiance. $R_d = P_{gross}$
I_{sat} (Ek)	Photosynthetic saturation coefficient. The crossing between α and P_{max} on a P/E-curve. Is given as the irradiance level where photosynthesis is optimum and crossing over from being undersaturated to becoming saturated.
LC	Light curve.
LL	Low light.
LoD	Instrument limit of detection.
ML	Medium light.
NPQ (ϕ_{NPQ})	Light induced regulated heat dissipation, or non-photochemical quenching. The energy from incoming light going to regulated heat dissipation.
NPQ_{max}	Maximum non-photochemical quenching.
P	Rate of photosynthesis.
PAR	Photosynthetic active radiations (400 - 700 nm).
PE curve	Photosynthesis vs. irradiance curve. Shows how photosynthesis responds to increasing light intensities as a saturation curve with EPAR on the x-axis and rETR on the y-axis.
P_{gross}	Gross photosynthesis
P_{max}	The maximum photosynthetic rate given as the maximum rETR.
P_{net}	Net photosynthesis. $P_{net} = P_{gross} - R_d$.
qP	Photochemical quenching. The energy from incoming light going to photochemistry.
R_d	Respiration in the dark.
rETR	Relative electron transport rate (arbitrary units. = $E \sigma_{PSII}' n_{PSII} (F_q'/F_v')$). A measure of the "speed" (effectiveness) of photosynthesis given as yield*irradiance. The higher the rETR the faster the electron transport and therefore higher photosynthesis.
UVR	Ultraviolet radiation.
α	The maximum slope of the P/E-curve. Is a value for the irradiance where photosynthetic effectiveness increases at the fastest rate.
σ	Sigma. Effective absorption cross section of PSII light harvesting antenna measured in $[nm^{-2}]$. An estimate of energy delivery effectiveness. The higher the value the more energy delivered and the more effective system.
$\tau_{1/2}$	Tau. Turnover time of PSII. How fast PSII is oxidized (reopened) after it's reduced (closed). Measured in [ms]. The higher the value, the faster PSII opens and closes and the more effective the system.
ϕ_{NO}	The fraction of energy from incoming light going to fluorescence and non-regulated heat dissipation.
